MECHANICAL ENGINEERING | PHYSICS | PRESERVATION OF THE ARCHITECTURAL HERITAGE | STRUCTURAL, SEISMIC AND GEOTECHNICAL ENGINEERING | SCIENCE, TECHNOLOGY, AND POLICY FOR SUSTAINABLE CHANGE | URBAN PLANNING, DESIGN AND POLICY | AEROSPACE ENGINEERING | ARCHITECTURE, BUILT ENVIRONMENT AND CONSTRUCTION ENGINEERING | ARCHITECTURAL, URBAN AND INTERIOR DESIGN | BIOENGINEERING | DATA ANALYTICS AND DECISION SCIENCES | DESIGN | ELECTRICAL ENGINEERING | ENERGY AND NUCLEAR SCIENCE AND TECHNOLOGY | ENVIRONMENTAL AND INFRASTRUCTURE ENGINEERING | INDUSTRIAL CHEMISTRY AND CHEMICAL ENGINEERING | INFORMATION TECHNOLOGY | MANAGEMENT ENGINEERING | MATERIALS ENGINEERING | MATHEMATICAL MODELS AND METHODS IN ENGINEERING

PhD Yearbook | 2026

Chair:
Prof. Salvatore Stagira

DOCTORAL PROGRAM IN PHYSICS

The Doctoral Program in Physics at Politecnico di Milano aims at attracting bright students with good scientific background and clear interest towards development and applications of new ideas and technologies. It offers a wide range of opportunities in the fields of advanced applied physics, such as photonics and optoelectronics (lasers, ultrafast optics), biomedical optics (optical tomography), vacuum technologies (thin film depositions), material technologies (microelectronics and nanotechnologies, micromechanical processing), and advanced instrumentation (electronic and atomic microscopy, nuclear magnetic resonance).

Scientific education and training to develop general research abilities in all areas of applied physics is increasingly needed by advanced technological companies. Through a general education in the basic areas of applied physics and a specific knowledge in condensed matter physics, as well as optics and lasers, the PhD Program aims at the development of an experimental approach to problem solving techniques and at the attainment of a high level of professional qualification.

The Doctoral Program has strongly experimental character. The contents are strictly related to the research activities carried out in the laboratories at the Department of Physics. They can be divided into two main areas:

a) Condensed Matter Physics, including photoemission; spin-resolved electronic spectroscopy; magneto-optics; X ray diffraction; magnetic nanostructures for spintronics; synchrotron radiation spectroscopy, positron spectroscopy, semiconductor nanostructures.
b) Photonics and Quantum Electronics, including ultrashort light pulse generation and applications; UV and X optical harmonics generation; biomedical applications of lasers; diagnostics for works of art; laser applications in optical communications; time domain optical spectroscopy and diagnostic techniques.

All research activities rely on advanced experimental laboratories located at Politecnico di Milano (Milano-Leonardo Campus and Como Campus) and are performed in collaboration with several international Institutions. Consistent effort is devoted to experimental research, development of innovative approaches and techniques, and design of novel instrumentation.

The educational program can be divided into three parts: 1) Courses specifically designed for the PhD program as well transdisciplinary courses; 2) Activities pertaining to more specific disciplines which will lay the foundation for the research work to be carried out during the Doctoral Thesis; 3) Doctoral Thesis. The thesis work is the major activity of the Program. It has a marked experimental character and will be carried out in one or more laboratories at the Department of Physics.
The students are also encouraged to perform part of their thesis work in laboratories of other national or foreign Institutions. Collaborations that may involve the PhD students are presently active with several national and international research and academic Institutions, such as: ETH-Zürich, EPL-Lausanne, Lund Institute of Technology, University of Paris-Sud, Ecole Polytechnique-Paris, University of Berkeley, University of Cambridge, University College London, Massachusetts Institute of Technology, Harvard University, European Space Agency, ENEA, Elettra-Ts, PSI-Villigen, Agenzia Spaziale Italiana, European Synchrotron Radiation Facility (ESRF-Grenoble), IFN-CNR, IIT–Istituto Italiano di Tecnologia.

Currently, the number of students in the three-year course is 130.

The PhD Program Faculty, who takes care of organizing and supervising teaching and research activities, consists of members (listed here below), who are all highly qualified and active researchers covering a wide spectrum of research fields. This ensures a continuous updating of the PhD Program and guarantees that the students are involved in innovative research work.

FAMILY NAME	FIRST NAME	POSITION*
BERTACCO	RICCARDO	FP
BRAMBILLA	ALBERTO	AP
CAIRONI	MARIO	ST
CALLONI	ALBERTO	AP
CERULLO	GIULIO	FP
COLUCCELLI	NICOLA	AP
COMELLI	DANIELA	AP
CONTINI	DAVIDE	AP
CREPALDI	ALBERTO	AP
CRESPI	ANDREA	AP
CUBEDDU	RINALDO	FP
DALLERA	CLAUDIA	FP
DELLA VALLE	GIUSEPPE	FP
DUÒ	LAMBERTO	FP
FARINA	ANDREA	ST
FINAZZI	MARCO	FP
GAMBETTA	ALESSIO	AP
ISELLA	GIOVANNI	FP
MARANGONI	MARCO	FP
MORETTI	MARCO	AP
NISOLI	MAURO	FP
PATERNÒ	GIUSEPPE MARIA	AP
PETTI	DANIELA	AP
PICONE	ANDREA	AP
POLLI	DARIO	FP
STAGIRA	SALVATORE	FP
TARONI	PAOLA	FP
TORRICELLI	ALESSANDRO	FP
VIRGILI	TERSILLA	ST
ZANI	MAURIZIO	AP

*Position: FP = Full Professor; AP = Associate Professor; ST = Scientist.

ULTRASHORT PULSES COMPRESSED BY A MPC FOR HIGH HARMONIC GENERATION

Marta Arias Velasco - Supervisor: Rocío Borrego Varillas

Ultrashort laser pulses are crucial for strong-field light-matter interaction, high-order harmonic generation (HHG), and time-resolved spectroscopic techniques such as time-resolved angle-resolved photoemission spectroscopy (tr-ARPES). However, the direct generation of few-cycle pulses from state-of-the-art laser systems operating at 800 nm and 1030 nm is fundamentally limited by gain bandwidth and technological constraints, making external pulse-compression schemes indispensable. While gas-filled hollow-core fibers (HCF) have traditionally been the standard approach for at 800 nm, multipass cell (MPC) techniques have recently demonstrated superior scalability, robustness, and performance for Yb-based systems at 1030 nm. In contrast, the potential of MPC-based pulse compression at 800 nm remains largely unexplored. Addressing this gap is important for establishing MPC-based pulse-compression schemes at 800 nm, complementing existing approaches at 1030 nm and broadening the available toolbox for ultrafast and strong-field applications.

This thesis aims to develop and optimize MPC-based post-compression schemes for generating ultrashort laser pulses, investigate their applications to HHG, and develop femtosecond extreme-ultraviolet (XUV) sources for tr-ARPES experiments.

MPCs enable an effective increase of the nonlinear interaction length while maintaining moderate peak intensities, making them especially attractive for a post-compression scheme aimed at achieving the few-cycle regime. In this configuration, the MPC operates as an off-axis optical resonator, typically consisting of two mirrors with a nonlinear medium between them. Under appropriate stability conditions, the beam undergoes multiple reflections between the mirrors, following a well-defined trajectory that traces a circular pattern on the mirrors.

Efficient pulse shortening relies on accurate mode-matching of the input beam to the cavity eigenmode. This ensures stable beam properties per pass through the cell. As the pulse propagates through the nonlinear medium, self-phase modulation induces spectral broadening by accumulating nonlinear phase. The increased bandwidth allows for subsequent temporal compression when the accumulated dispersion is properly applied.

To achieve efficient post-compression at 800 nm, an MPC-based schemes were designed, implemented, and systematically investigated. Different cavity geometries were explored to evaluate their performance in terms of spectral broadening, spatial beam quality, and achievable pulse shortening. The experimental results are compared with simulations based on a home-developed one-dimensional model, enabling the identification of the advantages and limitations of the different configurations.

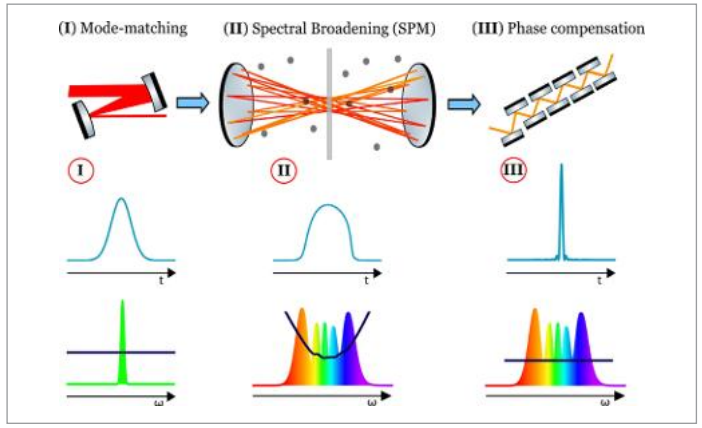

Fig.1 - Schematic representation of the most common implementation of a multipass cell with a bulk or gas nonlinear medium for spectral broadening. In the second and third row, the temporal and spectral evolution, respectively

Among the configurations investigated, the first scheme, based on a concave-concave (Cv-Cv) design following the Herriott cell formalism, incorporates two fused silica plates as a nonlinear medium separated by a vacuum system to avoid ionization in the focus region and prevent beam degradation. The setup also allows the introduction of a controlled amount of gas, enabling the MPC to operate in a hybrid configuration and providing enhanced control over nonlinear broadening. With this design, sub-20 fs Fourier-transform-limited pulse durations were achieved, with further shortening obtained upon argon injection. However, this design was not further investigated due to the poor spatial quality of the beam inside the optical cavity.

To overcome these limitations, a convex-concave geometry (Cx-Cv) was designed and implemented. This non-Herriott cavity supports folding of the optical path due to the absence of foci, enabling a more compact design with a footprint reduced by approximately a factor of three. Plane-chirped mirrors were incorporated into the folded geometry to partially compensate for accumulated dispersion. With this configuration, a compression factor of KK=2.3 was achieved while maintaining improved spatial beam quality.

In parallel, during my secondment at the Physics Department of Lund University with the Attosecond Physics Group, a compact post-compression method using a bulk MPC was employed to generate Fourier-transform-limited pulses with tunable durations ranging from 40 fs to 180 fs. This flexibility enabled a systematic study of the dependence of HHG on the driving pulse duration under identical focusing conditions and in the same generating medium. The post-compression stage was fully characterized both temporally and spatially, and the experimental results were supported by numerical simulations.

The main result shows that the maximum conversion efficiency (CE) does not necessarily occur for the shortest driving pulses. Instead, it is determined by the critical intensity required for phase matching, which depends on the pulse duration through the corresponding critical ionization degree. This interplay naturally defines an optimal pulse duration, τ_{opt}, that maximizes CE. The results highlight that HHG efficiency arises from a balance between the increasing single-atom response at higher intensities and the phase-matching constraints imposed by ionization dynamics.

Finally, this work establishes the foundation for a high-repetition-rate femtosecond XUV beamline dedicated to tr-ARPES experiments. A commercial gas-filled MPC operating at 1030 nm was characterized and validated as the post-compression stage of the driving laser system, delivering few-tens-of-femtosecond pulses suitable for HHG. Using these pulses, HHG in argon was demonstrated in the 20–50 eV spectral range, and the temporal properties of isolated harmonics confirmed the feasibility of few-femtosecond XUV probe pulses.

An alternative driving-field configuration, annular-beam geometry, was investigated to enable scaling toward high average power and to facilitate natural separation of the XUV radiation from the residual infrared field, providing a promising route toward robust and scalable operation at high repetition rates. These results establish a pathway to develop a stable, high-flux XUV source optimized for future tr-ARPES applications.

ULTRAFAST LASER-FABRICATED OPTOFLUIDIC PLATFORMS FOR SHORT-WAVELENGTH LIGHT AND LIQUID SHEET TARGETING

Alia Ashraf – Supervisor: Rebeca Martinez

Extreme Ultraviolet (EUV) radiation, covering the electromagnetic spectrum between 10 nm and 121 nm, represents a pivotal regime for both fundamental academic research and cutting-edge industrial applications. From a scientific standpoint, this spectral range enables the investigation of matter with nanometric resolution and provides a unique gateway for spectroscopic studies within the "water window" region. From an industrial perspective, advanced lithography utilizing EUV at 13.5 nm and beyond represents the state-of-the-art in the semiconductor industry for the manufacturing of silicon integrated circuits. The demand for high-brightness EUV sources and compatible optical components is critical; currently, this need is primarily met by large-scale facilities such as synchrotrons and free-electron lasers, or through commercial laser-induced plasma sources. In both instances, the large physical footprint and high operational costs strictly limit their accessibility to a select number of specialized laboratories.

An intriguing alternative for the generation of EUV radiation is the physical phenomenon known as High-order Harmonic Generation (HHG). HHG is a highly non-linear process arising from the interaction of an intense, focused ultrafast laser beam (1013 – 1015W/cm2) with a suitable non-linear medium, typically a noble gas jet. This interaction leads to the emission of coherent radiation in the form of high-order odd harmonics of the driving laser frequency, characterized by pulse durations on the atomic second timescale. While HHG sources offer a more compact and accessible alternative, their practical implementation is significantly hindered by the low conversion efficiency inherent to the process, as well as the technical challenges associated with manipulating the resulting radiation. Indeed, such high-energy photons are highly susceptible to absorption by the harmonic-generating medium itself, leading to source depletion, as well as by subsequent optical components, which are consequently restricted to cumbersome grazing-incidence configurations.

The central objective of my doctoral research is the development of integrated EUV and ultrashort UV laser sources, realized through the creation of intricate networks of hollow microstructures embedded within bulk fused silica. These structures, realized using the technique known as Femtosecond Laser Irradiation followed by Chemical Etching (FLICE), enable the precise confinement of the gas target and the manipulation of the driving field required to trigger the nonlinear interaction. What makes this approach unique is that, through the meticulous design of the glass chip, one can precisely control both the strong laser fields and the spatial distribution of the gas density, thereby optimizing generation efficiency at unprecedented levels.

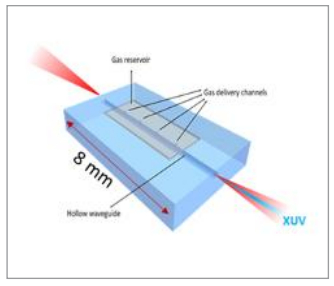

Fig.1

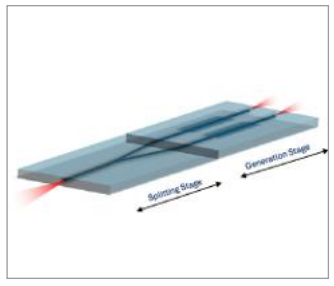

Fig.2

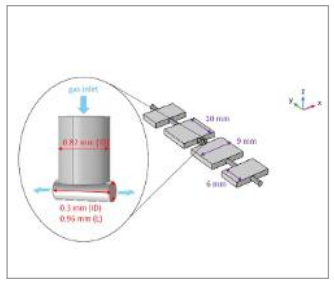

Fig.3

By exploiting the three-dimensional capabilities of FLICE, the HHG device is fabricated on one monolithically integrated fused silica chip measuring 8×10×1 mm, engineered with a 3D microchannel network for precise gas delivery. It features a hollow waveguide strategically connected to a top-side gas inlet through four vertical, micrometer-sized access holes. This architecture ensures a controlled supply of the non-linear medium directly to the interaction region where the driving laser field is confined. Both the optical and fluidic components are simultaneously defined within the substrate using a unified 3D laser irradiation process, ensuring perfect alignment and structural integrity as illustrated in fig. 1.

Another architecture developed by FLICE, the integrated HHG beam interferometer in which some extra functionalities are integrated. It is a monolithic glass device with a 35 mm long, designed to simultaneously generate two coherent EUV beams for high-contrast interference patterns. The architecture features a splitting stage where a130 µm waveguide splits into two symmetric arms using a sinusoidal profile to minimize radiative losses of the driving field, as illustrated in fig. 2. Within the subsequent generation stage, these arms are integrated with microfluidic gas inlets, leveraging the 3D capabilities of FLICE to add complex functionalities. This integrated approach ensures perfect phase stability and structural alignment, providing a robust platform for EUV interferometry that is unavailable in traditional bulky setups.

We aim to enhance the capabilities of the FLICE technique by developing a complex, differentially pumped integrated glass chip specifically designed to host high-intensity-driven nonlinear interactions while ensuring optimal gas distribution. As an illustration, Fig. 3 depicts a device that integrates differential pumping stages designed to evacuate the gas immediately following the generation process, thereby significantly reducing the probability of reabsorption of the emitted radiation. The device consists of a three-dimensional hollow network comprising a central UV-generation cell, a gas inlet, multiple pumping chambers for gas evacuation, and a pass-through channel aligned with the laser propagation axis, all integrated within fused silica to guarantee minimal gas permeability together with excellent mechanical and chemical stability.

All the chips are fabricated using Femtosecond Laser Irradiation followed by Chemical Etching (FLICE), showing its versatile capabilities to develop and adopt integrated waveguide components with the addition of different functionalities is achievable in a compact and monolithic platform.

COMPUTER GENERATED HOLOGRAPHY FOR AUGMENTED REALITY APPLICATIONS

Marco Astarita - Supervisor: Gianluca Valentini

Holographic displays are widely regarded as a leading candidate for next-generation three-dimensional visualization because they can shape the optical wavefront and, in principle, provide the full set of depth cues available to human vision. This capability is particularly attractive for augmented-reality (AR) near-eye systems, where comfortable visualization should be central to user-oriented design, and where conventional stereoscopic solutions can suffer from the vergence-accommodation conflict. In a holographic display, a three-dimensional virtual scene is encoded into a computer-generated hologram (CGH) and optically reconstructed by modulating coherent light with a reconfigurable diffractive device, most commonly a phase-only spatial light modulator (SLM). Overall, this enables pixel-level control over accommodation cues and depth.
Despite this potential, practical holographic near-eye displays are constrained by a set of challenges that span computation, image quality, and system integration. This research work addresses these limitations by developing novel strategies for efficient hologram generation and high-fidelity optical reconstruction, specifically tailored for AR applications.

Computational Strategies and Wireframe Holography
One of the primary hurdles in holographic displays is the significant computational power required to calculate CGHs in real-time, especially for complex 3D scenes. This thesis proposes a "wireframe holography" approach, which simplifies the representation of virtual objects into a set of oriented lines or segments. By leveraging the analytical properties of the Fourier transform for linear segments, the computational load is drastically reduced compared to point-cloud or polygon-based methods. This enables the generation of high-resolution holographic content at interactive frame rates, a crucial requirement for seamless AR experiences.
Furthermore, we explore the implementation of optimization algorithms such as the Compressive Sensing-based Weighted Gerchberg-Saxton (CS-WGS) algorithm. This method refines the phase distribution on the SLM to minimize reconstruction errors and improve image uniformity. By integrating these algorithms into a GPU-accelerated framework, we demonstrate that high-quality holographic video can be synthesized with minimal latency.

Image Quality and Zero-Order Suppression
The quality of holographic reconstructions is often degraded by physical artifacts, most notably the "zero-order" diffraction beam. This uncontrolled spot of light arises from the non-modulated portion of the beam reflecting off the SLM surface and can significantly reduce the contrast and dynamic range of the virtual image. In this work, an interferometric method for zero-order suppression is developed. By introducing a destructive interference pattern or utilizing specific optical architectures, the zero-order beam is effectively neutralized without the need for bulky physical masks or spatial filters that would otherwise increase the footprint of the AR headset. Additionally, the research investigates the impact of speckle noise—a characteristic graininess of coherent systems. We implement temporal averaging and phase-diversity techniques to mitigate speckle, ensuring that the reconstructed images are sharp and visually pleasing for the end-user.

Hardware Integration and Experimental Results
The proposed methods were validated through the design and characterization of a prototype holographic near-eye display. The system utilizes a high-resolution phase-only SLM and a compact laser source. Experimental results confirm that the "wireframe" approach provides a clear and stable 3D visualization with correct depth cues. The zero-order suppression technique effectively clears the central field of view, allowing for a high-contrast overlay of virtual content onto the real-world environment.

Conclusions and Future Perspectives
This research contributes to the advancement of holographic AR by providing a comprehensive framework that addresses both software and hardware challenges. The developed algorithms for wireframe holography and the interferometric zero-order suppression method represent significant steps towards making holographic near-eye displays a viable technology for everyday use. Future work will focus on the miniaturization of the optical engine and the integration of eye-tracking systems to further enhance the user experience and reduce computational requirements through foveated holography.

OBLIQUE PLANE MICROSCOPY USING DYNAMIC REMOTE FOCUSING

Vipin Balan - Supervisor: Andrea Bassi

Light-sheet microscopy has become one of the most powerful techniques for imaging biological samples from the microscale to the mesoscale due to its low phototoxicity, intrinsic optical sectioning capability, and large field of view (FoV). However, conventional light-sheet systems employ two orthogonally arranged objectives with limited working distances, which restricts their ability to image conventionally mounted samples. Oblique plane microscopy (OPM) overcomes this limitation by using a single objective for both illumination and detection, enabling light-sheet imaging of standard sample geometries. Since same objective is used for both excitation and detection, the light sheet must be introduced obliquely with respect to the optical axis. Imaging such a tilted plane is inherently challenging, as planes that are not coincident with the focal plane of the objective experience defocus across the field of view. In conventional OPM, this defocus is corrected using a remote focusing configuration incorporating a tilted objective, which re-images the oblique plane onto the camera sensor in perfect focus. Even though this approach retains all the fundamental advantages of light-sheet microscopy, the tilted remote focusing geometry leads to partial clipping of the primary objective's aperture. This reduces the effective numerical aperture (NA) and consequently degrades spatial resolution. To address this limitation, a full-aperture oblique plane microscope was developed using off-the-shelf optical components, enabling complete utilization of the imaging objective's numerical aperture. This is achieved by eliminating the tilted remote focusing configuration and replacing it with dynamic remote focusing using an electrically tunable lens (ETL). The ETL is a current-controlled optical element whose focal length varies proportionally with the applied input current within its operating range. By modulating the driving current, the axial focal position can be adjusted electronically without any mechanical translation of lens. This dynamic remote focusing, combined with synchronized rolling-shutter detection, enables accurate capture of the illuminated oblique plane without defocus. Following validation of the system, the microscope was enhanced by integrating a galvanometric mirror scanner for high-speed imaging. Additionally, a wavelength splitter was incorporated into the detection pathway, together with supplementary excitation, to enable dual-color imaging. The performance of the system was validated through imaging studies on diverse biological specimens, including the beating heart of zebrafish embryos and prepared optical slide samples.

INTERSUBBAND TRANSITIONS IN GE/SIGE QUANTUM WELLS FOR ADVANCED MID-INFRARED INTEGRATED PHOTONICS

Pietro Baldin - Supervisor: Giuseppe Della Valle

Driven by the relentless demand for miniaturized, lightweight, and efficient optical components, the field of nanophotonics has transformed how electromagnetic waves are manipulated at nanometric scales. Classical optical engineering relies on bulky refractive and diffractive lenses, prisms, and wave-guiding elements, but these traditional architectures rooted in macroscopic optics suffer from intrinsic geometric limitations, and scaling laws that prevent their integration into ultra-compact consumer electronics. Today, these bulky components face the prospect of being entirely replaced by flat-optics, thanks to the development of nanopatterned architectures known as metasurfaces, i.e. two-dimensional arrays of sub-wavelength scatterers designed to impart abrupt phase, amplitude, and polarization changes on incident wavefronts. Within the domain of flat-optics, a specific subclass known as nonlocal metasurfaces has distinctly gained prominence: while purely localized metasurfaces rely on the isolated responses of single-scatterer resonances, nonlocal metasurfaces function by supporting spatially extended and collective optical modes, that distribute electromagnetic energy across multiple adjacent unit cells. These advanced resonant frameworks are highly prized for their exceptional spectral and angular selectivities, generating sharp resonances with ultra-high Quality (Q-) factors. Furthermore, these architectures maintain excellent compatibility with standard scalable top-down nanofabrication techniques, and rely on commonly available dielectric materials. Prominent examples of nonlocal resonant phenomena include Guided Mode Resonances (GMRs) and quasi-Bound States in the Continuum (q-BICs).

From an experimental standpoint, transitioning nonlocal metasurfaces from theory to practical applications is a very challenging task: the collective nature of these extended resonances makes their macroscopic optical response very sensitive to the precise material properties and specific geometric features, with any difference from the nominal parameters potentially leading to strong deviations from their theoretical behaviour. In addition, since these modes rely on coherent interactions across thousands of nanostructures, another crucial role is played by finite-size effects, which arise from the physical truncation of the periodic array at its edges, and may drastically alter the resonances properties. More in general, inevitable fabrication defects - ranging from surface roughness to structural irregularities - lead to severe radiation leakage, resonance broadening, and overall degradation of the metasurface's optical performance.

Currently, the applied nanophotonics community faces a highly restrictive bottleneck: a distinct lack in the scientific literature of versatile, computationally efficient, and robust design methodologies specifically tailored for the unique physics of nonlocal metasurfaces. Traditional full-wave electromagnetic solvers, like Finite Difference Time Domain (FDTD) or Finite Element Method (FEM), require computationally prohibitive resources and massive time investments when attempting to accurately model spatially extended modes over vast areas with nanoscale resolution.

This computational challenge effectively prevents these sophisticated optical devices from being rapidly prototyped, and widely adopted for commercial and industrial optical applications.

This thesis introduces a comprehensive and highly versatile computational framework dedicated to the accurate simulation, comprehensive assessment, and rapid mathematical optimization of nonlocal metasurfaces. By strategically leveraging rigorous analytical physics tools, alongside customized semi-iterative reduced theoretical models, the proposed methodology effectively bypasses the computational bottlenecks inherently associated with "brute-force" solvers. This advanced framework not only accurately predicts complex nonlocal resonant behaviors with high fidelity, but also allows to systematically quantify the detrimental physical impact of geometrical imperfections and finite-size spatial truncation on real-life fabricated samples.

This advanced numerical expertise is subsequently applied to the rational forward-design of flat optics, across two highly impactful technological directions: Smart Vision applications, and complex nonlinear nanophotonics. In the first case, we focus specifically on the reals of Augmented Reality (AR) and wearable Eye-Tracking (ET) systems, for which physical constraints regarding device weight, optical transparency, and angular field-of-view are notoriously strict. Utilizing the computational framework, we successfully achieve advanced nonlocal metasurface designs where the metasurfaces are used as free-space optical combiners either in the near-IR or visible regions, ideally enabling efficient, ultracompact, and lightweight ET/AR wearable devices. These designs theoretically match the same performances of similar state-of-the-art metasurfaces that were recently proposed in the literature for these applications, and they also feature important improvements on some key functionality requirements: for example, for ET we propose metasurface designs that achieve an efficient nonlocal resonance in the near-IR with high-index substrates compatible with realistic prescription lenses materials, while for AR we achieve a multi-resonant RGB combiner with significantly reduced angular dispersions, whilst in both cases avoiding spurious rainbow effects and keeping an overall high average transparency in the visible.

The second half of the thesis focuses strictly on the application of nonlocal resonant phenomena to nonlinear effects, i.e. the changes on the optical properties (namely the permittivity) of nonlinear materials due to the complex, sub-picosecond transient dynamics of out-of-equilibrium charge carriers that are all-optically photo-excited. In the first application study, this physical exploration is leveraged to rationally design a lateral hybrid heterostructure, tailored for ultrafast all-optical diffraction management and dynamic beam steering: by manipulating how incident light diffracts on ultra-short femtosecond timescales, the nonlocal metasurface design we propose paves the way for an efficient and ultra-high-speed optical routing, and it could be easily extended to other commonly-available nonlinear dielectric materials, metasurface geometry, and spectral regimes, proving its effectiveness and versatility.

Lastly, we combiner nonlocal and nonlinear phenomena for another interesting application, i.e. the design of a chiral metasurface engineered to achieve true nonreciprocal transmission for circularly polarized incident light: by harnessing nonlinearly-driven symmetry breaking mechanisms, our metasurface acts as an optical isolator at the nanoscale, allowing light of a specific circular handedness to pass unimpeded in one direction while reflecting it in the reverse.

Overall, the theoretical models, simulations, and applied findings presented throughout this extensive work definitively demonstrate the huge potential of nonlocal metasurfaces for a plethora of important optical applications. The synergy between bespoke, highly efficient computational modeling on one side, and the precise, physically grounded engineering of spatially extended optical resonances on the other, can forge vital new pathways in applied nanophotonics, with this integrated approach effectively bridging the long-standing gap between industry-driven, practical smart vision technologies and the fundamental physics of novel, ultrafast light-matter interactions.

ULTRAFAST PROCESSES IN SOLID STATE MATERIALS: FROM HOT CARRIER DYNAMICS TO SPATIALLY-RESOLVED MAGNETIZATION DYNAMICS

Alessandro Baserga - Supervisor: Stefano Dal Conte

This doctoral thesis investigates out-of-equilibrium physical processes occurring on femtosecond timescales in solid-state materials relevant to advanced optoelectronics and spintronics. The work focuses on understanding how dimensionality reduction, defects, and heterostructure engineering influence charge carrier and spin dynamics. By employing ultrafast spectroscopic and microscopic techniques, various energy and spatial relaxation channels were isolated, providing a microscopic description of the light-matter interaction mechanisms governing the response of these systems under strong photoinduced non-equilibrium conditions.

The first chapter addresses the challenge of manipulating hot carrier lifetimes in graphene through chemical functionalization. Pristine graphene exhibits extremely rapid cooling times on the order of picoseconds, which limits applications requiring the preservation of a hot electronic distribution, such as photothermoelectric devices. We studied the effect of partial fluorination, which introduces sp^3 hybridized sites into the sp^2 graphene lattice, locally opening a bandgap and consequently improving graphene's electro-optical properties. However, defects introduced by fluorine act as scattering centres that significantly accelerate carrier cooling compared to pristine graphene. To overcome this limitation, previous studies designed and synthesized a van der Waals heterostructure composed of a graphene layer (Gr) and a partially fluorinated graphene layer (F-Gr), showing that the structure could combine the positive properties of fluorination while reducing its negative effects, resulting in a favourable trade-off. Our results demonstrate that the interaction between the two layers leads to defect passivation. In this configuration, excited carriers in the graphene layer can benefit from the bandgap introduced by functionalization without undergoing the accelerated decay caused by defects. This approach shows that interlayer coupling in 2D heterostructures enables the engineering of optical and transport properties, providing a powerful strategy for tailoring functionalized graphene systems.

A central part of this research concerns the study of mercury phosphorus selenide ($HgPSe_3$), a layered semiconductor belonging to the metal phosphorus trichalcogenides family. These materials are characterized by strong electron-electron, electron-magnon, and electron-phonon interactions, which make their relaxation dynamics highly complex. Using broadband transient absorption spectroscopy and time-resolved photoluminescence, we characterized the evolution of the hot carrier population and its coupling to the lattice. Data analysis revealed a hierarchy of relaxation times. An initial ultrafast carrier occurs within a few picoseconds, likely driven by electron-phonon scattering. Subsequently, the dynamics is dominated by carrier capture into intra-gap states associated to the material's intrinsic structural defects. We observed a luminescence emission centred at 1.3 eV, attributable to defect-mediated transitions, which, together with the known defect states emitting at 1.8 eV, acts as a bottleneck for the recovery of the ground state. The study of temperature and excitation density dependence revealed the onset of the hot-phonon bottleneck effect: at high excitation densities, the phonon system is unable to dissipate the carriers' thermal energy quickly enough, leading to a prolonged excited state population. This understanding is important for the optimizing $HgPSe_3$-based photodetectors, whose operational speed is intrinsically limited by these capture and relaxation processes.

The final part of the work shifts focus from charge to spin degrees of freedom, investigating laser-induced ultrafast demagnetization in Pt/CoFeB/MgO ferromagnetic thin films. Although the temporal dynamics of demagnetization in ferromagnets is well-documented, its spatial evolution on the nanometre scale remains less understood. We employ an innovative ultrafast holographic microscopy technique capable of distinguishing the two polarization components of laser beams to map magnetization variations with 100-fs temporal resolution and sub-micrometre spatial resolution. The holographic maps reveal that the demagnetization is spatially non-uniform and extend the region of direct interaction with the laser. Lateral heat and spin transport dynamics were observed to influence magnetization recovery. Specifically, we highlighted how the diffusion of hot electrons and heat contributes to a spatial variation of the magneto-optical signal. Magnetization recovery dynamics show a progressively faster decay trend with increasing distance from the centre of excitation, a behaviour consistent with heat dissipation processes mediated by electrons, the lattice, and magnons described by the three-temperature model. This study highlights the importance of spatial gradients in the design of optically written magnetic memories and proves that ultrafast holographic microscopy is a powerful tool for studying out-of-equilibrium processes in magnetic systems. It provides a powerful approach for investigating additional phenomena such as spin diffusion in real space, domain wall propagation, and the detection of spin waves.

Overall, the results presented in this thesis demonstrate that out-of-equilibrium processes in low-dimensional materials are intrinsically linked to their structure and spatial morphology. Through the investigation of $HgPSe_3$ shows how defects and intra-gap states predominantly govern the system's response time, acting as trapping centres that redirect hot carrier relaxation away from intrinsic pathways. Similarly, the study of graphene heterostructures reveals that the strategic combination of chemical functionalization and layer stacking enables fine control of electronic cooling, overcoming constraints imposed by doping and disorder. Furthermore, the exploration of magnetic systems confirms that spatial resolution is an essential requirement for deciphering the transport phenomena accompanying light-induced demagnetization. Ultimately, this thesis provides a comprehensive picture in which ultrafast spectroscopy serves as a fundamental tool for probing the complexity of electronic de-excitation processes. A deep understanding of these relaxation and energy transfer mechanisms represents a fundamental pillar for the future design of high frequencies energy-efficient optoelectronic and spintronic devices that fully exploit the unique properties of two-dimensional materials and thin-film layers.

ATTOSECOND DYNAMICS IN THE DEEP CONDUCTION BAND OF WIDE-BANDGAP INSULATORS

Simone Bonetti– Supervisor: Matteo Lucchini

Understanding how electrons move inside solids on their natural, sub-femtosecond time scale represents one of the most compelling challenges in condensed-matter physics. Accessing this regime is not only a matter of fundamental scientific curiosity but also a technological necessity. As present-day semiconductor electronics approach fundamental limits imposed by heat dissipation, alternative paradigms for information processing are actively sought. In this context, controlling solid materials directly with optical electric fields has emerged as a promising route toward faster signal processing, potentially extending operational frequencies by orders of magnitude beyond those achievable with voltage-driven architectures.

Within this broader effort, wide-bandgap insulators occupy a particularly attractive position. Their large energy gaps strongly suppress carrier injection when driven by off-resonant optical fields, enabling reversible and coherent light-matter interaction even under intense excitation conditions. Instead of promoting real carriers across the band gap, a strong infrared field can induce virtual excitations that follow the instantaneous value of the electric field. Such field-driven processes provide a clean platform for investigating ultrafast electron dynamics in a regime where long-lived population effects are absent. However, exploring these phenomena requires experimental techniques capable of resolving motion on the attosecond scale, where the optical waveform itself governs the evolution of electrons. Only by achieving sub-cycle temporal resolution can one directly track how electrons respond to the driving field within a fraction of its oscillation period.

In the present work, we measure attosecond electron dynamics in lithium fluoride (LiF), a prototypical wide-bandgap insulator characterized by an energy gap of nearly 14.5 eV. Owing to its large band gap, LiF provides an ideal model system in which strong-field excitation can drive coherent electronic motion without inducing permanent modifications of the material. These properties make it particularly suitable for isolating purely electronic contributions to the ultrafast optical response and for disentangling virtual processes from real carrier dynamics.

To access these processes experimentally, we employ attosecond transient reflection spectroscopy (ATRS), a pump-probe technique designed to probe non-equilibrium dynamics in solids with sub-femtosecond resolution. In this approach, a few-femtosecond infrared pulse acts as a pump that drives the system far from equilibrium. An attosecond extreme-ultraviolet (XUV) pulse serves as a probe, interrogating the material at controlled time delays relative to the pump. Both pulses are impinging at 72° angle of incidence. The XUV reflected light is collected and dispersed by a diffractive grating, allowing for detection of its spectrum. By scanning the delay between pump and probe it is possible to measure the pump-induced changes of LiF reflectivity over a broad spectral window, which in turn provides the time-dependent characterization of the electronic response with resolution below the optical cycle.

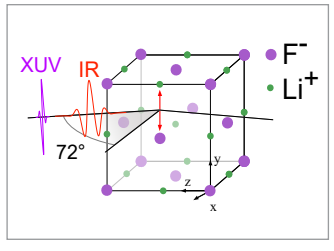

Fig.1 - Cartoon of ATRS experiment on LiF. The IR and XUV pulses are impinging on the LiF sample with a 72° angle of incidence. The red arrow indicates the polarization direction of the pulses, which are oscillating along the Li-F bond

A key aspect of the method lies in the absolute calibration of the pump-probe delay with respect to the infrared electric field. This calibration enables a direct correlation between the measured reflectivity modulations and the instantaneous value of the driving field, allowing a quantitative analysis of sub-cycle phenomena. Moreover, the nature of the LiF band structure allows for XUV transitions to probe its deep conduction band, thereby extending the investigation beyond the immediate vicinity of the band edge and into a spectral region that is typically inaccessible to conventional optical techniques.

Importantly, equilibrium reflectivity measurements in this energy range do not reveal pronounced resonant structures, which underscores the necessity of a time-resolved approach to uncover hidden dynamical features.

The pump-probe experiments reveal only transient signals characterized by oscillations at twice the driving frequency, commonly referred to as 2ω oscillations. This behaviour indicates a response that is phase-locked to the square of the infrared electric field. The observation of such sub-cycle modulations demonstrates that the electronic excitation in LiF follows the optical waveform on its natural timescale, providing direct evidence of field-driven dynamics in the strong-field regime. Two main components can be clearly identified in the measured response. The first is a broadband modulation extending over a wide spectral region in the extreme-ultraviolet range. Its smooth energy dependence and robust 2ω character are fingerprint of virtual charge dynamics induced by the strong infrared field. The second contribution is more localized in energy and exhibits a behaviour that is reminiscent of the dynamic of excitons, although no sharp excitonic resonances are visible in the static reflectivity. In other words, the experiment suggests the driving field is activating a high-lying excitonic state embedded within the conduction band continuum, a state that remains hidden under equilibrium conditions.

To support this interpretation, advanced theoretical modelling is employed. Simulations performed within an independent-particle framework, where electron-hole correlations are neglected, successfully reproduce the broadband component of the signal, confirming its origin in field-driven virtual charge dynamics. In contrast, the localized exciton-like feature does not appear within this approximation. It emerges in the calculated response only when electron-hole interactions are explicitly included. This comparison clearly indicates that the latter contribution originates from excitonic dynamics, demonstrating that electron-hole correlations can play a decisive role in shaping the ultrafast optical response even in spectral regions that, under equilibrium conditions, appear free of distinct excitonic resonances.

The coexistence of virtual carriers and excitons on the attosecond timescale illustrates the complexity of strong-field light-matter interaction in wide-bandgap insulators. In particular, field-driven virtual charge and exciton dynamics appear to be intertwined in the deep conduction band of LiF. This finding broadens the conventional view of excitons as quasiparticles that predominantly contribute to low-energy, near-gap optical responses, and instead indicates that excitonic effects can persist and play a significant dynamical role even at much higher energies when the system is driven far from equilibrium.

In conclusion, this study establishes ATRS as a powerful tool for detecting excitonic states that remain hidden under equilibrium conditions. More broadly, it advances our understanding of electron dynamics in solid-state materials and contributes to a deeper comprehension of non-equilibrium phenomena in condensed-matter physics.

ENGINEERING OF LIGHT SENSITIVITY IN CHLAMYDOMONAS REINHARDTII

Anna Bosc - Supervisor: Giuseppe Maria Paternò

This PhD thesis is positioned at the interface between biophotonics and the physics of active biological systems, with the aim of quantitatively understanding and modulating the phototactic behavior of the microalga Chlamydomonas reinhardtii using non-genetic optical and biophysical approaches. The organism is treated as an active microswimmer in which optical information is converted into a directional mechanical response through coupled electro-physiological and dynamical processes. Within this framework, the thesis explores the use of membrane-targeted phototransducers as tools to perturb the bio-physical parameters governing motility.
The first objective of the work was the quantitative characterisation of phototaxis in Chlamydomonas reinhardtii as a function of the illumination wavelength. Using controlled light stimulation protocols combined with macroscopic and single-cell imaging, distinct dynamical regimes were identified: avoidance responses under near-UV illumination and robust phototactic responses under green and blue light. In the latter spectral range, a transition regime emerges, in which both the sign and amplitude of the phototactic response critically depend on the properties of the light source and on the physiological state of the cell. This regime provides a particularly sensitive operating point to probe the response of the system to external perturbations.

To resolve the intrinsic heterogeneity of cellular behavior, a single-cell behavioral phenotyping workflow based on trajectory tracking was developed. Cell populations were classified into distinct dynamical states—stationary, confined motility, and directional motion—allowing for a statistical description of swimming dynamics. Motion was quantified using the mean squared displacement (MSD), both in steady-state conditions through power-law fitting to discriminate different motility regimes, and in a time-resolved form aligned to stimulus onset to capture transient phototactic responses.

From a biophysical perspective, phototaxis in *Chlamydomonas reinhardtii* arises from a transduction chain linking light perception to flagellar dynamics. The eyespot apparatus, composed of blue-light photoreceptors coupled to pigmented shading structures, generates a periodic modulation of the perceived light intensity due to cell body rotation during swimming. This modulation is converted into an asymmetric intracellular signal that differentially regulates the beating of the two anterior flagella. The resulting flagellar asymmetry induces controlled trajectory curvature and net phototactic steering. Because this process relies on the electrical and mechanical properties of the plasma membrane, phototaxis is expected to be sensitive to perturbations of its bio-physical state.

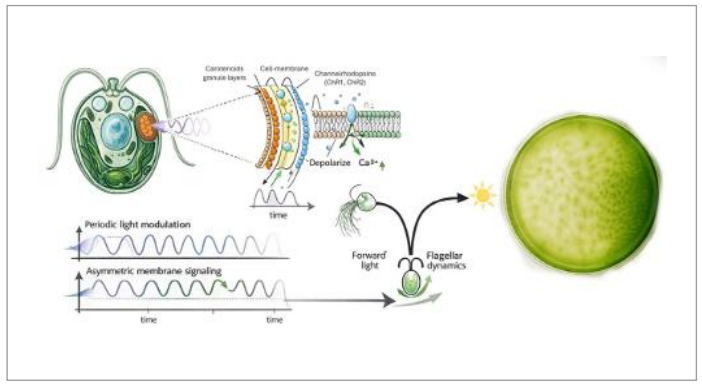

Fig.1 - Bio-physical mechanism of phototaxis in Chlamydomonas reinhardtii.
Periodic modulation of the light signal due to cell body rotation and eyespot shading is converted into a modulation of the membrane potential (mediated by Channelrhodopsins photoreceptors). This signal induces an asymmetric modulation of flagellar beating, resulting in a curved swimming trajectory and net phototactic steering. Perturbations of membrane bio-physical properties provide an effective non-genetic route to control the phototactic response

Based on this rationale, after characterising wild-type behaviour, several non-genetic phototransducers were tested to modulate motility. Among them, Ziapin2 proved particularly effective. Ziapin2 is an amphiphilic molecule that inserts into the cell membrane and undergoes conformational changes, thereby acting as a perturbation of membrane mechanical and electrical properties.
The introduction of Ziapin2 produces marked and systematic effects on microswimmer dynamics. Increasing concentration and incubation time lead to a progressive reduction of basal motility, accompanied by an increase in the stationary fraction and a prevalence of confined motion. In the blue-light stimulation regime, where control cells exhibit a well-defined phototactic response, Ziapin2 significantly suppresses directional motion and reduces the amplitude of the light-induced MSD response.
In addition, chlorophyll fluorescence measurements were used as probes of the physiological and photochemical state of the system. Photosystem II fluorescence induction curves show systematic dependencies on Ziapin2 concentration and incubation time, consistent with enhanced quenching processes or modified fluorescence yield. Exploratory FLIM measurements during phototaxis experiments further suggest that the observed dynamical perturbations are accompanied by measurable changes in single-cell fluorescence dynamics.
Overall, this work provides a quantitative description of phototaxis as an emergent phenomenon arising from the coupling between optical stimulation, membrane-mediated transduction, and flagellar dynamics. The results demonstrate that the behavior of a biological microswimmer can be modulated in a controlled, non-genetic manner, offering a bio-physical framework relevant both for fundamental studies of active matter and for applications in optical control and biohybrid system design.

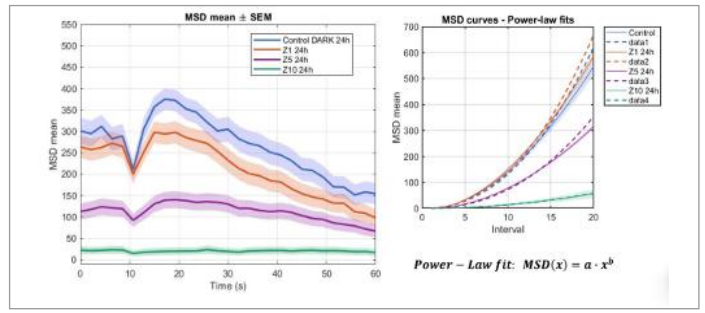

Fig.2 - Ziapin2 suppresses microswimmer dynamics and phototactic response quantified by MSD analysis.
MSD analysis of Chlamydomonas reinhardtii trajectories after 24 h incubation in control conditions and with increasing concentrations of Ziapin2 (1, 5 and 10 uM). Left: Time-resolved MSD aligned to the phototaxis stimulation protocol (phototaxis starts at 10 sec), showing a progressive reduction of motility amplitude and stimulus-induced response with increasing Ziapin2 concentration. Right: MSD time-lag analysis with a power-law model revealing a systematic decrease in both amplitude and scaling exponent with increasing perturbation. The results indicate a transition from persistent, directed motion toward confined or weakly diffusive regimes

STRATEGIES FOR HIGH-PERFORMANCE PRINTED AND DOWNSCALED ORGANIC TRANSISTORS

Martino Cambiaggio – Supervisor: Mario Caironi

Organic electronics has emerged as a promising technology for the fabrication of lightweight, flexible, and potentially sustainable electronic systems, offering unique advantages such as solution processability, compatibility with low-temperature substrates, and additive manufacturing. These features make organic electronics particularly attractive for large-area and distributed applications, including wearable devices and the Internet of Things (IoT), where low-cost, scalable production and reduced environmental impact are increasingly important. Moreover, the increase in availability of additive technologies draws the industrial interest for rapid prototyping techniques and on-demand fabrications. However, despite the rapid growth of the field and the availability of high-performance organic semiconductors, the practical implementation of printing technologies in organic electronics remains limited by a significant performance gap with respect to more established solution-based deposition techniques. This gap, typically, arises from the increase complexity in controlling the film formation and the morphology during printing, which prevent achieving the optimal conformation. At the same time, in general, performances reported by organic electronic devices are still strongly limited for the requirements of several applications. For instance, wireless-communication technologies for wearable, logistics and IoT devices, require high-frequency operations still unmatched by organic electronic devices. The reasons of this lack of performance can be traced back to the needs of highly downscaled dimensions for high-frequency operations and to the lack of effective strategies to enhance charge injection and transport in organic electronic devices. In my thesis these limitations are addressed through two complementary experimental studies aimed at advancing the fabrication and performance of solution-processable organic field-effect transistors (OFETs). The first section investigates the inkjet-printing compatibility of the high-mobility C_8-BTBT:C_{16}IDT-BT semiconductor blend. By systematically studying the role of printing parameters, particularly platen temperature and drop spacing, it is shown that printing at a substrate temperature of T=60 °C combined with postdeposition thermal annealing enables to retrieve an optimal morphology through controlled solvent evaporation and self-organization of the C_8-BTBT small-molecule (Fig.1a-d). Under optimized conditions, the blend was successfully integrated into inkjet-printed OFETs, including printed source, drain, and gate electrodes on flexible parylene-C substrates (Fig.1d). By introducing the molecular dopant $C_{60}F_{48}$ directly into the ink, saturation mobilities up to 8 $cm^2V^{-1}s^{-1}$ and linear mobilities exceeding 6 $cm^2V^{-1}s^{-1}$ were obtained, values comparable to those reported in literature with state-of-the-art solution-based deposition techniques. These values represent the highest mobilities reported to date for solely inkjet-printed organic semiconductors (i.e. without any prior pre-patterning of the substrate), effectively closing the performance gap with other solution-based deposition techniques.

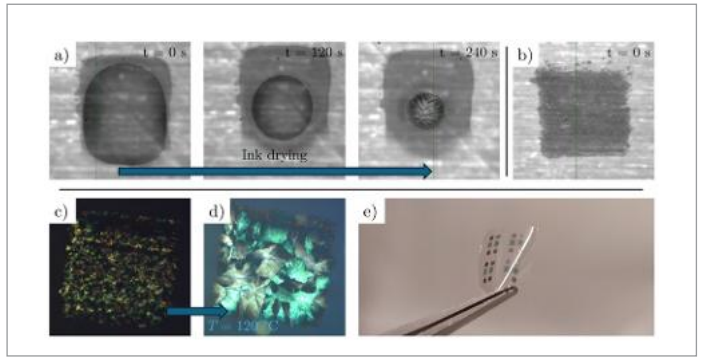

Fig.1 - a-b) Different printing temperatures (room temperature (a) and T=60 °C (b)) lead to different drying modes, changing the transport phenomena within the drying film, ultimately leading to different film morphologies. c-d) Effect of a post-printing thermal annealing at T=120 °C on the film printed at T=60 °C, obtaining the optimal polycrystalline film morphology. Microscope picture in cross-polarized light before (c) and after (d) the thermal annealing. e) Picture of the final devices on a self-standing flexible parylene-C substrate

The second part of the thesis addresses a fundamental limit in organic electronics: the absence of reliable strategies for spatially localized molecular doping. Localized doping is essential for reducing contact resistance and improving charge injection, particularly in short-channel OFETs, yet it remains difficult to achieve without compromising current modulation. In collaboration with the Institut de Ciència de Materials de Barcelona, a novel approach based on the molecular-gate concept proposed by Perevedentsev and Campoy-Quiles is introduced, in which Joule heating of the electrodes is used to locally activate dopant diffusion through a polymeric interlayer (Fig.2a). Proof-of-concept devices based on C16IDT-BT doped with tris(pentafluorophenyl) borane (BCF) demonstrated a clear enhancement in current injection and field-effect mobility, with saturation mobilities exceeding 2 cm2V–1s–1 in short-channel devices (3.5-5.5 µm), compared to almost two orders of magnitude lower values in pristine counterparts. By exploiting asymmetric doping and overlap-free device architectures fabricated via fs-laser sintering of the gate electrode (Fig.2b-e), a total gate capacitance of approximately Cg = 115 fF and a transition frequency of 50 MHz at –21 V were achieved, representing an order-of-magnitude improvement over bulk-doped devices with similar geometry. Overall, the results presented in this thesis broaden the applicability of inkjet printing to high-performance organic semiconductors and introduce a versatile strategy for localized dopant control. Together, these advances contribute to narrowing the gap between laboratory-scale demonstrations and practical high-speed applications of organic printed electronics.

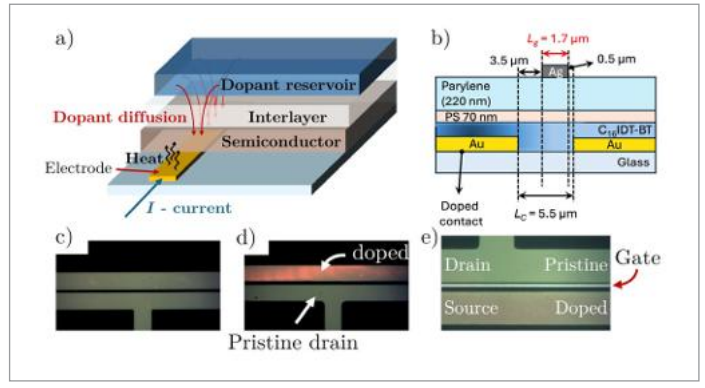

Fig.2 - a) Schematic of the localization of a molecular dopant via a controlled diffusion through a polymeric interlayer activated by the Joule heating of the electrode. b) Schematic of an asymmetric device with the organic semiconductor locally doped around the source electrode and a sintered gate electrode with no overlap with the contacts. c-d-e) Microscope pictures of: a pristine pair of electrodes (c), after the source electrode is doped (d) and of the full device with the sintered gate (e).

SECONDARY ELECTRON ENERGY SPECTROMETER FOR SCANNING ELECTRON MICROSCOPY

Wenzheng Cao - Supervisor: Anjam Khursheed

Since the invention of the scanning electron microscopy (SEM), the focused electron beam has been widely applied to fields such as material science, biology and semiconductor research.
It is not only used for imaging nanometer features, but also for analysing chemical composition and surface chemical state, by the electron beam induced X-ray, Auger electrons, and Backscattered electrons (BSEs).
Although the majority of electrons generated from the sample surface by the primary beam are secondary electrons (SEs) —with energies below 50 eV — they are primarily utilised for imaging in the SEM. In contrast, BSEs are employed not only for imaging but also for providing atomic contrast and crystallographic orientation information.
As described by the Chung-Everhart distribution, SEs usually exhibit an asymmetric, bell-shaped energy distribution resulting from inelastic scattering events, in which electrons from the primary beam transfer kinetic energy to electrons in the specimen, enabling their escape from the sample surface.
In addition to this main peak, previous studies conducted in dedicated ultra-high vacuum system have revealed fine features superimposed on the main peak. These features vary with the specimen and may offer potential for distinguishing materials composition and revealing band structure.
However, such experiments have rarely been performed in the SEM due to concerns over contamination and the lack of suitable SE energy spectrometers. Besides analyzing the fine features, research has shown that tracking the peak position and intensity of the SE spectrum in the SEM can enable quantitative evaluation of dopant concentration and insulation layer thickness. Overall, there is considerable potential for using SEs in the SEM, including the possibility of simultaneously acquiring topographical image with nanometer resolution and corresponding energy spectrum. The primary obstacle to realizing this capability is the absence of suitable SE spectrometers designed for the SEM environment.
In this thesis work, novel designs for SE energy spectrometers are proposed to address the previously mentioned challenge. Given the limited space in the SEM chamber and the need to minimize working distance for nanometer resolution, a 40° sector band pass type of SE analyser concept was developed. As shown in Figure 1, the analyser was positioned below the pole-piece and capture the secondary electrons emitted from the sample surface, located approximately 1.5 mm beneath the analyser. The input angle is designed to be 40° with an angular spread of ± 10°. A single biasing plate is employed to deflect and focus the secondary electrons onto a detector positioned at the crossover point. The entire analyser can be mounted on a retractable arm, allowing it to be withdrawn when not in use. The design was simulated and optimised using COMSOL, which predicts the analyzer to have a best relative energy resolution of 1.61% at a pass energy transmittance of 7.52%. These predicted levels of energy resolution and detector transmittance are comparable to high performance commercial energy analyzers, such as the cylindrical mirror analyser (CMA) which is widely used in surface science instruments, and comparable to the detector transmittance of the SEM when operating in its standard image mode of operation.
Two types of detectors were evaluated for this analyser, one operating in analog mode based on a scintillator and a photomultiplier, and the other works in pulse counting mode using a Channeltron electron multiplier. Under comparable situations, the pulse-counting detector demonstrates a tenfold improvement in signal-to-noise ratio at low primary beam current (40 pA). This advantage comes its discrete nature of operation, which is much less affected by the shot noise inherent in the primary beam than the analogue detector.
Figure 2 shows the 3D design of the 40° sector analyser, which was constructed compactly with a length of 10 cm and a height of 1cm. The analyser was tested in a commercial SEM using various samples. The acquired spectrum generally fits with the Chung-Everhart distribution, although background noise was observed at the low-energy end— likely due to tertiary electrons generated by BSEs striking the inner walls of the spectrometer. Experiment results indicated that applying a slight bias to the sample could mitigate this issue by shifting the entire spectrum away from the noise peak at the lower end.
To further eliminate the background noise, an alternative design based on a toroidal analyser and projection lens was proposed (Figure 3). This angle-resolved toroidal SE spectrometer not only enables a reduced working distance but also effectively filters out unwanted tertiary electrons through multiple focusing and deflection stages. Secondary electrons entering the spectrometer horizontally are focused by an electrostatic lens, deflected by a toroidal section, and finally projected by another electrostatic lens onto a microchannel plate (MCP) detector. This configuration allows simultaneous acquisition of both SE energy spectrum and angular distribution information, thereby providing richer information for material research.
In summary, SE spectrometers with different concepts were investigated in this work, and these results offer new possibilities for conducting SE spectroscopy in commercial SEMs.

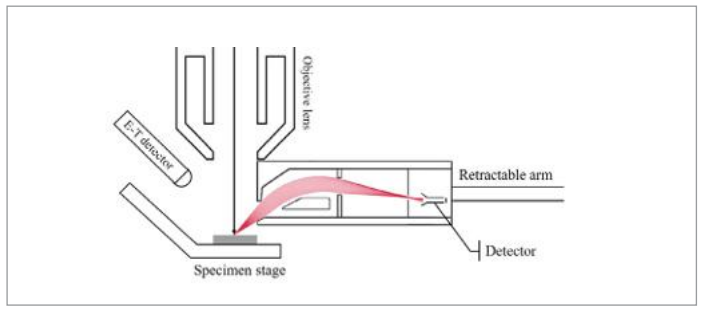

Fig.1 - Diagram of the 40° sector spectrometer inside a SEM

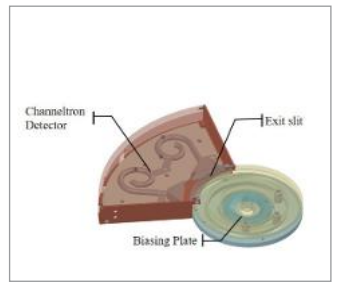

Fig.2 - 3D design of the 40° sector spectrometer

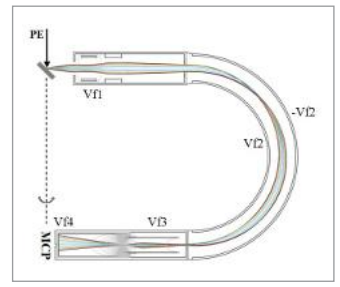

Fig.3 - Diagram of the angle-resolved toroidal spectrometer

ZERO-ORDER DIFFRACTION SUPPRESSION IN PHASE-ONLY HOLOGRAPHIC NEAR-EYE DISPLAYS

Alessandro Cerioni - Supervisor: Gianluca Valentini

Augmented Reality (AR) near-eye displays aim to seamlessly integrate digital information with the real world, but current solutions are still constrained by limited optical efficiency, bulky architectures, and visual artifacts. Among emerging technologies, holographic displays based on phase-only spatial light modulators (SLMs) represent a promising approach, as they enable physically accurate wavefront reconstruction and natural focus cues, addressing key limitations such as the vergence–accommodation conflict.

This doctoral research investigates computer-generated holography (CGH) as a viable pathway toward compact, high-performance AR eyewear, with a strong emphasis on real-world optical implementation. A critical challenge in phase-only holography is zero-order diffraction (ZOD), a dominant on-axis artifact arising from unmodulated light due to the finite fill factor of pixelated SLMs. This artifact significantly degrades image contrast and represents a major obstacle to the integration of holographic engines into wearable devices.

The main contribution of this work is the development and experimental validation of a camera-in-the-loop (CITL) interferometric technique for full-field ZOD suppression. The method operates directly at the hologram level by synthesizing a corrective optical field that destructively interferes with the residual zero-order component. Through a one-time calibration procedure, the amplitude and phase of the corrective field are retrieved with pixel-level precision, enabling near-complete suppression of the central artifact (up to approximately 99%) without reducing the field of view, compromising image fidelity, or introducing additional optical elements.

Unlike conventional approaches based on spatial filtering or off-axis encoding, which typically involve trade-offs in efficiency, compactness, or alignment complexity, the proposed solution achieves intrinsic suppression within the phase encoding process. This eliminates the need for bulky Fourier-plane filtering optics and allows the optical system downstream of the SLM to remain simple and compatible with waveguide-based architectures.

Experimental results demonstrate the robustness and generality of the method across a wide range of holographic scenarios, including point-cloud, planar, and multi-depth reconstructions. The correction preserves key image quality metrics, such as structural similarity and uniformity, while significantly improving contrast and removing central artifacts even under ambient illumination conditions representative of AR use cases. Furthermore, the retrieved corrective phase pattern is largely invariant with respect to the displayed hologram, enabling its reuse across different content with minimal adjustment.

Beyond the suppression of zero-order diffraction, this work provides a broader contribution to the field of holographic displays by addressing one of the fundamental limitations that has historically hindered their practical deployment. By embedding interference engineering into the CGH synthesis process, the proposed approach bridges the gap between laboratory demonstrations and scalable display technologies.

These results support the feasibility of compact, high-quality holographic engines for next-generation AR eyewear. Future developments will focus on extending the method to full-color time-multiplexed operation, integrating it into miniaturized optical architectures, and leveraging the same calibration framework for the correction of higher-order aberrations and system imperfections.

WIRELESS ENERGY TRANSMISSION BASED ON HIGH-POWER LASERS FOR SPACE APPLICATIONS

Giovanni Cichelli - Supervisor: Nicola Coluccelli

The progressive return to the Moon within the framework of international exploration programs has renewed interest in enabling technologies capable of supporting long-term surface operations. One of the most critical challenges concerns the delivery of electrical power to permanently shadowed regions, such as deep polar craters near the lunar South Pole, where sunlight is absent for extremely long periods. In this context, Laser Power Transmission (LPT) emerges as a compelling solution for wireless energy delivery, enabling continuous and targeted power supply to remote assets without the need for heavy cabling infrastructure. This doctoral research addresses the complete LPT chain, focusing on the optimization of photovoltaic array (PVA) architectures under monochromatic Gaussian illumination. Unlike conventional solar panels designed for broadband and quasi-uniform solar irradiance, LPT receivers operate under highly coherent, monochromatic, and spatially non-uniform beams. The Gaussian intensity profile of high-power lasers produces pronounced radial irradiance gradients, resulting in current mismatch among series-connected cells and localized thermal loading, thereby limiting the achievable optical-to-electrical conversion efficiency. To overcome these limitations, three innovative strategies were developed and numerically evaluated: the Ring-Shaped Design (RSD), the Tree-Shaped Design (TSD), and a Hybrid architecture combining the advantages of both (Figure 1).
The Ring-Shaped Design arranges cells along concentric paths, grouping regions with similar irradiance levels. This geometry mitigates mismatch losses by ensuring that each section operates under approximately uniform intensity.
The Tree-Shaped Design, instead, introduces radial segmentation into angular sectors, allowing a finer adaptation to the Gaussian intensity profile and reducing current imbalance across the panel.
Building upon these concepts, the Hybrid Design integrates radial and angular segmentation within a unified circular layout. The inner portion of the panel adopts a tree-based topology, while the outer sections implement a ring-like branching configuration to better accommodate the intensity decay toward the beam periphery. This dual strategy enables improved current balancing and enhanced Fill Factor under non-uniform illumination. Numerical simulations, incorporating detailed I-V and P-V modeling of temperature-dependent InGaAsP triple-junction cells, demonstrate that the Hybrid configuration achieves conversion efficiencies up to 39% at 20 kW input optical power. These performances are competitive with state-of-the-art space-qualified solar cells operating under ideal uniform illumination.
A crucial component of the study concerns long-term reliability in the harsh lunar environment. The PV receiver is exposed to displacement damage induced by high-energy protons and electrons, which degrade minority carrier lifetime and increase series and shunt resistances. The simulation framework incorporates experimentally derived remaining factors of the electrical parameters for radiation-induced degradation, enabling a comparative analysis between Beginning-of-Life (BoL) and End-of-Life (EoL) scenarios. Results indicate that The Ring-Shaped and Hybrid configurations maintain superior robustness, preserving conversion efficiencies up to approximately 27% at EoL under high radiation fluences. This resilience against radiation-induced shunting and mismatch confirms the suitability of the proposed architecture for multi-year lunar missions, including applications such as the European Large Logistic Lander (EL3) and surface-based in-situ resource utilization systems.
Beyond the receiver optimization, a parallel and independent line of research was devoted to the experimental demonstration of Soliton Self-Frequency Shift (SSFS). In particular, the generation of wavelength-tunable ultrafast pulses via SSFS in a nitrogen-filled Multipass Cell (MPC) was experimentally investigated. This approach addresses the need for wavelength-tunable, high-energy and high-power laser sources. Using 24-fs pulses from a Yb-based laser centered at 1030 nm, spectral shifting toward longer wavelengths was achieved by exploiting the rotational Raman response of molecular nitrogen (N_2). The MPC geometry enables multiple reflections within a gas-filled cavity, effectively increasing the nonlinear interaction length while avoiding the energy limitations and damage thresholds typical of hollow-core fibers. Dispersion was carefully managed through chirped mirrors providing controlled group-delay dispersion, allowing stable soliton formation and controlled spectral redshift (Figure 2).
The experimental results demonstrate efficient conversion to a shifted soliton peak at 1110 nm, with efficiencies reaching 35% and pulse energies up to 55 µJ. The system exhibited excellent beam stability and scalability, confirming gas-filled MPCs as a robust platform for high-energy ultrafast pulse generation for applications in High-Harmonic Generation and Nonlinear Microscopy.
In conclusion, this thesis numerically demonstrates the feasibility of laser-based wireless power transmission for lunar exploration. The proposed architectures achieve optical-to-electrical efficiencies up to 39% at BoL and remain highly competitive after substantial radiation exposure. These results confirm that LPT is a viable and efficient solution for enabling sustained operations in permanently shadowed lunar regions.

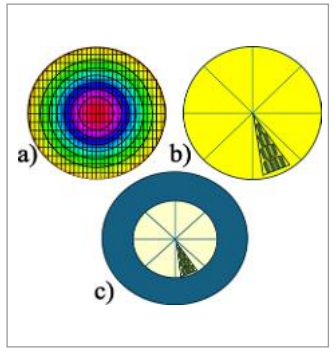

Fig.1 - a) Ring-Shaped Design; b) Tree-Shaped Design; c) Hybrid design

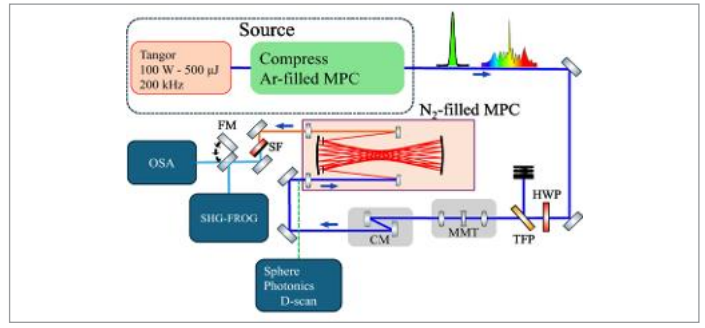

Fig.2 - Experimental setup SSFS. MPC: Multipass Cell; HWP: Half-Wave Plate; TFP: Thin-Film Polarizer; MMT: Mode-Matching Telescope; CM: Chirped Mirrors; SF: Spectral Filter; FM: Flip Mirror; SHG-FROG: Second-Harmonic Generation Frequency-Resolved Optical Gating; OSA: Optical Spectrum Analyzer

MEMS-RECONFIGURABLE SPINTRONIC AND MAGNONIC DEVICES

Maria Cocconcelli - Supervisor: Federico Maspero

The migration of wireless communication systems toward carrier frequencies above 6 GHz is redefining the fundamental limits of RF hardware. System performance is no longer dictated primarily by transistor switching speed, but by the ability to distribute, synchronize, and phase-align signals across increasingly large antenna arrays. In the upper microwave regime, beam steering and spatial multiplexing require precise, broadband, and continuously tunable control of phase and true time delay across many parallel channels.
At these frequencies, conventional semiconductor phase shifters and delay architectures face intrinsic scaling penalties. Conductor losses and parasitic reactances increase with frequency, phase linearity degrades, and wideband operation becomes progressively more difficult to maintain. True time-delay implementations are particularly constrained, since the achievable delay scales with physical path length or with the number of cascaded stages, directly increasing footprint, insertion loss, and complexity.
As array size and instantaneous bandwidth grow, these limitations accumulate, turning phase-control hardware into a dominant size, weight, and power (SWaP) bottleneck in next-generation RF front-end systems.
Magnonics provides an alternative wave-based platform for compact RF manipulation. Spin waves propagate in magnetically ordered materials as collective excitations of the magnetization and naturally operate in the microwave regime, with submicron wavelengths at gigahertz frequencies. Because spin-wave propagation does not involve net charge transport, Ohmic losses associated with electronic interconnects are fundamentally reduced. Moreover, phase accumulation is intrinsically encoded in propagation, enabling delay and phase-shifting functionalities without relying on long transmission lines or cascaded active components. This wavelength-based encoding offers a route to compact phase-control elements that do not scale directly with electrical path length.
A central technological barrier for practical magnonic systems is magnetic biasing. Most experimental demonstrations rely on bulky external electromagnets to define the operating point of the magnetic film, a solution incompatible with SWaP-constrained RF architectures. This work addresses that limitation through a fully integrated strategy combining permanent micromagnets for static on-chip bias generation with micro-electromechanical systems (MEMS) for dynamic reconfiguration.
As a first milestone, deterministic control of spin-wave propagation was demonstrated through the on-chip integration of SmCo permanent micromagnets with a CoFeB magnonic conduit. The micromagnets, symmetrically positioned with respect to the waveguide, generate a localized transverse stray magnetic field in the region between them. By adjusting the magnet–conduit separation, the local magnetic field in the waveguide can be tuned over several mT. Micro-focused Brillouin light scattering measurements show that this local field modulation shifts the dispersion relation of Damon–Eshbach spin waves, producing reversible changes in attenuation length and accumulated phase depending on the relative orientation of the stray and external fields. For small separations, decay length variations exceeding 50% and phase shifts of several radians are achieved. These results establish permanent micromagnets as passive, zero-static-power elements capable of locally engineering spin-wave transport.
Building on this concept, a fully standalone silicon-integrated magnonic device was realized that operates without any external magnetic field. Permanent SmCo micromagnets combined with soft magnetic flux concentrators generate transverse bias fields up to 20.5 mT directly on chip. The device integrates coplanar waveguide antennas for all-electrical excitation and detection within a compact footprint of approximately 100 × 150 μm^2. Zero-field spin-wave propagation is demonstrated up to 8 GHz. By tailoring magnet geometry and spacing, the device functions as a passive phase shifter with phase variations exceeding 120° at 6 GHz and as a time-delay element reaching delays up to 180 ps. The resulting delay density highlights the intrinsic compactness of magnonic phase encoding compared with conventional transmission-line approaches.
Voltage-controlled reconfigurability is subsequently introduced through MEMS actuation. A soft magnetic element mounted on a piezoelectric cantilever is flip-chip bonded above the magnonic waveguide. Application of a low actuation voltage induces mechanical deflection, modifying the vertical separation between the micromagnet and the conduit and therefore the local stray field experienced by propagating spin waves. This mechanism enables localized and reversible tuning of spin-wave propagation. By mechanically adjusting the micromagnet position, the accumulated phase can be continuously varied and the spin-wave excitation band shifted within the 6-12 GHz range.
Together, these results establish on-chip magnetic biasing, compact standalone operation, and low-power electrical reconfigurability within a single platform. The integration of permanent micromagnets and MEMS control enables compact, tunable magnonic phase shifters and time-delay units operating above 6 GHz, directly addressing phase-control bottlenecks in advanced RF front-end architectures.

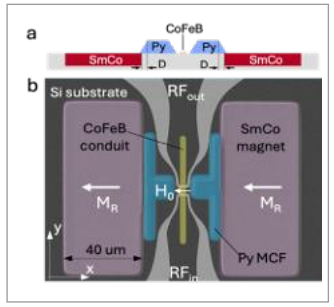

Fig.1 - Standalone silicon-integrated magnonic device enabling zero-field spin-wave propagation: (a) cross-sectional schematic; (b) scanning electron microscope image with false colors

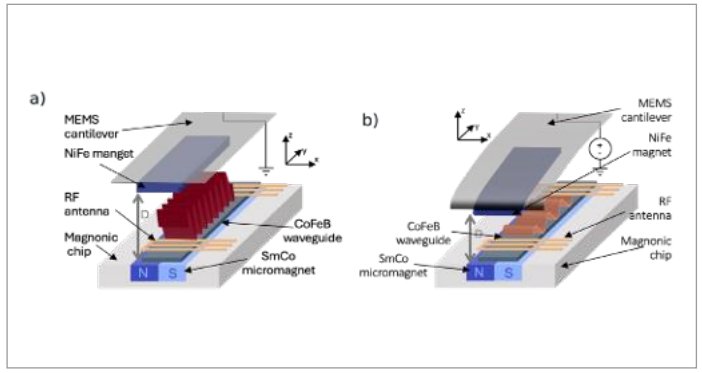

Fig.2 - MEMS-actuated magnonic device: (a) zero actuation voltage; (b) applied voltage with cantilever deflection and modified magnetic bias

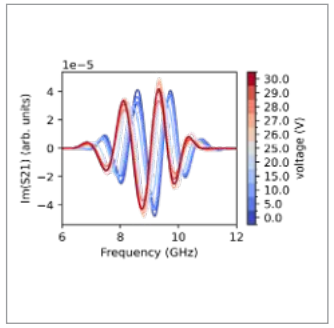

Fig.3 - Voltage-controlled broadband signal modulation in the 7–11 GHz range enabled by MEMS displacement of an integrated micromagnet

ADVANCING NEAR-INFRARED SPECTROSCOPY FOR MEASURING HUMAN HEMODYNAMICS ACROSS DOMAINS

Letizia Contini - Supervisor: Rebecca Re

Introduction

Human hemodynamics emerges from the continuous interaction between local metabolic demands and systemic regulatory mechanisms and represents a fundamental marker of tissue health and function. Vascular regulation ensures that oxygen delivery and extraction dynamically adapt to physiological needs, supporting both basal metabolism and task-related activity. For this reason, the study of hemodynamic processes is central in several research fields, from physiology and sports science to neuroscience and clinical research. However, investigating hemodynamics in vivo remains challenging as most conventional techniques are invasive, costly, or poorly suited for repeated, long-term measurements. Within this context, diffuse optical spectroscopy has emerged as a powerful class of non-invasive methods for probing tissue oxygenation and microvascular dynamics. By exploiting the interaction of near-infrared light with biological tissues, Near-Infrared Spectroscopy (NIRS) provides access to hemoglobin concentration and oxygenation changes several centimeters below the skin surface. Among NIRS approaches, Time-Domain Near-Infrared Spectroscopy (TD-NIRS) offers unique advantages. TD-NIRS is based on the injection of picosecond laser pulses into tissue and the detection of re-emerging photons using single-photon detectors and fast timing electronics. By measuring the time-of-flight of photons, TD-NIRS enables quantitative and depth-resolved estimation of optical and hemodynamic properties of the probed medium, allowing the separation of different tissue layers contributions.

This PhD research investigated how TD-NIRS can be exploited to characterize hemodynamic dynamics across different tissues and experimental paradigms.

The work combined numerical simulations, instrumental development, and in vivo measurements to advance both the methodological foundations and applications of TD-NIRS. In parallel, complementary applications of Continuous-Wave NIRS (CW-NIRS) were explored in developmental and social neuroscience contexts.

Hemodynamics in the cerebral cortex

A first major contribution of this thesis concerns the characterization of spontaneous cerebral hemodynamic oscillations and their interaction with systemic physiological rhythms. Even at rest, the cerebral microvasculature exhibits structured oscillatory activity arising from endothelial, neurogenic, myogenic, respiratory, and cardiac control mechanisms. These oscillations reflect the ongoing regulation of cerebral blood flow and oxygenation and can be used as relevant markers of vascular health and brain-body interactions. By exploiting the high temporal resolution and intrinsic depth sensitivity of TD-NIRS, this work demonstrated that such oscillatory components can be resolved non-invasively in the human brain. Numerical simulations showed that TD-NIRS enables depth-resolved sensitivity to cerebral and extracerebral compartments, while experimental measurements confirmed the detectability of multiple oscillatory components in in vivo data. Importantly, the results showed that TD-NIRS can be used to study the coupling between cerebral hemodynamics and systemic rhythms, providing a window into brain-body physiological interactions during both resting-state conditions and induced perturbations.

Then, this work addressed a key methodological limitation of depth-resolved TD-NIRS analyses: the reliance on assumed geometrical models of the probed tissue. Using a bilayer model to describe cerebral and extracerebral compartments, simulations revealed that inaccuracies in the assumed superficial layer thickness can significantly distort the frequency-domain features of reconstructed hemodynamic signals. Such errors lead to spectral distortions and inter-layer signal leakage, complicating data interpretation. Building on this, a novel data-driven framework was proposed to estimate effective tissue model parameters directly from TD-NIRS data, exploiting task-induced periodic perturbations within the cerebral compartment. Preliminary validation on in vivo datasets demonstrated the feasibility of this approach and its potential to reduce dependence on external anatomical measurements.

Hemodynamics in the skeletal muscle

The thesis further extended oscillatory hemodynamic analysis to applications of TD-NIRS in human skeletal muscle. Like the brain, skeletal muscle exhibits spontaneous hemodynamic oscillations at rest, reflecting the interplay between local microvascular regulation, autonomic inputs, and systemic rhythms. In addition, muscle hemodynamics undergo adaptations during exercise, as blood flow and oxygen delivery increase to meet elevated metabolic demand.

While CW-NIRS has been widely used to monitor relative changes in muscle oxygenation during exercise and recovery, the systematic study of oscillatory dynamics within the muscle microcirculation has remained largely unexplored, particularly using TD-NIRS. This work addressed this gap by investigating both basal oscillatory activity and task-induced adaptations during sustained isometric exercise. By comparing participant groups differing in age and training habits, the analysis revealed meaningful differences in oscillatory power distribution across physiological frequency bands. During exercise, systematic redistributions of oscillatory power were observed, reflecting the dynamic engagement of different vascular control mechanisms in response to increased metabolic demand. This demonstrates that TD-NIRS can capture not only average oxygenation changes, but also frequency-specific signatures of microvascular regulation. As such, oscillatory metrics derived from TD-NIRS show promise as non-invasive indicators of muscle vascular function and health, with potential applications in sports science, rehabilitation, and clinical physiology.

Functional and social hemodynamics

During a secondment period abroad, the research expanded to novel applications of CW-NIRS in developmental and social neuroscience. In these contexts, traditional analysis approaches often struggle due to atypical, delayed, or overlapping hemodynamic responses, particularly in infant and child populations or in naturalistic experimental designs.

A first contribution introduced a data-driven method for modelling task-evoked hemodynamic responses without imposing a fixed canonical response shape. This approach addresses a longstanding methodological limitations in the NIRS literature: while general linear model (GLM) methods can handle fast-paced designs, they often perform poorly when assumptions about canonical hemodynamic responses are violated, whereas block-averaging methods are model-free, but can be used limitedly to slow, strictly structured tasks. The proposed framework combines the strengths of both approaches, enabling flexible modelling of atypical and overlapping responses commonly observed in developmental settings.

A second contribution investigated the reliability of NIRS-based hyperscanning for studying inter-brain synchrony during social interaction. By adopting analysis strategies designed to disentangle genuine inter-brain coupling from shared physiological, task-related, and environmental confounds, this work demonstrated that CW-NIRS can provide meaningful measures of neural synchrony when appropriate controls are applied. These results support the use of NIRS in social neuroscience while highlighting the importance of rigorous methodological design.

Conclusions

Overall, this thesis advances diffuse optical spectroscopy by demonstrating novel applications of TD-NIRS across tissues and research domains, introducing data-driven methodological solutions to improve depth-resolved analysis, and highlighting the flexibility required to extend NIRS techniques to complex physiological and developmental settings. By integrating simulations, instrument development, and in vivo studies, the work contributes to a more robust and interpretable use of NIRS for probing human hemodynamics.

TIME- AND MOMENTUM-RESOLVED SPECTROSCOPY OF 2D SEMICONDUCTORS IN STRONG COUPLING REGIME

Cristina Cruciano - Supervisor: Stefano Dal Conte

Light-matter interactions underpin a wide range of linear and nonlinear phenomena, such as absorption, scattering, harmonic generation and optical parametric amplification. For decades, enhancing these interactions has been one of the main goals of many research groups, driven, on one hand, by the opportunity to explore new physical regimes and, on the other, by the need to advance technologies.

In this context, optical nanophotonic resonators, like microcavities and metasurfaces, provide a perfect platform for this interaction enhancement, enabling access to new regimes, including the so-called strong coupling regime. In this regime, energy exchange between light and matter occurs faster than their respective decay rates, leading to the formation of new quasi-particles, known as polaritons. These hybrid light-matter states exhibit novel properties and open new avenues for technological applications, including the field of quantum information science.

Over the past two decades, two dimensional (2D) materials and, in particular, single-layer transition metal dichalcogenides (TMDs) have revolutionized the way light-matter interactions are realized. Their unique combination of atomic-scale thickness, indirect-to-direct bandgap transition and spin-valley selectivity have attracted significant attention for both fundamental studies and applications. Owing to their strong bound excitons which remain stable up to room-temperature, their ability to be exfoliated into homo- and hetero structure and their spin-valley selectivity, TMDs have rapidly become the focus of a large number of studies.

In this thesis, we explore different approaches to achieve and control the strong light-matter coupling regime in TMD-based microcavities and metasurfaces. By means of momentum-resolved (k-space) and ultrafast optical spectroscopic techniques we are able to investigate both static and dynamic behaviour of these structures.

In particular, by exploiting the nonlinear nature of excitons in bilayer (BL) MoS_2 and by integrating them into a microcavity, we enhance the nonlinearity of the resulting polaritons. This approach enables us to demonstrate the ultrafast sub-ps reversible switching of the strong coupling regime using extremely low pulse energies, of the order of few pJ (see Figure 1). In addition to previous experiments, by leveraging on the large oscillator strength and binding energy of a monolayer (ML) WS_2 we demonstrate Rabi oscillations at room temperature in a microcavity. By tuning the measurements parameters, such as pump fluence and angle of incidence, we are able to control the period of these oscillations.

We also show that exploiting the natural anisotropy of ReS_2, the topological features of a C4-symmetry metasurface can be modified to support polaritonic flatbands (Fig. 2(a)) accessible with linearly polarized light.

We further enhance light-matter interactions by integrating a monolayer WS_2 into a polarization-independent radial quasi bound state in the continuum (qBIC) structure with an enhanced Q-factor. Moreover, we observe the presence of OAM modes in the photoluminescence (PL) signal suggesting a transfer of such eigenstates to the qBIC-exciton-coupled emission (Fig. 2(b)).

Lastly, we analyse the anisotropic angular dispersion of a WS_2 metasurface in connection with the exciton-polariton dynamics of the structure. Specifically, we studied how the coupling and the detuning between excitons and qBIC can strongly alter the coherent and incoherent relaxation dynamics of polaritons (Fig. 3(a)). Finally, we demonstrated coherent oscillations between lower polariton and exciton states in this system, suggesting a non-trivial coherent coupling between bright and dark excitons through the qBIC photonic mode (Figs. 3(b-c)).

Our work provides a comprehensive perspective on strong-light matter interactions, highlighting their versatility and potential across different nanophotonic platforms.

By demonstrating multiple approaches to achieve and control the strong coupling regime, it paves the way for further exploration of novel physical phenomena and the development of advanced functionalities. In particular, these results open new opportunities for both fundamental studies and the realization of next-generations quantum and photonic technologies.

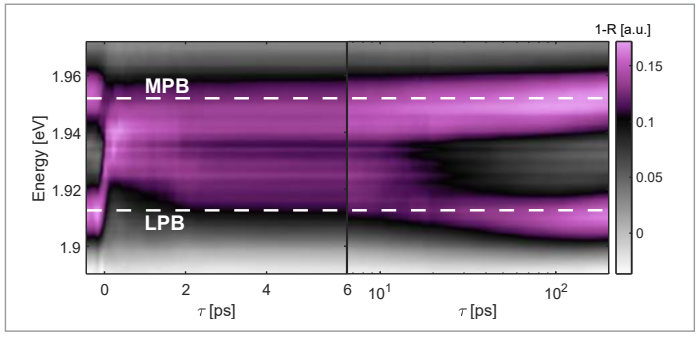

Fig.1 - Non-equilibrium optical response of BL MoS2 measured as a function of energy and delay time showing the switching of the lower and middle polariton branches (LPB and MPB, respectively) from the strong (at negative delays) to the weak coupling regime (first 2 ps). The strong coupling regime is restored for longer time delays

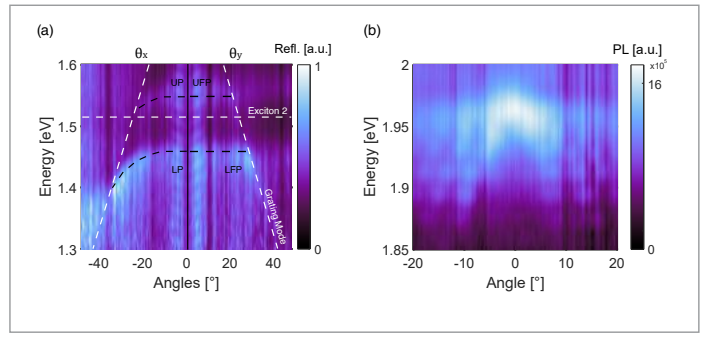

Fig.2 - (a) k-space measurements on the ReS2 metasurface. The left part displays the cut along θ_x where the polaritonic branches are visible (UP, LP); the right part displays the cut along θ_y where the flat polaritonic branches are visible (UFP, LFP). (b) Cross-section of the PL k-space hypercube taken along ky showing a periodically modulated multi-parabolic dispersion for the TM mode

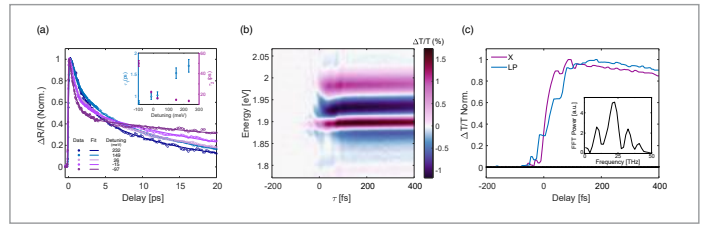

Fig.3 - (a) Lower polariton temporal traces (dots) fitted with a multi-exponential model (solid line). The inset shows the values for τ1 and τ2 extracted from the fit. (b) Pump-probe map of the WS_2 metasurface. (c) Normalized temporal traces extracted at LP and X energies. The inset shows the FFT performed on the oscillatory component of LP traces

DEFECT CHARACTERIZATION OF GE-ON-SI AND SIGE HETEROSTRUCTURES FOR ADVANCED OPTOELECTRONIC AND SPIN-QUBIT APPLICATIONS

Afonso de Cerdeira Oliveira - Supervisor: Giovanni Isella

A wide range of advanced microelectronic and photonic applications, including infrared photodetectors, spintronic devices, and monolithic optoelectronic integration on CMOS-compatible substrates, require high-quality material platforms compatible with silicon technology. In this context, epitaxially grown germanium-on-silicon (Ge-on-Si) has emerged as a cost-effective and technologically scalable solution, while providing superior electronic and optical properties of germanium and extending the optical functionality into the infrared spectral range. However, the large lattice mismatch between Ge and Si (approximately 4.2%) introduces significant strain during the epitaxial growth, which is partially relieved through the formation of dislocations. These defects may propagate through the epilayer as threading dislocations, where they could act as non-radiative recombination centers, and ultimately deteriorating device performances.
The first part of this work focuses on the epitaxial growth and defect density reduction of Ge layers on silicon substrates. Ge layers were deposited by low-energy plasma-enhanced chemical vapor deposition (LEPECVD) and subsequently subjected to thermal cycling annealing (TCA) employing different maximum annealing temperatures and number of cycles. These post-growth processes were intended to promote threading dislocation interactions and their annihilation. By optimizing both epitaxial growth parameters and the thermal annealing process, the threading dislocation density was reduced from $2.2 \times 10{-}9cm{-}2$in as-grown layers to values below $1.0{\times}10{-}7cm{-}2$ for 1500 nm-thick Ge-on-Si layers. Importantly, the annealing protocols employed yielded layers with thicknesses, crystalline quality and surface roughness suitable for subsequent device fabrication.
The epitaxial growth and post-annealing treatments were supported by an extensive structural, morphological and optoelectronic characterization through high-resolution X-ray diffraction, atomic force microscopy, high-resolution scanning transmission electron microscopy (Fig. 1), defect etching processes and photoluminescence measurements (Fig. 2). The extensive characterization of defect evolution under high-temperature processing enabled a detailed analysis of the interplay between detrimental effects such as silicon diffusion and surface roughness, and the threading dislocation density and defect-type transitions. This analysis clarified the trade-offs governing the overall process and offered a better comprehension of Ge layers optimization for different application requirements.
In the second part of the work, defect-engineering strategies were systematically optimized for Ge-on-Si layers and SiGe heterostructures, with the objective of enabling and supporting a range of emerging application domains. These activities included the deposition and thermal treatment of Ge-on-Si layers and SiGe graded buffers for integration of III-V materials within Si technology through the direct epitaxial growth of gallium antimonide with reduced density of antiphase boundaries, targeting the realization of III-V laser sources monolithically integrated into Ge-based mid-infrared photonic integrated circuits. In parallel, low-defect-density Ge epitaxial layers selectively grown within Si and SiO_2 trench architectures were investigated as an alternative to confine threading dislocations at the trenches interface, with the objective to achieve a material platform for future single-photon avalanche diode devices. Finally, SiGe graded buffer heterostructures complemented with constant composition layers for complete film relaxation were developed to suppress defect propagation and impurity incorporation in Ge quantum wells structures to exploit hole spin qubit applications, enabling enhanced confinement of a two-dimensional hole gas. In this context, hole mobility of 608000 cm2V-1s-1, demonstrating transport properties competing with the current state-of-art performances.
Closing the cycle from the investigation of fundamental defect properties in germanium to the exploitation in functional devices, a Ge-on-Si bias-tunable dual-band photodetector was exploited to achieve discrimination between transparent solvents.
The device is based on monolithic integrated layers of silicon and germanium incorporating p-i-n junctions in a back-to-back architecture, enabling a bias-controlled responsivity (Fig. 3). By varying the polarity and magnitude of the applied external bias, the relative contribution of the individual photodiodes can be selectively tuned. The net photocurrent is determined by the difference between the photocurrents generated in each junction, having an open-circuit voltage condition dependent on a ratio proportional to the individual photocurrents of each junction.
The introduction of transparent solvents between the light source and the detector modifies the optical power impinging on the dual-band detector, leading to a shift in the external bias at which the open-circuit occurs, enabling discrimination between different solvents through small voltage variations, with measurable shifts as low as 3 mV.
Such cost-effective devices operate at pixel level, and under uniform illumination conditions and benefit from the extended spectral sensitivity provided by the integrated germanium photodiode. Moreover, the acquisition of information in the form of a ratio between spectral regions enables novel sensing approaches.
In this context, defect engineering plays a critical role in enabling device functionality by minimizing dark current and noise, which are essential for achieving high sensitivity and reliable discrimination. A detailed understanding of control of defect-related recombination mechanisms in Ge-on-Si heterostructures therefore provides a pathway toward the fabrication of advanced photonic devices and the development of new sensing concepts.

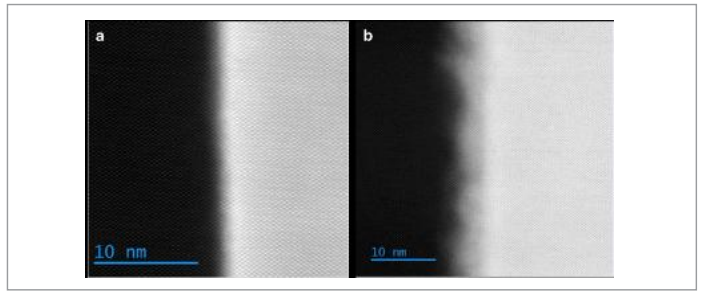

Fig.1 - Cross-sectional STEM-HAADF (Z-contrast) images of Ge-on-Si layers (a) in the as-grown condition and (b) after thermal cycling annealing treatment. The post-annealed sample exhibits an approximately 10 nm-thick interfacial region, in which a $Si_{1-x}Ge_x$ alloy has formed between the silicon substrate and the germanium layer, consistent with silicon interdiffusion during high-temperature processing.

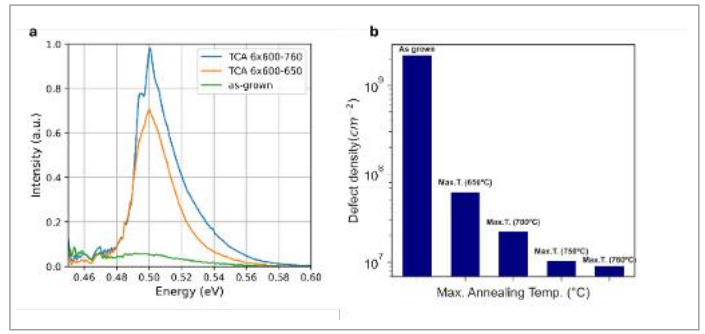

Fig.2 - Effect of thermal cycling annealing at different maximum temperatures on defect-related properties in Ge-on-Si layers: (a) Photoluminescence spectra of Ge-on-Si layers highlighting radiative recombination associated with defect-related energy levels (b) threading dislocation density determined after selective etching of defective regions and subsequent etch-pit counting by scanning electron microscopy

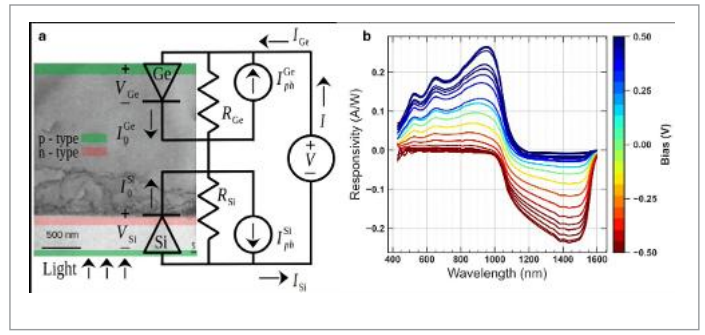

Fig.3 - (a) Ge-on-Si dual-band detector equivalent circuit superposed to a TEM cross-section image. The doping profile is schematically represented by green (p-type) and red (n-type) shaded area (b) Bias-dependent responsivity of the Ge-on-Si dual-band detector. Positive and negative values of the responsivity are associated with photocurrent flowing in opposite directions in the dual-band device

BRIDGING INSTRUMENTATION AND DATA FUSION IN MULTIMODAL HYPERSPECTRAL IMAGING FOR CULTURAL HERITAGE ANALYSIS

Alessia Di Benedetto - Supervisor: Daniela Comelli

Hyperspectral imaging (HSI) has become a key analytical tool for the non-invasive investigation of delicate materials, particularly in the field of Cultural Heritage (CH). HSI provides a spectrum at each spatial pixel and, depending on acquisition and excitation conditions, it can probe different physical phenomena to enable the identification of materials over extended surfaces.
However, considering the specific field of CH, artworks are intrinsically complex samples, often characterized by heterogeneous material composition due to the multiple chemical species present, as pigments, binders, varnishes and degradation compounds.
Within this context, the analysis of a single modality is often insufficient to achieve a comprehensive understanding of the object. The present work addresses this limitation through the development of innovative strategies for multimodal HSI, which exploits the combination of complementary imaging techniques, with the aim of achieving a comprehensive understanding of the sample.
Therefore, the objective of this thesis is the integration of multimodality in both hybrid HSI setups and dedicated data fusion strategies.

A first major contribution concerns the design and development of two innovative hybrid multimodal setups. Specifically, the design of hybrid systems is fundamental to guarantee the spatial co-registration between modalities, ensuring pixel-by-pixel correspondence and simplifying subsequent data analysis.
The first system is a Raman-Photoluminescence (PL) raster-scanning microscope developed for the mapping of micro-samples. The system integrates multiple excitation paths and a shared collection path within a single optical system, enabling sequential acquisition of Raman and PL maps. The complementarity between Raman, highly specific for molecular identification, and PL spectroscopies, particularly sensitive to luminescent compounds, enables a more comprehensive characterization of complex stratigraphies and pigment powders.
The second setup is a multimodal and multiscale camera based on the TWINS interferometric hyperspectral camera. The system enables the sequential acquisition of reflectance and PL data simply by switching the illumination source, while maintaining the camera fixed. The system operates in both large field of view (FOV), allowing for the analysis of large areas on the order of tens of centimetres, and in macro configurations, imaging details of about one centimetre in FOV. This setup exploits the complementarity between reflectance, which is sensitive to surface and colour variations, and PL, sensitive to luminescent compounds and chemical changes, as degradation.
Each dataset, originating from these setups, is structured as a 3D datacube, where the first two dimensions correspond to the spatial coordinates, while the third one contains hundreds of spectral bands. This intrinsic high dimensionality requires advanced multivariate techniques to extract meaningful information. Therefore, in this thesis, several multivariate algorithms were investigated, as Non-negative Matrix Factorization (NMF) and Uniform Manifold Approximation and Projection (UMAP), to assess the pros and cons of each approach depending on the probed physical phenomena.
Beyond the exploitation of multimodality in the collection process, this work strongly focuses on multimodality in the analysis process through the design of innovative spectral data fusion strategies. Indeed, rather than investigating each HSI dataset independently, this research proposes a unified approach in which the datasets are combined prior to the analysis, enabling the extraction of more robust and physically meaningful components.
Specifically, the data are stacked along the spectral dimension into a single dataset, following a block-scaling step where each modality is scaled to achieve balanced contribution from different spectral shapes and dimensionality.
The effectiveness of this approach is demonstrated in real case studies. Specifically, the fusion of reflectance and transmittance modes, combined with NMF analysis, enabled the recovery of concealed text in glued ancient manuscript pages (Fig. 1). Similarly, fused reflectance and PL datasets, analysed through UMAP, improved the discrimination of degradation levels in artificially photoaged polymer samples.
Finally, a key component of this work is the development of MUSA (Multimodal fUsion framework for Spectral imaging Analysis), an innovative napari-based software integrating visualization, dimensionality reduction, spectral unmixing and data fusion within a user-friendly interface (Fig. 2). MUSA is specifically designed to handle multiple co-registered HSI datacubes simultaneously, facilitating multimodal workflows and ensuring reproducibility of the analysis.
Overall, this research establishes a comprehensive multimodal framework that combines setup innovation and advanced multivariate data fusion.
By ensuring the intrinsic co-registration at the acquisition stage, exploited with the design of hybrid setups, and integrating complementary spectral information at the analysis stage, the proposed approach significantly enhances material discrimination in complex cultural heritage samples.

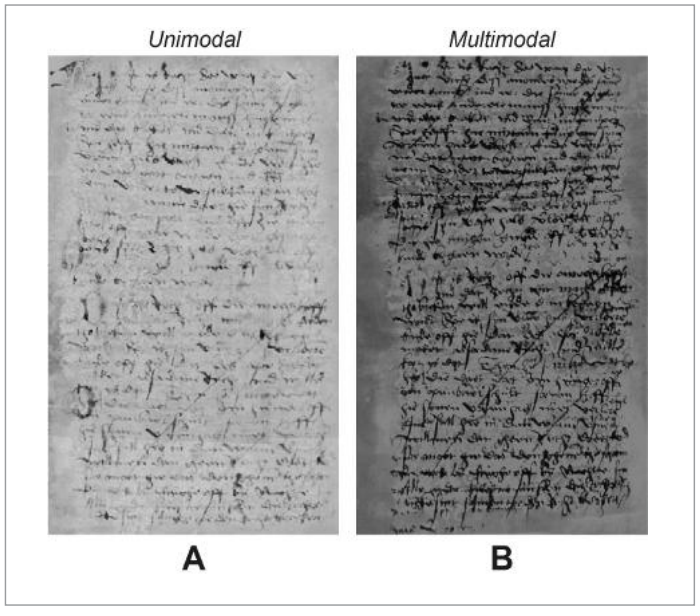

Fig.1 - Comparison between unimodal and multimodal approaches for the retrieval of hidden text beneath glued manuscript pages. (A) Unimodal NMF analysis applied to the transmittance dataset acquired from the back side of the page. (B) Multimodal analysis combining reflectance and transmittance datasets acquired from the back side of the page, resulting in an improved contrast and enhanced readability of the concealed text

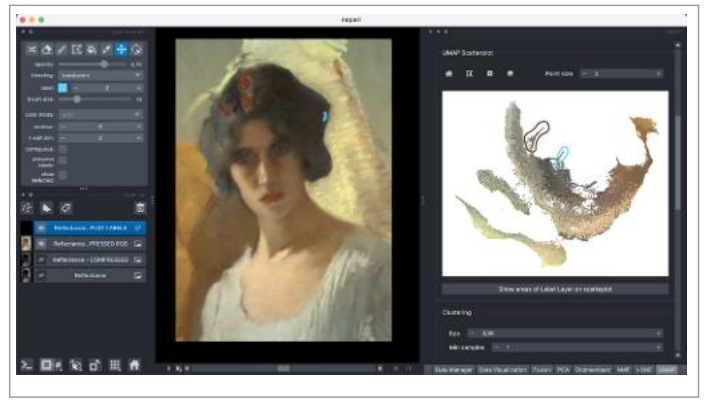

Fig.2 - MUSA software for HSI analysis implemented as a napari plugin. The interface shows a reflectance dataset of a painting loaded in the viewer, with the corresponding UMAP embedding displayed in the analysis panel (right). Two clusters selected in the scatterplot are highlighted in the RGB image.

SCALABLE CHARACTERIZATION TECHNIQUES FOR INTEGRATED PHOTONIC DEVICES IN A FEMTOSECOND LASER WRITTEN PLATFORM

Niki Di Giano - Supervisor: Francesco Ceccarelli

Linear optical networks constitute a core technology for both classical and quantum photonics, enabling applications that range from optical signal processing and analog optical computing to quantum interferometry, communication, and computation. Universal Photonic Processors (UPPs) are integrated optical devices that provide a scalable hardware platform for such applications by implementing arbitrary unitary transformations through meshes of reconfigurable 2-by-2 unit cells (Fig. 1). «Calibration» in this sense means obtaining an accurate model representing the relationship between the control variables of the reconfigurable cells and the implemented unitary transformation.

Femtosecond Laser Waveguide Writing (FLWW) in glass is a fabrication platform that offers several advantages such as rapid prototyping, three-dimensional optical structure writing, and substrate machining at the micro-scale. This platform, together with photolithography-based methods to fabricate resistive heaters on top of the glass substrate, enables the creation of highly performant UPPs. However, the behavior of FLWW UPPs is affected by fabrication imperfections and, critically, by thermal cross-talk between the densely packed resistive heaters, which complicates modeling and calibration. All these factors contribute to making high fidelities more difficult to achieve.

This work presents a comprehensive experimental study of calibration and operation strategies for FLWW UPPs, with a focus on scalability, automation, and high-fidelity performance. Fully automated calibration pipelines are developed, reducing the total calibration time from multiple l days to a few hours, while enabling completely automated and scalable optimization algorithms. On a 6-mode processor, the proposed approach achieves an average amplitude fidelity of 0.9979 ± 0.0009. Leveraging the speed of the automated calibration, a single-matrix optimization method based on current fine-tuning is demonstrated, increasing the mean amplitude fidelity for selected target matrices up to 0.9996 on average, highlighting fine-tuning as a viable strategy to push past the limits of the calibration in FLWW UPPs for a variety of applications.

The robustness of the calibrated devices is further investigated with respect to polarization effects. Despite waveguide birefringence that is intrinsic to the fabrication platform, the experiments show that the polarization state of the input light alters the average fidelity of the UPP only by a negligible amount even when confronting opposite polarization states, without the need to recalibrate the device.

Scalability is addressed through the extension of the calibration setup to larger meshes and through the introduction of machine-learning-based «digital twin» models trained on large matrix datasets. The proposed setups are capable of both gathering the data and applying the algorithms autonomously. Using these methods and setups, a 6-mode processor achieves an average amplitude fidelity of 0.9978 ± 0.0008, an 8-mode processor achieves an average amplitude fidelity of 0.9948 ± 0.002, while a 12-mode device achieves 0.9907±0.0063, with single matrix acquisition times below 10 seconds (Fig. 2).

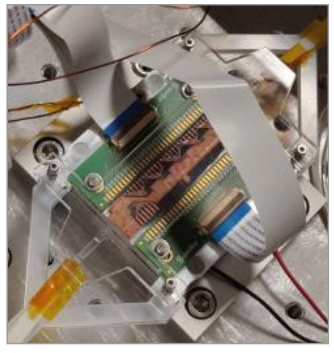

Fig.1 -A picture of a UPP fabricated with FLWW. This UPP is a 6-mode device with a Bell structure, featuring input and output fiber arrays and a Peltier cell to control the temperature. Two ribbon cables connect the custom PCBs to the resistors fabricated on the glass, enabling control over the currents flowing in the resistors.

From the point of view of mitigating side-effects in UPPs, thermal cross-talk is investigated in detail through vacuum-enhanced device operation. By operating the UPP at medium vacuum conditions (3×10^{-2} mbar), heat transfer is reduced, leading to a marked increase in thermal isolation between adjacent heaters. Quantitative cross-talk metrics show an improvement of an order of magnitude when transitioning from air to vacuum. While vacuum conditions modify the thermal dynamics of the system, introducing longer thermalization times for individual heaters, simulations show that the effective global reconfiguration time (Time-To-Matrix, TTM) remains comparable. These results highlight vacuum operation as a viable pathway to suppressing thermal cross-talk in large-scale FLWW UPPs without fundamentally compromising reconfiguration speed.

Beyond amplitude-only characterization, an interferometric phase retrieval technique based on a dedicated interface chip is introduced, enabling access to physically meaningful phase information and full fidelity evaluation. This approach allows the measurement of complex matrix elements, constituting one of the first demonstrations of full (amplitude and phase) matrix and fidelity measurements in a FLWW UPP with a Clements-type architecture. Using the proposed calibration methods and measurement technique for the UPP, fidelities between 0.9935 and 0.9993 are measured for selected matrices, fully accounting for the complex nature of the unitaries.

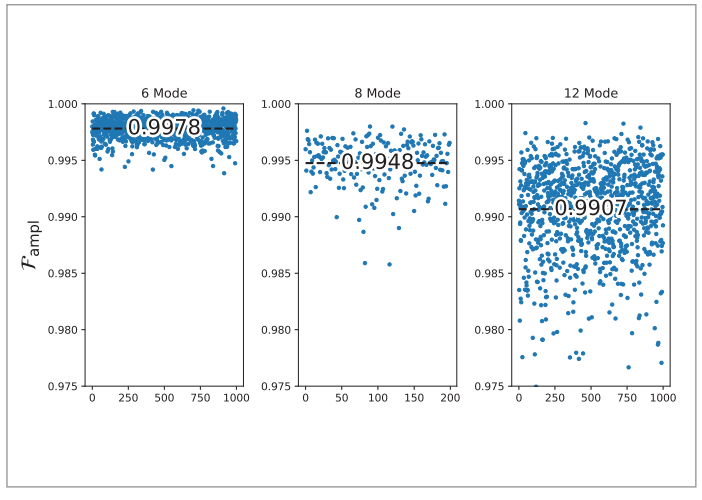

Fig.2 - a comparison between the fidelitites obtained by using this method on UPPs of different sizes (6, 8 and 12 modes)

Finally, a complementary investigation of a novel methodology for the characterization of multimode waveguides is presented. By acquiring large datasets of output intensity patterns under varying excitation conditions and applying Principal Component Analysis (PCA), the number of modes supported by the structure is inferred from the dominant principal components. Experimental results on two different fibers (1550BHP and 780HP) at five different wavelengths ranging from 405 nm to 925 nm are carried out, demonstrating qualitative discrimination of multimodal behavior which is consistent with theoretical expectations. This approach establishes a low-cost, data-driven framework for multimode waveguide characterization and provides a foundation for future extensions toward quantitative mode analysis.

Overall, this work demonstrates a scalable and experimentally validated toolbox for the calibration and high-fidelity operation of FLWW integrated devices, providing a solid foundation for their deployment in advanced classical and quantum photonic applications.

MID-INFRARED UNIPOLAR PHOTONIC DEVICES BASED ON P-DOPED GE/SIGE QUANTUM WELLS

Marco Faverzani - Supervisor: Jacopo Frigerio

Significant research interest has recently focused on the mid-infrared (MIR) spectral range, specifically the "fingerprint region" which contains the fundamental roto-vibrational modes of most molecules. Photonic devices operating within this window thus allow for the precise detection, identification, and quantification of chemical species, enabling applications in healthcare, security, and environmental monitoring. This research addresses the growing demand for efficient, integrable, and scalable MIR technologies by establishing a group-IV material platform which exploits intersubband (ISB) transitions in p-doped Ge-rich SiGe quantum wells (QWs). The work focuses on three main objectives: the fundamental investigation of ISB transitions in square and parabolic SiGe QWs, the demonstration of a waveguide-integrated quantum well infrared photodetector (QWIP), and the preliminary assessment of the strong light-matter coupling regime in group-IV heterostructures.

First, the fundamental investigation of SiGe multiple QWs is presented, focusing on the growth and characterization of square and parabolic QWs. Both heterostructures were designed to achieve MIR ISB transitions and grown by low-energy plasma-enhanced chemical vapour deposition (LEPECVD). Their crystalline quality and compositional profile were assessed by X-ray diffraction measurements, atom probe tomography and scanning transmission electron microscopy. Dichroic transmission spectroscopy was used to determine the ISB absorption spectra (Figure 1a). At a sheet hole density of 5×10^{11} cm^{-2} and low temperature, a dominant absorption feature is found in square QWs at 8.5 µm. However, as soon as temperature or doping are increased, a second peak appears at longer wavelengths along with a higher-energy shoulder. In parabolic QWs, instead, a single absorption line is present up to carrier densities exceeding 10^{12} cm^{-2}, which does not shift with doping and temperature (Figure 1b). At larger doping levels, band non-parabolicity becomes dominant and the absorption spectra get more structured. In both cases, theoretical absorption spectra calculated with an advanced tight-binding model provided an excellent agreement.

The design and realization of a waveguide-integrated QWIP featuring square SiGe QWs is then discussed. Room-temperature electro-optical characterization revealed a polarization-dependent response featuring three peaks between 7 and 10 µm, consistent with ISB absorption spectra. Although the measured responsivity remains moderate compared to III-V QWIPs, these proof-of-concept results represent a crucial milestone toward efficient fully-integrated MIR photodetection. A second-generation miniaturized device is currently under development, aimed at reducing the footprint, thus enabling actual integration within Si-based photonic integrated circuits (PICs).

Finally, the possibility of achieving the ISB strong coupling regime in SiGe QWs at MIR wavelengths was assessed. Electromagnetic simulations were performed to design and analyze conventional metal-insulator-metal (MIM) and hybrid metal-insulator-semiconductor (MIS) microcavities enclosing parabolic SiGe QWs, confirming the appearance of two ISB polaritons in both architectures. To practically realize such microcavities, hyper-doped Ge and SiGe layers were developed as highly-reflective semiconducting mirrors. Using pulsed laser melting, electron densities well beyond 5×10^{19} cm^{-3} were obtained, resulting in plasma frequencies lying in the MIR (Figure 2). The thermal stability of these materials was studied to determine suitable growth temperatures for the deposition of the heterostructure which prevent complete dopant deactivation. Preliminary regrowth experiments were conducted using these layers as substrates, demonstrating the deposition of crystalline overlayers, although severe deactivation occurred under all tested conditions, likely due to the detrimental effect of the LEPECVD plasma. Further optimization of the growth parameters is thus required to enable the realization of monolithic MIS microcavities.

The fabrication of conventional MIM cavities is also being pursued by growing the heterostructure on SOI substrates, forming the bottom metallic mirror via wafer bonding and exposing the QWs surface by wet etching, using SiO_2 as a stopping layer, and mechanical polishing.

In conclusion, this work establishes the maturity and potential of Ge-rich SiGe heterostructures as a versatile platform for MIR photonics. Building upon these results, future efforts will focus on integrating these components into PICs and demonstrating the ISB strong coupling regime in the group-IV material platform.

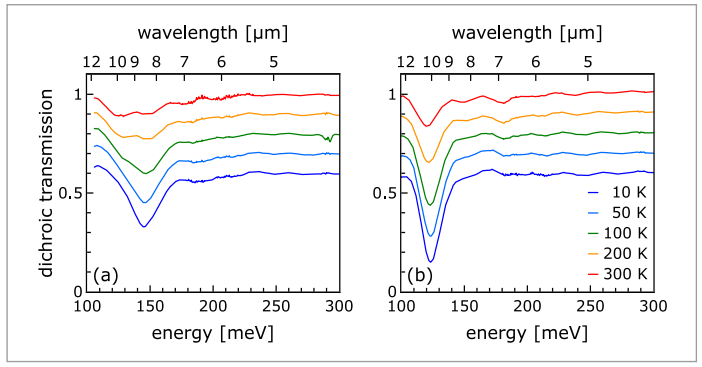

Fig.1 - Temperature-dependent dichroic transmission spectra of (a) square (n2D ≃ 5×10^{11} cm^{-2}) and (b) parabolic (n2D ≃ 1.2×10^{12} cm^{-2}) QWs.

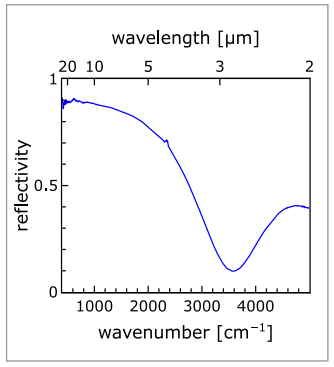

Fig.2 - MIR reflectivity spectrum of laser-annealed Ge

CONNECTING STRUCTURE AND FUNCTION IN NANOMATERIALS THROUGH ULTRAFAST SPECTROSCOPY

Diego Florio - Supervisors: Franco V. A. Camargo, Tersilla Virgili

Designing functional nanomaterials requires understanding how photoexcited states evolve on ultrafast timescales, as processes from femtoseconds to nanoseconds ultimately determine macroscopic behavior. This thesis investigates these phenomena using ultrafast spectroscopy, a technique capable of directly probing excited-state dynamics and revealing the microscopic mechanisms governing light-matter interactions. By combining ultrafast spectroscopy with controlled nanomaterial engineering and complementary structural characterization, this work explores how nanoscale architecture shapes photophysical behavior across a variety of nanostructured systems.

The first part of the thesis explores nanostructures designed for ultrafast, label-free biosensing. In particular, the work investigates how combining metallic and dielectric nanomaterials can enhance the optical response to environmental changes. To this end, a hybrid metal-dielectric platform was developed by coating a silica opal - an ordered assembly of dielectric nanospheres forming a three-dimensional photonic crystal - with a thin gold layer. The hybrid structure is not a mere superposition of opal and gold: due to the curvature of the spheres, the metal layer naturally evolves into nanocaps supporting localized surface plasmon resonances absent in the continuous gold film. Ultrafast spectroscopy shows that the plasmonic transient response of the hybrid structure is strongest at a spectral position and under specific excitation conditions defined by the photonic crystal. This pronounced and sharply defined response, combined with the intrinsic environmental sensitivity of the plasmon, enables detection of bacterial adsorption as measurable spectral shifts and rapid changes in the transient dynamics. These results demonstrate that plasmonic-photonic architectures can convert nanoscale environmental changes into distinct ultrafast optical signatures, offering a proof-of-concept approach for the real-time detection of biological species.

The second part of the thesis focuses on semiconductor-metal hybrid nanocrystals designed for photocatalytic hydrogen generation. In these systems, the semiconductor absorbs light, while a metal domain acts as a catalytic site that extracts photoexcited electrons and drives water splitting to generate molecular hydrogen. A key challenge is understanding how the structure and chemical nature of the metal cocatalyst influence both charge separation and catalytic reactivity. Another longstanding issue is to design environmentally friendly systems that do not rely on heavy metals, mainly cadmium. Using cadmium-free ZnSe nanorods decorated with gold as a model system, this work investigates the photocatalytic performance for different gold loadings, from atomically dispersed sites to larger metallic domains. Ultrafast spectroscopy revealed that electron transfer from the semiconductor to gold occurs efficiently across the different metal morphologies. However, photocatalytic activity does not simply follow charge-transfer efficiency. Instead, the results show that isolated single-atom catalytic sites can outperform larger metallic tips, highlighting the dominant role of atomic-scale chemical reactivity. Ultrafast spectroscopy also revealed the influence of surface trapping processes, emphasizing the importance of controlling the semiconductor surface in order to fully exploit the catalytic properties of the metal sites. Building on this insight, the study then explores a different model system based on ZnSe/ZnS core-shell quantum dots coupled to gold domains. In this architecture, the ZnS shell provides surface passivation but simultaneously introduces a tunneling barrier for electron transfer to the metal. By independently tuning shell thickness and gold domain size - from isolated atoms to sub-nanometric clusters and crystalline tips - the work disentangles the interplay between surface passivation, charge extraction, and catalytic activity. Ultrafast spectroscopy directly links structural modifications to carrier dynamics, revealing that optimal photocatalysis emerges from a balance between trap suppression and efficient interfacial electron transfer.

In parallel with their use in photocatalysis, quantum dots have also been investigated as building blocks for next-generation light-emitting devices, including lasers and quantum light sources, due to their size-tunable optical properties and high photoluminescence efficiency. In these systems, strong quantum confinement leads to pronounced Coulomb interactions between charge carriers, which can trigger Auger recombination, a fast many-body nonradiative process that benefits single-photon emitters but limits devices relying on multiexciton states. Understanding and controlling Auger recombination is therefore essential for optoelectronic applications. Among the strategies proposed to address this challenge, a recent approach involves fusing two quantum dots into a dimer structure, forming a quantum dot molecule. In the last part of this thesis, exciton and multiexciton dynamics are studied using ultrafast spectroscopy, both in isolated CdSe/CdS core-shell quantum dots and in these quantum dot molecules. The experiments reveal that electronic coupling between the two cores of a dimer enables the formation of spatially segregated multiexciton states, in which excitons reside in separate cores. This spatial separation reduces electron-hole overlap and significantly slows Auger recombination compared to isolated quantum dots. Stochastic kinetic modeling reproduces the observed dynamics by correctly accounting for exciton-number statistics and the recombination pathways available in both monomers and dimers. A complementary theoretical analysis performed on monomers further clarifies the origin of higher-order nonlinear signals in TA measurements, showing that they do not correspond directly to quantum dots containing a specific number of excitons but instead arise from sequential Auger recombination cascades triggered by higher initial exciton populations.

Together, the studies presented in this thesis demonstrate how ultrafast spectroscopy provides a direct link between nanoscale structure and functional photophysics of advanced materials, spanning applications from sensing to energy conversion and optoelectronics.

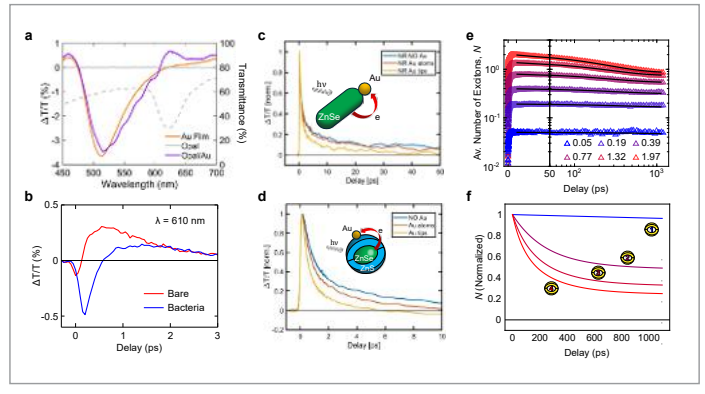

Fig.1 - (a,b) Hybrid metal-dielectric platform for ultrafast label-free biosensing (a) Spectra of the relative differential transmission change (ΔT/T) measured at 500 fs after excitation of Opal/Au (purple), Au Film (orange), and Opal (solid grey). The steady-state transmittance spectrum of the Opal is also shown (dashed grey). (b) ΔT/T dynamics at ≈610 nm for the Opal/Au in the absence (red) and presence (blue) of bacteria. (c,d) **Photocatalytic semiconductor-metal hybrid nanoparticles** (c) Normalized ΔT/T dynamics of the bleach recovery at 380 nm, corresponding to the first excitonic transition of the ZnSe nanorods, upon excitation at 330 nm for pristine ZnSe nanorods (NR No Au, light blue), single-atom-decorated nanorods (NR Au atoms, orange), and Au-tipped nanorods (NR Au Tips, yellow). (d) Normalized ΔT/T dynamics of the bleach recovery at 435 nm, corresponding to the first excitonic transition of the ZnSe/ZnS quantum dots, upon excitation at 400 nm for pristine ZnSe/ZnS quantum dots (No Au, light blue), single atom-decorated quantum dots (Au atoms, orange), and Au-tipped quantum dots (Au Tips, yellow). (e,f) **Multiexciton dynamics in quantum-confined nanocrystals** (e) Fluence-dependent ΔT/T dynamics (colored scatter plots) and stochastic kinetic fits (black lines) of the bleach recovery at 575 nm, corresponding to the first excitonic transition of the CdSe/CdS quantum dots, upon excitation at 400 nm normalized to the average number of excitons per quantum dot, N. (f) Simulated normalized dynamics of the first excitonic transition of the CdSe/CdS quantum dots for an initial number of excitons n0 from 1 to 4.

TR-MOKE IMAGING OF SPIN-WAVE INTERACTIONS WITH DIRECT-LASER-WRITTEN YIG PATTERNS

Piero Florio - Supervisor: Edoardo Albisetti

Co-Supervisor: Daniela Petti

The growing demand for faster and more energy-efficient information processing is driving exploration into wave-based computing paradigms beyond conventional charge electronics. In wave-based signal processing, information is encoded in the amplitude, frequency, or phase of propagating excitations, enabling inherently parallel operations based on interference and diffraction. Among the various physical platforms under investigation, magnonics which exploit spin waves has emerged as a particularly promising candidate for on-chip signal transport and processing.

Spin waves combine several distinctive advantages. Their wavelengths can reach the nanometer scale at microwave frequencies enabling device miniaturization well beyond that of photonic systems operating at comparable frequencies. At the same time their group velocities can approach tens of kilometers per second supporting fast signal transmission. Crucially spin wave propagation does not rely on charge motion thereby suppressing Joule heating and offering a pathway towards highly energy-efficient information technologies.

A key material platform for integrated magnonics is yttrium iron garnet (YIG), an insulating ferrimagnet distinguished by its exceptionally low magnetic damping and correspondingly long spin-wave propagation lengths. Over the past decade substantial progress in material growth and nanofabrication has enabled the realization of individual magnonic elements in YIG including waveguides, interferometers and logic prototypes. As the field advances attention is shifting from individual components to scalable architectures. Drawing inspiration from photonic integrated circuits, the development of large-scale magnonic networks relies on the identification of universal building blocks such as waveguides, phase shifters and directional couplers that can be interconnected to implement complex linear and interference-based functionalities. Achieving this level of integration requires fabrication strategies that combine low magnetic damping, sub-micrometer precision and high throughput. Conventional lithographic patterning followed by reactive ion etching (RIE) introduces edge roughness and structural damage leading to increased damping and a substantial reduction of spin-wave propagation lengths in patterned structures. In the context of my PhD I worked on a direct laser writing approach based on localized modifications of the magnetic properties of YIG thin films to define specific geometries for wave propagation. The process operates under ambient conditions and reaches writing speeds up to 3 mm^2/min allowing an entire wafer to be patterned on the timescale of minutes. Compared with focused ion beam techniques our approach eliminates the need for vacuum systems and ion optics, significantly reducing experimental complexity and cost while offering a direct and scalable route to device fabrication.

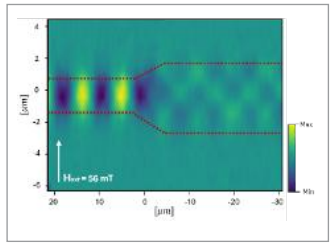

Fig.1 - Time-resolved imaging of spin wave propagation in a variable-width waveguide: Tr-MOKE (Time-Resolved Magneto-Optical Kerr Effect) map showing the propagation of a spin wave within a waveguide fabricated by laser nanopatterning, featuring a progressive symmetric widening from 2 µm to 4 µm along the propagation direction. The spin wave is excited at 3.06 GHz by a stripline antenna positioned to the left of the measurement area. An external magnetic field (56 mT) is applied as reported. The red dashed line represents the interface between the laser-irradiated region (paramagnetic) and the non-irradiated region (ferrimagnetic) that constitutes the guiding channel.

The samples used in this work consist of 100 nm thick single crystal yttrium iron garnet films grown via liquid phase epitaxy on GGG substrates. Spin-wave nanostructures were patterned using a commercial maskless laser writing system equipped with a diode laser. The system sequentially exposes the sample surface point by point allowing precise control over the delivered laser power while achieving diffraction-limited spatial resolution. While pristine YIG is a ferrimagnet supporting spin-wave propagation the irradiated regions become paramagnetic effectively suppressing spin-wave transport. By exploiting this laser-induced phase change it is possible to directly define magnonic nanostructures in a single step without the need for etching or additional material processing.

The technique used to characterize the aforementioned devices is called Time Resolved Magneto-Optical Kerr Effect (Tr-MOKE), a stroboscopic technique that allows visualization of spin wave propagation in magnetic materials. The core of the technique lies in the synchronization between excitation and signal detection: an antenna, fabricated on the sample through conventional lithography, is excited by an RF generator, producing an oscillating magnetic field that excites spin waves. In order to measure their propagation, the Magneto-Optical Kerr Effect (MOKE) is exploited: a train of polarized laser picosecond pulses striking the magnetized surface, undergoes a slight polarization rotation, proportional to the oscillating out-of-plane (OOP) magnetization component.

Thanks to the integer ratio between the frequency of the spin wave and the repetition rate of the laser, each picosecond laser pulse probes the wavefront always at the same phase of the oscillation. In this way, the system works like a stroboscope, "freezing" the ultrafast motion of the wave at a precise phase in its cycle. The measurement occurs point by point: the laser, focused into a spot with a diameter smaller than 1 micron, measures the MOKE signal at a given position. The sample is then moved to scan an area or a line. By combining all measured points, a spatial snapshot of the propagating spin wave is reconstructed and visualizable as the 2D map shown in **FIGURE 1** that represents the first variable-width waveguide prototype I realized during my PhD. The experiment shows a symmetric widening in a nanopatterned waveguide acting as a modal filter. The red dashed line represents the interface between the laser-irradiated region (paramagnetic) and the non irradiated region (ferrimagnetic) that constitutes the guiding channel. The image, obtained by point-by-point sampling of the magnetic oscillation phase, reveals the modal structure of the wave along the waveguide: in the narrower region (2 µm), the excitation frequency intersects the simulated fundamental mode (n=1), while in the wider region (4 µm) it intersects the higher-order mode (n=3). This change in the modal configuration is attributable to the different demagnetizing fields in the two regions, which locally modify the dispersion relation and cause a mode shift, in full agreement with theoretical expectations.

INTEGRATED HIGH FREQUENCY PC-MIM NANORECTENNA ARCHITECTURE: DESIGN, SIMULATIONS AND FABRICATION

Martina Foschi - Supervisor: Remo Proietti Zaccaria

A rectifying antenna, also known as rectenna, is a device composed of an antenna coupled to a diode. The peculiarity of this system is its capability to capture electromagnetic radiation and turn it into electricity or, vice-versa, to turn input electricity into electromagnetic radiation. Specifically for the first scenario, the AC electromagnetic signal is collected by the antenna and converted into DC current by the rectifying diode. Due to the possibility to operate in a broad spectrum of frequencies, rectennas can be employed in different technological applications. This characteristics has driven interest in their use across diverse fields, ranging from wireless power transmission to energy harvesting systems. Traditionally, rectennas were primarily limited to microwave and radio frequency applications. However, the development of nanoantennas and the studies on ultrafast nanodiodes has paved the way for rectennas in principle capable of functioning at near infrared and visible frequencies. Indeed, in order to work at such high frequencies, a rectenna comprises a nanoantenna and a metal-insulator-metal (MIM) diode, the latter theoretically capable of operating on the scale of hundreds of THz/few PHz, corresponding to a switching time of the order of femtoseconds (fs). Furthermore, owing to the advancements in the micro/nano-fabrication field, it has been possible to merge in a single solution the receiving antenna and the rectifying diode, to form the so called the point contact metal-insulator-metal (PC-MIM) rectenna. In this configuration, a sharp metallic tip (or nanocone) duals as receiving nanoantenna and as top electrode of the MIM diode. The sharp tip is then brought into contact with a insulator-metal bilayer, to compose the rectifying junction. To date, this architecture has proved to be the most effective architecture in this frequency range, leading to an increase of two orders of magnitude in the state-of-the-art efficiency. Even though, this type of architecture brings some difficulties especially in terms of practical device implementation. For this reason, in this thesis we propose a more versatile high-freqeuncy rectenna architecture based on the integration of a PC-MIM junction within a patch antenna structure. In details, the patch antenna carries two different functions, namely it serves as efficient receiving antenna and as support for the metallic nanocone that, with the addition of the two thin layers (metal and insulator), completes the PC-MIM architecture. Figure 1.a and 1.b illustratee the two different nanorectennas configurations

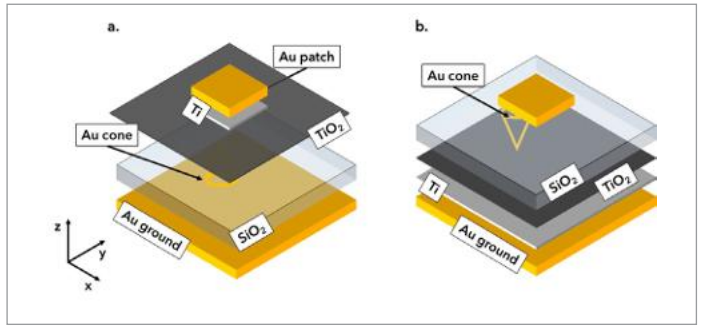

Fig.1 - 3D graphic illustration of the two architectures that follow the proposed new rectenna design. Both architectures are based on the patch antenna that is a three-layer system composed of a Au patch layer, a SiO2 substrate and a Au ground layer. The two configurations differ from each other by the nano cone positioning and the consecutive placement of the thin TiO2 insulating layer and the Ti layer forming the PC-MIM diode. Namely, a) illustrates Geometry #1 with the nanocone pointing towards positive z values, while b) illustrates Geometry #2 with the nanocone pointing towards negative z values

that result from the different positioning of the nanocone in the SiO2 layer (facing upwards or downwards), respectively Geometry #1 and Geometry #2. When excited with a linearly polarized plane wave, this system can convert the receiving radiation into a TM0 mode (also known as radial mode) within the nanocone. This is an important aspect as, if a proper metal is chosen, this kind of mode can realize adiabatic compression, leading to a strong Surface Plasmon Polaritons (SPPs) concentration at the apex of the cone itself, regardless the dimensions of the cone apex. Indeed, a small tapering angle is a critical parameter in a PC-MIM as the SPPs to electron-hole pairs conversion scales up inversely proportional to the square of the curvature radius. In turn, this produces a high concentration of hot electrons available for tunnelling through the insulating layer, namely photocurrent. This work involves two main parts including electromagnetic simulations and fabrication protocol development. Given the aforementioned scenario, firstly we have developed the geometrical design of the new rectenna architecture. Indeed, through finite element method simulations we have studied this problem in order to obtain the best electromagnetic performance, maximizing the SPPs concentration at the cone apex. Moreover, a comparison between our results and the simulated data related to the state-of-the-art (from literature), suggests that this new rectenna device could achieve better results in terms of quantity of hot electrons available for tunneling at the cone apex, possibly leading to an increased photocurrent (Figure 2).
The second part of this thesis is focused on the fabrication of the rectenna device following Geometry#2. This activity resulted in a complex three-dimensional nanoscale architecture which had to overcome significant fabrication challenges. The resulting fabrication protocol involves different fabrication steps that include metal and oxide layers deposition, dry etching of conical apertures in a SiO2 substrate, multi-layer electron beam lithography patterning and alignment, and selective gold electroplating.
Finally, a proof of concept of patched PC-MIM rectenna was achieved and then extended in an array configuration (Figure 3.a-b) so to provide the most suitable structure for realistic applications.

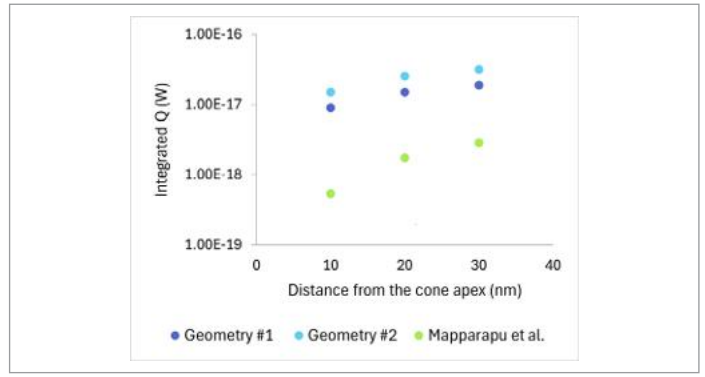

Fig.2 - Power loss density Q integrated in a volume defined by 10-20-30 nm distance from the cone apex calculated in both geometries. Comparison with the state-of-the-art shows a one-fold increase in the absorbed power by the tip that can be used as as an estimator for the hot electrons available for tunneling at the MIM barrier

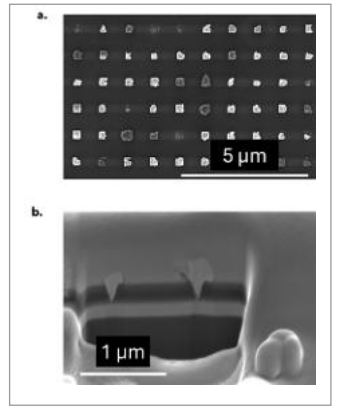

Fig.3 - a) SEM image of a small area of the 80 x 80 µm device array. This image the top view of the rectenna device from which the patch layer is visible on top of the SiO2 substrate. b) Cross section SEM image of two devices fabricating following Geometry #2, showing the etched nanocone in the SiO2 substrate, electrochemically filled together with the patch layer

EDIBLE RECHARGEABLE BATTERIES

Valerio Galli – Supervisor: Mario Caironi

Edible electronics is an emerging research field that aims to develop a completely safe-to-eat technology by studying and exploiting the electronic properties of food-derived materials and food additives. Edible devices can be degraded within the body at the end of their operational life, without any risk. This technology thus offers the opportunity to replace standard electronics across various sectors. In medicine, the development of ingestible smart pills is attracting significant attention for monitoring the GI tract. However, the use of these devices is associated with a nonnegligible risk of retention and consequent complications. Edible systems can replace ingestible electronics, eliminating the need for medical supervision during administration. In the agrifood sector, edible smart tags can be directly applied to food to monitor and prevent spoilage or counterfeiting. Edible devices can also be implemented in sensor networks to monitor environmental parameters without contributing to electronic waste or environmental pollution. Advances in edible electronics depend on the development of reliable power sources that ensure the stable operation of edible electronic systems.

Among all possible solutions, batteries appear to be the best candidate as they can deliver current at a defined potential and have high energy densities. The development of a safe-to-eat battery strictly relies on material selection. Edible materials have therefore been investigated to identify the best candidates for battery redox-active and auxiliary materials. Edible inks were formulated combining small redox-active molecules, activated carbon as a conductive additive, and ethyl cellulose as a binder, and their deposition onto gold-laminated ethyl cellulose edible current collectors enabled the development of edible battery electrodes. After detailed electrochemical characterization, quercetin and riboflavin have been selected as the best edible redox-active molecules for the cathode and the anode, respectively. Both molecules undergo a reversible redox reaction, enabling the realization of a rechargeable battery, with a cell voltage of ~0.65 V. Finally, the first edible rechargeable battery was assembled using a NaHSO4 aqueous electrolyte, nori as a separator, and beeswax as an encapsulant. This first prototype had a capacity of 10 µAh, and all materials used did not exceed the EFSA ADI levels. The potential applications of this battery, however, were limited by the design and the low capacity of the first prototype. For this reason, the battery was redesigned to facilitate interconnection with other devices by adopting a coplanar electrode architecture. The capacity was also doubled to 20 µAh by increasing the electrode mass loading. Operational stability over two weeks and environmental stability across 0-37 °C validated the use of edible batteries in scenarios such as healthcare and agrifood. For the first time, the compatibility of edible rechargeable batteries with other edible electronic components was demonstrated by powering edible sensors and logic circuits, paving the way for the development of a completely safe-to-eat technology. The potential of these batteries extends beyond edible electronics. Interconnections with traditional passive resistive sensors and the development of a 3-cell battery to power an IoT environmental sensor enable the replacement of traditional batteries in applications where safety and sustainability are crucial.

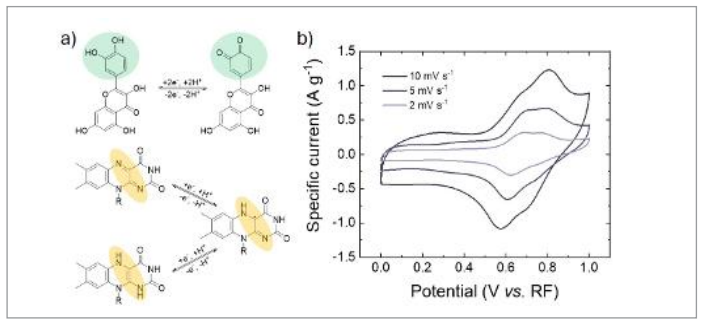

Fig.1 - a) Redox reactions of quercetin and riboflavin. b) Cyclic voltammograms of the edible rechargeable battery

In addition to the aforementioned scenarios, integrating edible batteries into smart pills is among the most promising and important applications, as it could eliminate many safety concerns associated with ingestible technologies. For this reason, a strategy for miniaturizing edible rechargeable batteries without performance loss was developed. New edible redox-active inks with increased conductivity were formulated, enabling an increase in electrode mass loading to 8 mg cm^{-2}. This enabled the design of a miniaturized battery that fits in a 000-sized pill, with a capacity of 60 µAh. The battery capacity can be further increased to 120 µAh by adopting a double-cell parallel configuration within the same pill volume. Finally, the feasibility of integrating edible batteries into smart pills was demonstrated by assembling a hybrid pill and powering a CMOS ring oscillator with just ~0.65 V. The technological breakthrough of edible electronics would not be possible without translating laboratory devices into real-world applications. As a first example of this process, edible rechargeable batteries were gastronomically revisited, and chocolate batteries were realized in a food-grade kitchen using only materials from the food supply chain. The showcase and tasting of these batteries at the 2025 World Expo in Osaka demonstrate that edible electronics can indeed be edible. The results presented mark a fundamental advancement in edible electronics and beyond. Edible rechargeable batteries represent a breakthrough in battery technology and offer unprecedented opportunities due to their safety and sustainability. This work lays the foundation for future advances and new solutions in healthcare, food science, and environmental monitoring.

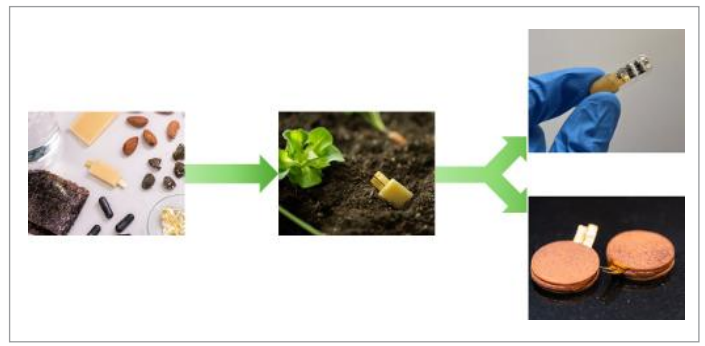

Fig.2 - Edible rechargeable battery development timeline

FERROELECTRIC CONTROL OF CHIRAL MAGNETIC INTERACTIONS IN HAFNIA-BASED MULTIFERROIC HETEROSTRUCTURES

Giovanni Gandini - Supervisor: Christian Rinaldi

Integrated circuits (ICs) have been at the heart of the computational revolution, playing a central role in the rise and development of the information era. However, as the demand for data processing and storage continues to grow, current computing architectures are approaching fundamental physical limits in energy efficiency and heat dissipation. In this context, spintronics offers a paradigm shift: by exploiting the electron's intrinsic spin rather than solely its charge, it enables the design of devices capable of overcoming the limitations of conventional electronics. Nevertheless, efficiently manipulating magnetic states remains a central challenge. Traditional current-driven approaches are limited by Joule heating and substantial energy dissipation, highlighting the importance of achieving electric-field control of the magnetization. Although Voltage Control of Magnetic Anisotropy (VCMA) enables efficient tuning, its reliance on a continuously applied bias renders the effect intrinsically volatile.
To overcome this limitation, my PhD research focused on integrating ferroelectric materials into spintronic heterostructures. Ferroelectric oxides provide a natural route to non-volatility through their remanent polarization, which persists even after removal of the switching bias. In this framework, hafnium–zirconium oxide (HZO) is particularly attractive: unlike conventional perovskite ferroelectrics, it is fully compatible with CMOS fabrication processes and retains robust ferroelectricity down to nanometric thicknesses, making it ideally suited for scalable spintronic applications. In this work, we demonstrate ferroelectric control of the interfacial Dzyaloshinskii–Moriya interaction (i-DMI) in perpendicularly magnetized TiN/HZO/Co/Pt heterostructures. The i-DMI is a chiral antisymmetric exchange interaction that favors orthogonal alignment between neighboring spins and plays a fundamental role in stabilizing complex magnetic textures such as skyrmions and chiral domain walls. A key step in this research was stabilizing a ferroelectric phase in initially amorphous TiN/HZO/Co capacitors through careful optimization of thermal treatments and electrical training. Identifying a processing window in which ferroelectricity and ferromagnetism could robustly coexist was essential, as high-temperature annealing typically degrades magnetic thin films.
The optimized conditions stabilized the polar orthorhombic phase of HZO (with remanent polarization around 12 μC/cm^2), while preserving perpendicular magnetic anisotropy and retaining approximately 88% of the pristine saturation magnetization.
The impact of ferroelectric polarization reversal on the ferromagnet was systematically investigated using in-operando Magneto-Optical Kerr Effect (MOKE) and electrical transport measurements. These experiments revealed a non-volatile and hysteretic modulation of magnetic coercivity (around 30%) synchronized with ferroelectric polarization reversal, reported in Fig. 1. Importantly,

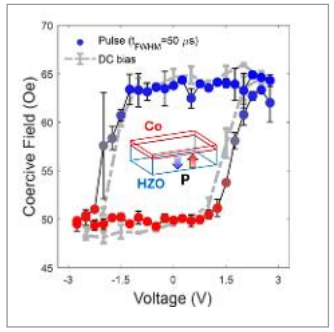

Fig.1 - Hysteretic modulation of magnetic coercivity upon ferroelectric polarization reversal. The coercive field, measured both under constant bias (grey line) and at remanence (coloured dots), exhibits identical behaviour, demonstrating that the modulation is governed by the non-volatile polarization state rather than by the applied electric field

this modulation is independent of pulse duration down to the sub-microsecond regime, closely follows ferroelectric switching dynamics, and induces negligible changes in saturation magnetization. Such observations effectively rule out magneto-ionic mechanisms driven by oxygen migration, which are common in ferromagnet/oxide systems but typically slow and degradation-prone. Furthermore, the effect proved to be long-lasting, with minimal variation over several days and no additional changes under voltage biases below the ferroelectric coercive field. Together, these results confirm both the robustness of the non-volatile state and the purely ferroelectric origin of the modulation.
The central achievement of this work lies in identifying the microscopic mechanism underlying the ferroelectric modulation of macroscopic magnetic properties. Brillouin light scattering measurements directly probed the interfacial Dzyaloshinskii–Moriya interaction, revealing a pronounced modulation, up to approximately 70%, upon polarization reversal. The consequences of tuning this chiral interaction were further explored through wide-field MOKE microscopy, which demonstrated controlled modulation of magnetic domain nucleation and expansion, as shown in Fig. 2. Micromagnetic simulations bridged the gap between microscopic interactions and macroscopic observables, accurately reproducing the experimentally observed magnetic behaviour upon varying the DMI strength. Overall, the results indicate that the coupling originates from a polarization-driven modulation of interfacial spin–orbit interactions, likely governed by a Rashba-type mechanism at the partially oxidized Co/HZO interface, as further supported by *ab initio* calculations.
Looking ahead, these findings open compelling perspectives for future spintronic technologies. Because DMI governs the morphology, stability, and dynamics of chiral magnetic textures, its electric-field modulation provides a promising pathway for information encoding in topological spintronic devices. Moreover, the coupling between ferroelectric polarization and interfacial spin–orbit physics lays the groundwork for integrating this material platform into devices exploiting spin-to-charge and charge-to-spin conversion phenomena. Ultimately, this work shows that ferroelectric polarization can serve as a non-volatile control knob for chiral magnetic interactions, opening new possibilities for electrically programmable magnetic systems. The ability to non-volatilely tune interfacial DMI enables a new generation of reconfigurable spintronic devices, where information can be encoded not only in the orientation of magnetization but also in the topology and chirality of spin textures.

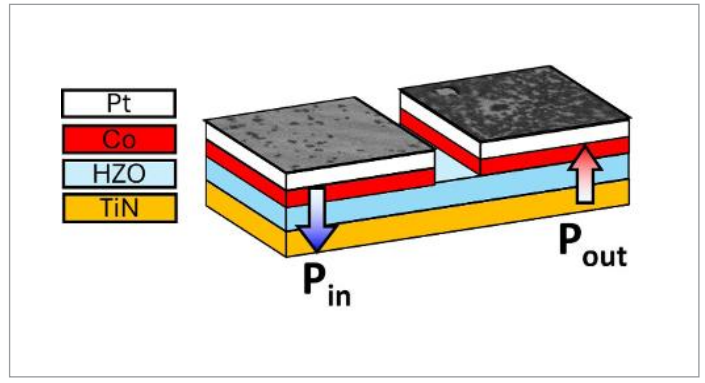

Fig.2 -Effect of ferroelectric polarization reversal on magnetic domain nucleation. Wide-field MOKE images were acquired starting from a saturated state (light grey) and applying a short magnetic field pulse to trigger magnetization reversal. Upon polarization reversal, a clear change in the density of nucleated domains (darker regions) is observed. The polarization state associated with larger interfacial DMI (outward polarization) exhibits enhanced domain nucleation, highlighting the impact of ferroelectrically tuned chiral interactions on reversal dynamics

ELECTRON-PHONON COUPLING IN LAYERED MATERIALS BY THZ SPECTROSCOPY

Federico Grandi - Supervisor: Eugenio Cinquanta

The terahertz (THz) spectral region (0.5-10 THz) is a unique and elusive band of the electromagnetic spectrum. Past challenges in generating and detecting radiation in this regime led to the concept of a "THz gap". However, scientific and technological interest has driven the discovery of novel techniques, closing this gap and opening the THz window for diverse applications ranging from telecommunications to materials characterization.

THz time-domain spectroscopy (THz-TDS) allows for the full reconstruction of the THz pulse's electric field in both amplitude and phase. This coherent detection enables the direct extraction of a material's complex optical parameters without the need for Kramers-Kroning relations. THz-TDS, hence, results in a powerful tool for studying the fundamental properties of solids, as the millielectronvolts photon energy matches fundamental low-energy excitations like free charge carriers in the conduction band and low-energy dipole-active phonons. In conventional semiconductors, like Silicon, the THz response is dominated by native free carriers' absorption, as no dipole-active phonons are generally present in the far-infrared. Upon perturbation in an Optical Pump-THz Probe (OPTP) experiment, the ultrafast injection of free charges is traced by the THz probe, resulting in a Drude transient response. In systems with the presence of strong dipole-active phonons, like perovskite semiconductors, the soft modes could couple with the photoinjected charges resulting in the formation of polaronic quasiparticles, sign of electron-phonon coupling. Ultrafast THz-TDS thus emerges as an effective tool to investigate the out-of-equilibrium dynamics and interplay between photoexcited charge carriers and the crystal lattice.

The research conducted during this PhD relied on a custom-built THz spectrometer equipped with optical pump-probe capabilities. To reliably detect the transient changes of the dielectric response of materials, improvements were made to the experimental setup to enhance both the signal-to-noise ratio (SNR) and the dynamic range (DR) of the time-domain acquisitions. Traditionally, data acquisition relies on a lock-in amplifier to extract the signal generated by the detection of THz radiation. To optimize this, a novel acquisition scheme was implemented, exploiting the combined use of a boxcar averager in series with the lock-in amplifier. This configuration increased the SNR allowing to reliably acquire signals almost ten times less intense than what the setup was capable of. Additionally, the deployment of an active beam-pointing stability system neutralized laser-induced instabilities, allowing for highly reliable retrievals of the material parameters.

Thanks to these optimizations, we could investigate the static and ultrafast dynamic conductive phenomena governing metal phosphorous trichalcogenides (MPX3), focusing on the layered semiconductor HgPSe3. This material exhibits high sensitivity to light across a broad spectrum, ranging from X-rays to the visible,

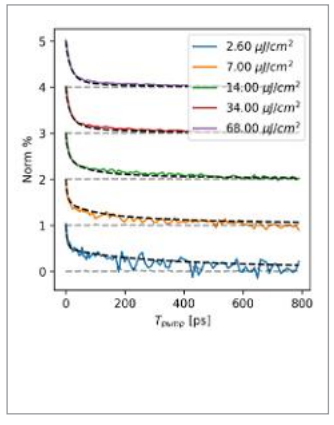

Fig.1 - Optical pump - THz probe response of HgPSe3 at 78K with 400 nm excitation at different fluences with decay fitted via monomolecular decay channels

making it a promising candidate for broadband photodetector applications. The primary motivation for probing $HgPSe_3$ in the THz regime was to map its intrinsic conductive capabilities and to uncover the links between its free charge carriers and the low-energy vibrational modes (such as shear and breathing motions) arising from its layered structure. Before this work, the interplay between these specific phonon modes and the photoexcited carrier populations had not been observed. From a broader perspective, the study of the el-ph coupling in layered materials is of pivotal significance to explain the transport properties of this class of material, targeting applications in nanoelectronics.

Static THz characterization of $HgPSe_3$ revealed the presence of clear, sharp vibrational resonances, which preliminary Density Functional Theory (DFT) simulations attributed to the rigid relative motion of the layers. Temperature-dependent studies of these modes showed distinct broadening as the temperature increased, driven by the increasing strength of temperature-dependent lattice anharmonicities.

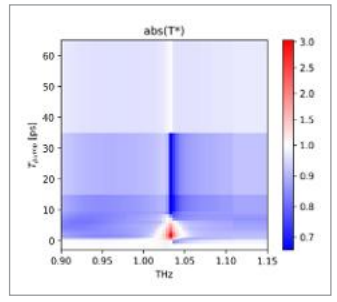

Fig.2 - (A) Comparison of the generated XUV signal (blue) in He for its optimal pressure and the trnasmitted signal through a polycrystalline Si 100nm thin-film indicating the the L2,3 absorption edge at 99eV. (B) Differential absorption map for a cumulative 80 min transient measurement on Si after implementing Principal Component Analysis (PCA).

Time-resolved OPTP measurements unveiled a highly complex, temperature-dependent transient response. At cryogenic temperatures, the primary phonon resonance is initially quenched immediately following photoexcitation, resulting in increased THz transmission. This negative change in the transient dielectric properties recovers within a few picoseconds. The most robust physical explanation for this phenomenon is a photoexcited carrier-induced overdamping of the phonon resonance, which suppresses the ground-state absorption feature. Following this initial few-picosecond window, the system enters an opposing regime: the hot carrier population loses energy to the lattice, driving the lattice out of equilibrium. This state reduces the available anharmonic decay channels, leading to an underdamping of the resonance.

Conversely, at higher temperatures, the thermal population of anharmonicities dominates the phonon response. Consequently, photoexcited carriers can no longer induce the initial overdamping effect. Instead, by driving the lattice out of equilibrium, the carriers immediately restrict the available recombination channels, leading purely to the underdamping effect. This manifests as an overall increase in the absorption of the phonon mode and a resulting positive transient change in the material's dielectric parameters.

By analyzing the integrated frequency response as a function of the pump-probe delay, it became evident that the primary mechanisms governing carrier recombination in HgPSe3 are monomolecular. These decay channels can be attributed to interactions with either the out-of-equilibrium phonon population or the presence of specific mid-gap trap states. These insights provide a critical understanding of the intrinsic limiting factors for charge conductivity in this semiconductor, establishing a foundational model for its conductive behavior under broadband photoexcitation.

Parallel work was initiated to design and construct a next-generation THz spectroscopy beamline based on a laser source featuring higher repetition rates and superior baseline stability. Once completed, this beamline will utilize an advanced pulse compression system, incorporating both a multipass cell and a hollow-core fiber, to achieve even broader THz bandwidths, promising access to the higher-frequency dynamics of complex layered materials.

PHOTONIC INTEGRATED DEVICES VIA FEMTOSECOND LASER MICROMACHINING FOR QUANTUM APPLICATIONS

Giulio Gualandi - Supervisor: Giacomo Corrielli

The advent of quantum technologies is expected to profoundly transform the way information is processed, transmitted, and measured. Unlike classical approaches, quantum technologies rely on the preparation and manipulation of genuine quantum states, where phenomena such as superposition and entanglement provide powerful resources for solving problems that are intractable for classical algorithms. Moreover, quantum carriers enable intrinsically secure communication protocols. Among the available physical platforms, photons represent particularly attractive carriers of quantum information: they are robust against environmental decoherence, can propagate over long distances, and are naturally compatible with existing optical fiber infrastructures. When combined with recent advances in integrated optics, photonic systems enable the development of compact, stable, and scalable platforms for both fundamental quantum experiments and real-world technological applications. A major challenge in the field is scalability, which drives the transition from bulk optical implementations to integrated photonic approaches. Integration is essential for moving quantum technologies beyond proof-of-principle demonstrations toward widespread deployment. While some applications, such as quantum key distribution, have already reached real-world implementation, many others still require intermediate technological milestones toward large-scale, fault-tolerant systems. In this context, quantum photonics research aims both to enable near-term applications and to develop the building blocks for future quantum technologies.

This thesis focuses on the fabrication and characterization of integrated photonic circuits using femtosecond laser micromachining (FLM) in glass. This technology represents a versatile and powerful platform for the rapid prototyping of three-dimensional photonic circuits, enabling the realization of waveguides, interferometric structures, resonators, and reconfigurable photonic processors without the need for clean-room facilities. The same fabrication technology was systematically employed throughout this work to realize multiple devices targeting different applications, demonstrating its flexibility and technological maturity. The work presented in this thesis spans a broad range of devices for quantum communication, fundamental quantum physics experiments, and fundamental components for integrated photonic platforms. Particular emphasis was placed on the complete experimental cycle, including device design, fabrication optimization, optical characterization, and integration within complex experimental setups.

The fabricated devices exhibit low propagation losses, low birefringence, and excellent compatibility with standard fiber components and commercial optical hardware. These characteristics make FLM-fabricated circuits particularly attractive for quantum photonics, where stability, low noise, and reproducibility are critical requirements.

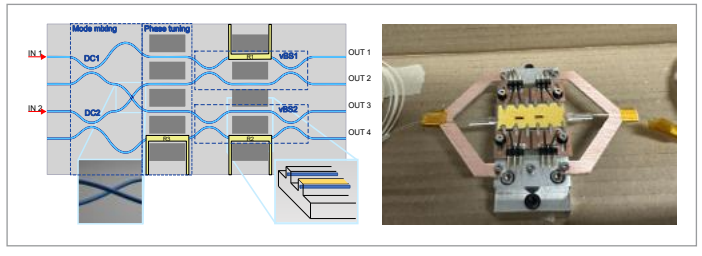

Fig.1 - **Schematic layout of the FLM-fabricated device for continuous-variable quantum communication (left) and photograph of the assembled chip (right).** The schematic highlights the two central modes crossing in three dimensions, enabled by FLM, and the trenches fabricated alongside the waveguides. The right panel shows the assembled chip with input/output fibers glued to the chip facets and electrical connections routed to a custom PCB attached to the device pins.

A first class of devices includes receivers for discrete-variable and continuous-variable quantum communication protocols operating at telecom wavelengths. A time-bin quantum key distribution receiver was fabricated exploiting the intrinsically low birefringence of laser-written waveguides. A dedicated post-fabrication correction was implemented to compensate residual birefringence effects, enabling full polarization-insensitive operation. The device demonstrated near-unity interference visibility and precise temporal matching with the transmitter, and it is currently deployed in a real quantum communication network for field testing. In parallel, a coherent receiver for continuous-variable quantum protocols was developed. The device successfully demonstrated heterodyne detection with high common-mode rejection ratio and long-term operational stability, confirming its suitability for practical quantum communication scenarios.

Another key result of this thesis is the demonstration of hybrid integration between photonic integrated circuits and single-photon detector arrays. By directly coupling a laser-written Photonic Integrated Circuit (PIC) with a Single-Photon Avalanche Diode (SPAD) array, high photon detection efficiency and negligible crosstalk were achieved, resulting in record system detection efficiencies for integrated PIC–SPAD platforms. The coupling scheme provides high tolerance to micrometric misalignment, enabling the use of compact and cost-effective positioning systems and opening the path toward fully integrated systems combining photon generation, manipulation, and detection within a single platform operating at room temperature.

Interferometric circuits for fundamental quantum photonics experiments with genuine single photons were also fabricated using FLM, exploiting its three-dimensional capabilities to simplify the circuit layout. In this context, a three-arm interferometer was realized to enable experimental tests of Born's rule. The device features high-quality directional couplers, providing high extinction ratios and excellent calibration stability, and has been integrated into an international effort to perform the test using single-photon sources based on emitters in hexagonal boron nitride (hBN).

A second device was designed for the heralded generation of Bell states, enabling the creation and manipulation of entangled states with single-photon inputs. Path-to-polarization conversion was successfully implemented, allowing different qubit encoding schemes.

In addition, this thesis demonstrates the first tunable integrated ring resonator fabricated with FLM, achieving a Q factor at critical coupling exceeding 8×10^5. By driving the two thermo-optic phase shifters, precise tuning of the resonance wavelength over more than one free spectral range was achieved, along with active control of the Q factor. These characteristics make the resonator suitable for applications requiring reconfigurable spectral responses, including tunable optical filters, gyroscopes, and integrated sensing systems.

These results collectively demonstrate the effectiveness of femtosecond laser micromachining as a unified fabrication platform for integrated quantum photonics. By realizing multiple devices targeting diverse applications, this work contributes to advancing the scalability, robustness, and technological readiness of photonic quantum technologies for future real-world deployment.

ULTRAFAST LIGHT-WAVE-DRIVEN CHIRO-OPTICAL INTERACTIONS IN LOW-DIMENSIONAL SYSTEMS

Francesco Gucci - Supervisor: Stefano Dal Conte

At the interface between two-dimensional materials and ultrafast lasers, valleytronics offers the opportunity to realize light-driven control of the quantum properties of matter. The momentum location of a quasiparticle in one of the multiple degenerate, yet inequivalent, conduction band minima, is leveraged as the information bit. Transition metal dichalcogenide monolayers are naturally inversion-symmetry-broken crystals, in which the K and K' valleys can be selectively addressed with circularly polarized light. This property makes them the prototypical platform for valleytronics. However, once a valley population is initialized, it decays on timescales of hundreds of femtoseconds, thus far preventing relevant technological applications. Here, we present novel approaches and techniques to manipulate the valley pseudospin with lightwaves within its decoherence time and to advance the understanding of chiro-optical interactions in valleytronic platforms.
In particular, we show that a pair of linearly polarized phase-locked pulses with orthogonal polarization can lead to coherent initialization of valley polarization. We employ the setup in Fig.1**a** to generate the pair of pulses and to record the single-color time-resolved Faraday rotation (TRFR), sensitive to the excitonic valley imbalance. The first pulse induces a coherent superposition of valley states. Then, by timing the interpulse delay with sub-femtosecond precision, we induce coherent valley-selective transitions (see Fig. 1**b**). Modifying the pump delays on a sub-cycle timescale yields excitation of opposite valleys (see Fig. 1**c**). Our findings are supported by first-principles simulations. With trains of four pulses (see Fig. 1**d**), we demonstrate logic operations on the valley degree of freedom, i.e. switch (Fig. 1**e**) and amplification (Fig. 1**f**). Our protocol allows for 10 THz operation rates at room temperature.
We expand on TRFR by presenting a full ultrafast chiro-optical spectroscopy technique. Employing a birefringent interferometer and an optical polarization bridge detection scheme (see Fig. 2**a**), we access the energy-resolved complex chiro-optical susceptibility of a material, . The imaginary and real parts of correspond, respectively, to circular dichroism (CD) and optical rotatory dispersion (ORD). Employing a pump-probe scheme, we record the transient evolution of CD and ORD on ultrafast timescales. Our self-heterodyned ellipsometric approach allows us to reach unprecedented sensitivity (< 50 microdegrees). We benchmark this spectrometer on gold nano-helicoids, corroborating our experimental findings with full-wave simulations (see Fig. 2**b**). Moreover, we record the temporal evolution of photoinduced chiro-optical activity in a lead halide perovskite, exhibiting optical selection rules similar to TMD monolayers (see Fig. 2**c,d**).
We also explore different regimes by driving a WS_2 monolayer with carrier-envelope-phase-stable, linearly polarized, non-resonant pulses. We show that intense mid-infrared pulses induce a dramatic symmetry breaking, highly dependent on the relative orientation between the radiation polarization and the TMD crystallographic directions. We track the sub-cycle temporal evolution of the second-harmonic generation of a second ultrashort near-infrared pulse. Our findings reveal a clear field-driven valley selectivity encoded in the temporal phase shift of the signal with respect to the driver pulse. A simple model, underpinned by symmetry arguments, provides a qualitative explanation of the observations.
Overall, our findings advance the understanding of ultrafast valley and chiro-optical dynamics in two-dimensional materials and their link with optical nonlinearities. They also establish new pathways for lightwave control of valley degrees of freedom beyond conventional optical selection rules.

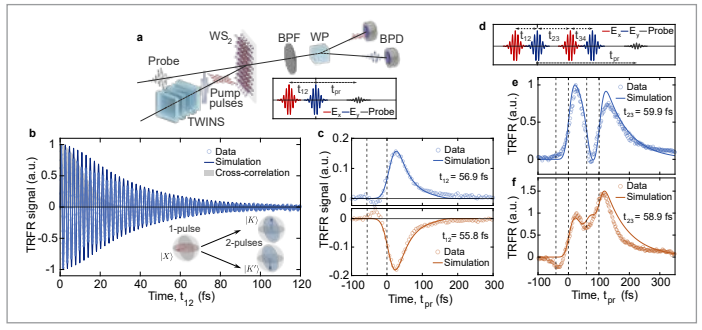

Fig.1 - Multi-pulse valley polarization initialization and manipulation. **a.** Sketch of the experimental setup (TWINS: birefringent interferometer, BPF: band-pass filter, WP: Wollaston prism, BPD: balanced photodiodes). **b.** TRFR signal measured after interaction with a pair of perpendicularly polarized pulses. The pump-probe delay (tpr) is held fixed, whereas delay between the two pump replicas (t_{12}) is continuously shifted. The bottom-right inset depicts a sketch of the underlying physical mechanism through the Bloch sphere picture. **c.** TRFR traces for fixed t_{12} and varying tpr. Depending on the value of t_{12} , the pulse sequence results in the excitation of K (t12 = 56.9 fs, blue trace) or K' (t12 = 55.8 fs, orange trace) valley. **d.** Scheme of the pump pulses train. **e.** The interpulse delays have been chosen to switch off the polarization after interaction with the third pulse ($t_{12} = t_{34}$ = 41.2 fs and t_{23} = 59.9). The fourth pulse switches the valley polarization on again. **f.** Same as e, but for a different delay between second and third pulse (t_{23} = 58.9), resulting in the amplification of the signal. The dashed lines depict the arrival times of the pump pulses.-

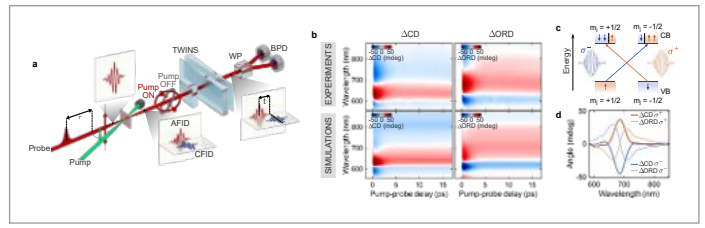

Fig.2 - **a.** Sketch of the experimental setup. After transmission through a chiral sample, the probe polarization can be described as the sum of achiral (AFID) and chiral (CFID) free-induction fields. The TWINS interferometer introduces a delay t between the components. A WP and BPD enable recording of chiral interferograms. A Fourier transform of the chiral interferograms gives access to the complex chiro-optical susceptibility. **b.** Transient CD and ORD experimental maps and full-wave simulations for the gold nano-helicoids. **c.** Selection rules in lead-halide perovskites. **d.** Transient CD and ORD spectra at a fixed delay for σ+(orange) and σ−(blue) photo-excitation.

DYNAMICS OF COLLECTIVE EXCITATIONS IN TRANSITION METAL COMPOUNDS

Andrea Iudica - Supervisors: Margherita Zavelani-Rossi, Giuseppe Paternò

This PhD thesis investigates the dynamical properties of quantum materials in which multiple interaction channels, such as electron-electron, electron-phonon, and spin interactions, contribute to the formation of the ground state. In these systems, the independent-electron approximation underlying standard band theory is often insufficient, particularly in transition metal compounds where partially filled d orbitals enhance correlation effects. As a result, a range of phenomena such as Mott insulating behavior, charge-density-wave order, and excitonic effects can emerge, reflecting the interplay between different microscopic interactions.

A central aspect of this work is the description of these materials in terms of collective excitations, i.e. quasiparticle-like modes arising from the coupling between electronic, lattice, and spin degrees of freedom. The properties of these excitations depend on the relative strength of the underlying interactions (e.g. Coulomb repulsion, electron-phonon coupling, exchange interactions), and are directly reflected in the optical response of the system. In particular, features such as spectral-weight redistribution and the formation of energy gaps provide information on the nature of the underlying order. However, in equilibrium, different interaction channels often produce similar signatures, making it difficult to unambiguously identify the dominant mechanisms responsible for a given phase. The thesis tackles this problem by adopting an **out-of-equilibrium perspective**, where ultrafast optical excitation is used to impulsively perturb the system and monitor its relaxation in real time. This approach enables what can be described as a *time-domain classification of interactions*: different microscopic processes unfold on characteristic timescales, from femtosecond electronic dynamics to picosecond lattice and spin responses. By tracking these dynamics, one gains direct insight into the hierarchy of couplings that stabilize the ground state, information that is hardly acessible through static probes alone .

At the heart of the experimental methodology lies **ultrafast broadband time-resolved optical spectroscopy**, the unifying tool of the thesis. This technique combines femtosecond temporal resolution with wide spectral coverage—from the mid-infrared to the deep ultraviolet—allowing simultaneous access to both low-energy collective modes and high-energy electronic excitations. Its multidimensional nature is a key strength: while the spectral domain captures transient modifications of the electronic structure, the time domain reveals coherent oscillations associated with phonons, magnons, and amplitude modes. This dual sensitivity provides a comprehensive view of nonequilibrium electrodynamics, enabling the direct observation of spectral-weight transfer and the coupling between different degrees of freedom.

A major emphasis of the thesis is the **versatility of broadband spectroscopy across a wide variety of materials**, demonstrating its universal applicability to distinct classes of quantum systems:

- In **titanium nitride (TiN)**, a moderately correlated metal, the work reveals a previously hidden electron-phonon coupling channel through the activation of a coherent zone-edge phonon. This mode, enabled by defect-mediated processes, modulates interband transitions and provides a direct probe of the coupling between lattice and electronic degrees of freedom.
- In the layered compound **1T-$TaSe_2$**, a prototypical charge-density-wave system, broadband spectroscopy captures the ultrafast melting of the CDW phase. The experiment correlates large spectral-weight redistribution with the collapse of electronic order, while simultaneously resolving the nonlinear dynamics of the amplitude mode, highlighting the interplay between electronic and lattice instabilities.
- In **anatase TiO_2**, the thesis reports evidence for a **momentum-indirect excitonic state**, combining ultrafast deep-UV spectroscopy with time-resolved photoluminescence and many-body calculations. This result emphasizes the importance of phonon-assisted processes and points toward the formation of excitonic polarons, showcasing the richness of exciton physics in correlated semiconductors.
- Finally, in the two-dimensional antiferromagnet **CrSBr**, the development of a novel **broadband magneto-optical Kerr effect (MOKE)** technique enables the reconstruction of the full complex magneto-optical response with unprecedented sensitivity. This methodological advance allows the investigation of the coupling between excitonic resonances and magnetic order, opening new avenues for studying spin-dependent phenomena in low-dimensional systems.

Across these case studies broadband ultrafast optical spectroscopy is employed to track the temporal and spectral evolution of the optical response following photoexcitation. This allows one to monitor both spectral-weight redistribution and coherent dynamics, providing complementary information on electronic excitations and coupled collective modes. By resolving the response over a broad energy range and on femtosecond timescales, the technique enables the identification of distinct dynamical components associated with different interaction channels, offering additional constraints compared to equilibrium measurements. Overall, the results presented in this thesis demonstrate that broadband time-resolved optical spectroscopy is a versatile tool for investigating the nonequilibrium properties of quantum materials. Its combined temporal and spectral resolution allows simultaneous access to processes occurring on different energy and time scales, including electronic relaxation, lattice dynamics, and collective excitations. While the interpretation of the data remains system-dependent and often requires complementary theoretical and experimental input, the approach provides a coherent framework for studying the interplay of interactions in correlated systems. In this sense, it contributes to a more detailed characterization of the mechanisms governing their dynamical behavior, and to the broader effort of understanding how external perturbations influence complex condensed matter systems.

ADVANCED MICROFLUIDIC PLATFORMS FOR SOFT-X INTEGRATED PHOTONICS

Abedin Kamal - Supervisor: Salvatore Stagira

High-order harmonic generation (HHG) in gases is a key process in ultrafast and attosecond science, enabling the production of coherent extreme-ultraviolet (EUV) and soft X-ray radiation for spectroscopy, imaging, and interferometric applications. Despite its scientific impact, conventional HHG implementations based on gas jets or capillaries remain limited by intrinsically low conversion efficiency, experimental complexity, and long-term stability issues. These limitations motivate the development of compact, robust, and controllable HHG platforms capable of supporting phase-sensitive and application-oriented EUV/XUV photonics.

This thesis investigates high-order harmonic generation (HHG) in fused-silica microfluidic hollow-core waveguides with diameters between 70 and 130 µm, fabricated by the FAST group at Politecnico di Milano using femtosecond-laser micromachining. In contrast to conventional free-space gas-jet and capillary geometries, microfluidic waveguides enable extended interaction lengths on the millimeter scale together with precise control of the gas density inside a mechanically robust and vacuum-compatible structure. The HHG experiments are implemented within a multi-chamber vacuum system, in which a controlled pressure gradient is established along the beamline: pressures of the order of 10^{-4} mbar are reached in the HHG generation chamber due to gas injection into the microfluidic device, while differential pumping reduces the pressure to approximately 10^{-7} mbar in the downstream spectrometer chamber. The generated extreme-ultraviolet (XUV) radiation is transmitted along the beamline, spectrally dispersed by a grazing-incidence grating, and detected using a micro-channel plate coupled to a phosphor screen, with the resulting signal recorded by a visible CCD camera.

Using the output of an amplified Ti:Sapphire laser system delivering 800 nm femtosecond pulses with a duration of 35 fs, pulse energies of approximately 400 µJ, and a repetition rate of 1 kHz, harmonic generation up to photon energies of about 130 eV is demonstrated. The generated XUV radiation exhibits photon fluxes ranging from 10^9 to 10^{12} photons s^{-1}, depending on the gas species, pressure, and waveguide geometry. Systematic experimental studies performed with different noble gases, gas pressures, and waveguide diameters demonstrate a high degree of control over the harmonic spectrum, cutoff position, and conversion efficiency, establishing microfluidic HHG devices as stable, reproducible, and tunable chip-scale EUV/XUV sources (Figure 1). In addition, preliminary experiments employing mid-infrared driving wavelengths confirm the compatibility of the microfluidic platform with high-pressure operation and stable thermal behavior, highlighting the scalability of the approach toward higher photon energies and future extension into the soft X-ray and water-window spectral regions.

Building on this source architecture, the work implements phase-stable EUV interferometry using both spatial and temporal schemes. An integrated EUV spatial interferometer is realized through a microfabricated Y-splitter device that embeds two spatially separated HHG sources within a single chip, enabling far-field EUV interference. In parallel, a common-path temporal interferometer based on the Translating-Wedge-based Identical pulses eNcoding System (TWINS) is employed to generate phase-locked infrared pulse replicas with attosecond delay control. These tools enable stable delay scans and provide the basis for phase-resolved HHG measurements (Figure 2).

The interferometric capabilities of the microfluidic platform are exploited for polarization-sensitive in-situ HHG spectroscopy as well as for integrated EUV beam conditioning and lithographic demonstrations. Using orthogonally polarized, phase-locked 800 nm pulse replicas generated in a common-path configuration, delay-resolved HHG measurements in argon reveal clear dynamical signatures of the 3p Cooper minimum, including persistent spectral suppression, modulation broadening, and a dispersive phase anomaly corresponding to an effective group-delay excursion of approximately 200–250 attoseconds (Figure 3). In parallel, the microfluidic approach is extended to chip-integrated EUV beam filtering through a geometry-based infrared rejection scheme that suppresses the co-propagating infrared driving field while preserving EUV transmission, achieving an XUV transmission efficiency of approximately 30% without relying on external thin-film filters. Building on this integrated filtering capability, a proof-of-principle EUV lithography experiment is demonstrated, including controlled exposure and interference-pattern imprinting using an integrated EUV interferometer, thereby highlighting the potential of microfluidic HHG devices as compact, stable, and multifunctional sources for coherent EUV/XUV photonics, phase-sensitive ultrafast spectroscopy, and laboratory-scale lithographic applicati.

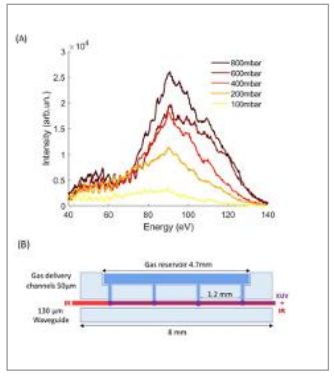

Fig.1 - (A) Generated XUV signal for HHG in He with 800nm driving pulses for various pressures of helium injected in the microfluidic device. (B) Schematic of the microfluidic device

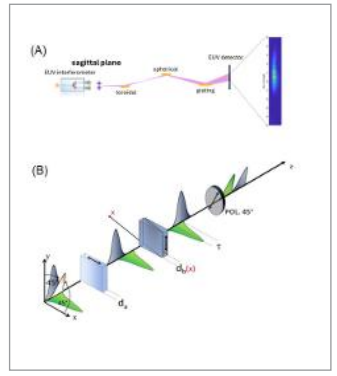

Fig.2 - A) Experimental setup for the characterization of the EUV integrated interferometer. (B) Working principle of the birefringence-based TWINS interferometer

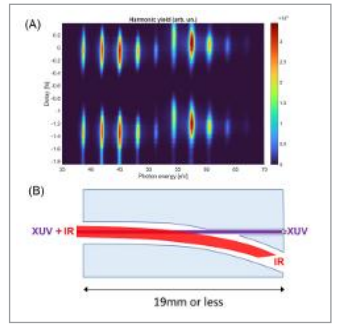

Fig.3 - A) Delay-resolved high-harmonic generation (HHG) spectrogram in argon, showing the harmonic yield as a function of photon energy and relative delay. (B) schematic of the microfluidic device used for infrared filtration, shown from the side

ADVANCED METHODS IN TIME-DOMAIN DIFFUSE OPTICS FOR BIOMEDICAL APPLICATIONS

Abhirami Krishnan - Supervisor: Antonio Pifferi

Time-domain diffuse optical spectroscopy (TD-DOS) is a non-invasive optical technique for the quantitative characterization of highly scattering media, such as biological tissues. It is based on the detection and analysis of the temporal distribution of photons after multiple scattering and absorption events within the medium. By measuring the time-of-flight of detected photons, TD-DOS enables the independent retrieval of tissue absorption and reduced scattering coefficients, while providing intrinsic sensitivity to probing depth. These features make TD-DOS particularly well suited for biomedical applications, including functional tissue monitoring, tissue oximetry, and diffuse optical tomography.

Although TD-DOS has demonstrated strong potential in both research and clinical contexts, current implementations are often limited by two main factors: the relatively small number of detection channels that can be operated simultaneously and the restricted spectral range typically confined to the near- infrared region. This doctoral research addresses both limitations by developing advanced time-domain methods aimed at improving scalability in multichannel detection and extending spectral coverage, while preserving quantitative accuracy and depth sensitivity.

The first part of this work focuses on increasing the effective number of detection channels in TD-DOS systems based on time-correlated single-photon counting (TCSPC). Modern TCSPC electronics offer excellent temporal resolution and high sensitivity, but their architecture usually limits the number of available hardware input channels. This constraint restricts the number of detectors that can be connected simultaneously and therefore limits spatial sampling, multi-distance measurements, and broadband acquisition.

To overcome this bottleneck, a delay- based multiplexing strategy was developed, in which signals from multiple detectors are encoded using controlled electrical delays and acquired through a reduced number of TCSPC inputs. Detector identity is then reconstructed in post-processing by comparing photon arrival times to a reference signal. This approach allows several detectors to share the same timing electronics, effectively multiplying the number of acquisition channels without significantly increasing system complexity. The multiplexed TD-DOS system was validated through a comprehensive experimental and numerical study. Ground-truth measurements, Monte Carlo simulations, and standardized phantom experiments following the MEDPHOT protocol were used to assess reconstruction accuracy, linearity, and cross-talk between channels. The results demonstrate that individual detector time-of-flight distributions can be reliably reconstructed and that accurate optical property estimates are preserved when using multiplexed detection. Additional in vivo measurements further confirmed the robustness and applicability of the method under realistic experimental conditions.

The second major contribution of this thesis is the extension of TD-DOS into the short-wave infrared (SWIR) spectral region, up to 1700 nm. The SWIR range provides access to strong and distinct absorption features of key tissue constituents such as water, lipids, and collagen, which are only partially accessible in the conventional near-infrared window. By combining a broadband supercontinuum light source with single-photon detectors optimized for longer wavelengths, time-resolved measurements were performed on phantoms, real samples, and in vivo tissues. These studies demonstrated enhanced spectral contrast and improved sensitivity to tissue composition and structure, highlighting the added value of SWIR time-domain measurements.

Finally, the developed methods were applied to multiwavelength and time- resolved monitoring of physiological processes, including thermal perturbations and cold-induced stimulation. The results illustrate the capability of TD-DOS to capture functional and depth-dependent changes in tissue properties over time, reinforcing its potential for dynamic and non-invasive tissue assessment.

Overall, this doctoral research advances the state of the art in time-domain diffuse optics by introducing scalable multichannel detection strategies and extending quantitative measurements into the SWIR region. As photon-counting detectors, broadband light sources, and data analysis methods continue to evolve, the approaches developed in this work contribute toward more versatile, depth- resolved, and information-rich optical tools with strong potential for future biomedical and clinical applications.

FEW-FEMTOSECOND UV–XUV TIME-RESOLVED PHOTOELECTRON SPECTROSCOPY OF ORGANIC MOLECULES

Lorenzo Mai - Supervisor: Maurizio Reduzzi

Photoinduced processes determine how organic molecules convert absorbed light into function, underpinning applications in light harvesting, sensing, and molecular optoelectronics. For many organic chromophores, the strongest absorption bands lie in the ultraviolet (UV), where excitation accesses highly reactive regions of the excited-state energy landscape and multiple relaxation pathways compete on ultrafast timescales. Within the first few femtoseconds after excitation (1 fs = 10^{-15} s), electron density reorganizes while nuclear motion begins, and their interplay drives the system across the excited-state landscape toward a specific photochemical outcome. In this regime, electronic and nuclear motion are strongly coupled, and resolving their earliest evolution is essential because it determines how relaxation pathways branch at conical intersections and ultimately shapes the molecular response. Capturing such dynamics experimentally is challenging due to the extreme temporal resolution required. This thesis addresses this challenge within the TOMATTO project by employing UV–XUV time-resolved photoelectron spectroscopy (TRPES) on organic molecules of optoelectronic relevance. A UV laser pulse initiates the dynamics, and an extreme-ultraviolet (XUV) laser pulse ionizes the molecules at controlled time delays: the resulting photoelectron spectra provide a snapshot of the evolving molecular wavepacket. The work exploits two complementary UV-XUV TRPES setups: the first offers a compromise between temporal and spectral resolution, enabling population flow between electronic states to be mapped with ~20 fs resolution; the second setup pushes the temporal resolution to the few-femtosecond limit (~3 fs), allowing even faster details to be resolved directly, including coherent vibrational wavepackets and extremely rapid changes in electronic character.

A first case study is acetylacetone, a prototypical polyatomic system for nonadiabatic relaxation. Combining both beamlines with theoretical support allows a study of its ultrafast dynamics with unprecedented detail. With ~20 fs resolution we extract the dominant relaxation timescales and the main vibrational coherences initiated by UV excitation, while the ~3 fs measurement captures the details at the onset of population redistribution. Together, the data map onto the mechanism in Fig. 1, in which nuclear motion drives rapid branching through successive conical-intersection passages that imprint distinct signatures in the TRPES observables.

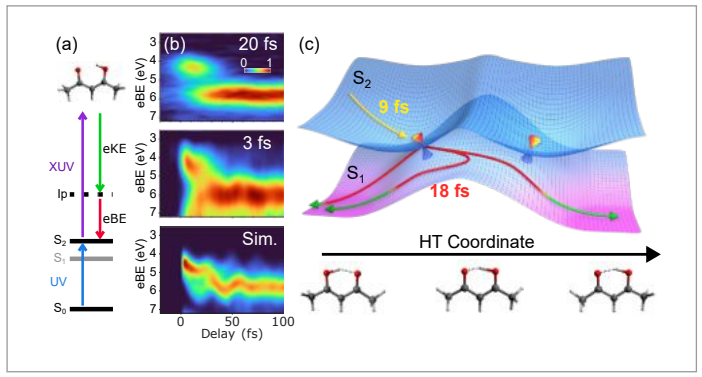

Fig.1 - UV–XUV TRPES of acetylacetone. (a) UV pump–XUV probe ionization scheme. (b) Time–energy maps at 20 fs and 3 fs resolution (and simulation), showing the onset of relaxation and vibronic motion. (c) Schematic excited-state landscape summarizing the early-time relaxation mechanism

The thesis then turns to chemical control of these ultrafast processes by using aldehyde (-CHO) substitution as a simple, systematic handle to tune the earliest relaxation steps after UV excitation via UV-XUV TRPES across families of aromatic and heteroaromatic chromophores. Across the series studied - including aldehydes of benzene, furan, pyrrole and thiophene - a consistent spectroscopic motif emerges: the aldehyde group redirects population away from short-lived, often dissociative dynamics typical of the parent molecules and into a more persistent excited-state channel, consistent with a photoprotective role across different molecular backbones.
As an emblematic example, the thiophene series (Fig. 2) shows how aldehyde functionalization reshapes early-time relaxation. In thiophene, UV excitation leads to short-lived dynamics on ring-centered states; upon -CHO substitution a distinct, long-lived photoelectron signature appears, consistent with rapid population transfer into an aldehyde-centered excited-state pathway. The efficiency of this transfer depends on the substitution position, directly linking formylation to a measurable change in early-time pathway selection that propagates to longer-time dynamics.
Overall, the thesis delivers an experimentally supported set of principles for steering ultrafast nonradiative relaxation in organic molecules. It shows that access to the few-femtosecond regime is essential to disentangle coupled vibronic motion and rapid electronic reordering, and it demonstrates that targeted functionalization - especially aldehyde substitution - can bias early-time pathway selection toward specific outcomes. These insights provide a foundation for extending UV-XUV TRPES to larger functional motifs relevant to organic optoelectronics, where controlling ultrafast pathway selection can become a practical design lever for improving performance and stability.

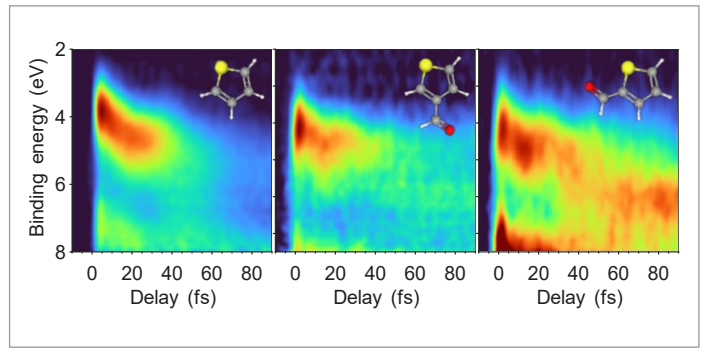

Fig.2 - Aldehyde (-CHO) functionalization reshapes early UV-excited dynamics in thiophene and thiophene aldehydes: comparative UV-XUV TRPES maps show rapid transfer from short-lived ring-centered states into a longer-lived carbonyl-centered channel, with efficiency controlled by substituent position

BLISTERS IN INTERCALATED HOPG: MECHANICAL PROPERTIES OF INDIVIDUAL STRUCTURES STUDIED BY COMBINED HIGH-RESOLUTION MICROSCOPY AND SPECTROSCOPY

Marco Menegazzo - Supervisors: Gianlorenzo Bussetti, Andrea Li Bassi

Blisters and bubbles are recurrent morphological features in layered van der Waals materials and are commonly regarded as defects originating from interfacial contamination, gas evolution, or electrochemical processes. While pressurized bubbles in atomically thin membranes such as graphene have progressively been recognized as model systems for membrane mechanics and strain engineering, analogous structures formed within bulk layered crystals have rarely been investigated as individual mechanical systems. In electrochemically intercalated highly oriented pyrolytic graphite (HOPG), blisters are typically treated as secondary morphological consequences of intercalation rather than objects possessing their own mechanical identity.

This thesis focuses on blisters formed in electrochemically intercalated HOPG and investigates their mechanical properties at the level of individual structures. Electrochemical intercalation in acidic media induces localized swelling of the upper graphite layers, leading to the formation of blisters with micrometric radii (typically between 1 and 2 µm) and heights of several tens of nanometres, around 100 nm.

These geometrical parameters make them ideal candidates for quantitative mechanical and spectroscopic investigation. Atomic force microscopy (AFM) provides high-resolution topographic reconstruction of individual blisters, allowing accurate determination of radius and height. Beyond imaging, AFM nanoindentation experiments quantify their elastic response. The effective Young's modulus extracted from the indentation curves is significantly lower than that of bulk graphite, decreasing from values on the order of ~100 GPa for the pristine basal plane to the range of 1–10 MPa for blistered regions. This strong reduction indicates that the swollen graphite layers behave as compliant membranes rather than as rigid bulk material.

Through AFM, it was also possible to probe their mechanical nature via controlled manipulation experiments. By deliberately pushing blisters laterally with the AFM tip, it is possible to displace them across the surface. In further experiments, blisters were mechanically cut by scanning the tip along a defined path. After cutting, the swollen region collapses and the basal plane underneath shows no residual topographic trace of permanent damage. These observations demonstrate that blister formation corresponds to elastic deformation of confined graphite layers.

The central part of the thesis is the development of a correlative AFM–Raman approach in which morphology and vibrational response are measured on the same region within a combined experimental setup. Raman spectroscopy probes the characteristic vibrational modes of graphite, in particular the G band (associated with in-plane optical phonons) and the 2D band (second-order overtone sensitive to electronic and structural properties). By acquiring Raman maps directly over AFM-characterized areas, a pixel-to-pixel correspondence between topography and Raman signal is achieved. This direct spatial correlation is essential for assigning spectroscopic features specifically to individual blisters. A statistical analysis performed over multiple blisters shows that both G and 2D bands systematically exhibit a redshift relative to the surrounding pristine basal plane. Comparison with literature on graphene and few-layer systems indicates that such redshifts are consistent with tensile strain. The internal strain is independently estimated from blister morphology measured by AFM, using a spherical-cap model that relates curvature to tensile deformation. When the strain calculated from geometry is compared to the Raman shift, a clear linear relationship emerges: larger geometrical strain corresponds to larger redshift. This statistical correlation establishes that, in these structures, the redshift is a direct signature of tensile strain.

Once this redshift–strain equivalence is established at the micrometric scale, tip-enhanced Raman spectroscopy (TERS) is employed to probe the local vibrational response within single blisters at sub-diffraction resolution. TERS measurements reveal that the Raman shift already differs from that of the surrounding basal plane at the blister perimeter, indicating that boundary conditions impose modified strain states even at the edge. Moving progressively toward the centre of the blister, the redshift increases, reaching its maximum at the apex.

By combining quantitative AFM mechanics, statistically validated AFM–Raman correlation, and nanoscale TERS mapping, this thesis demonstrates that HOPG blisters behave as confined pressurized membranes embedded within a bulk graphite crystal. This reinterpretation shifts their status from accidental defects to mechanically meaningful subsystems and provides a consistent framework for understanding strain localization and membrane behaviour in multilayer van der Waals materials.

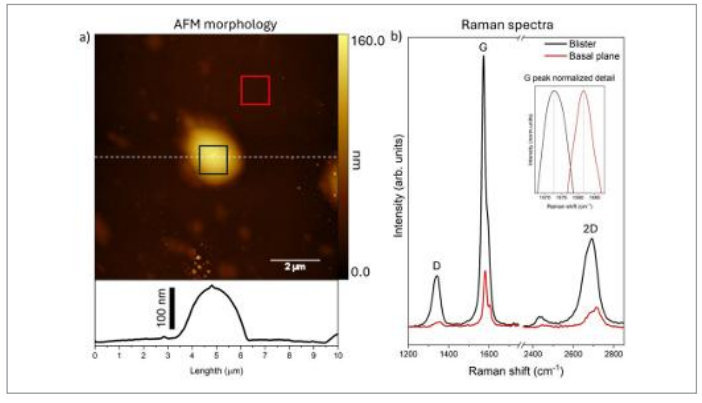

Fig.1 - a) AFM scan of a blister b) Raman spectrum of the selected regions

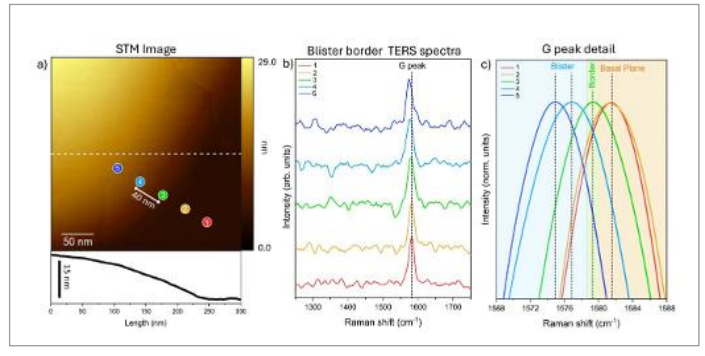

Fig.2 - a) STM image of the border of the blister, the number in the circle indicates the position of the respective TERS spectra, V_{bias} = 0.1 V, I_T = 900 pA. b) full TERS spectra of the 5 point indicate in panel a. c) Detail of the G peak presented in panel b

CHARGE DENSITY WAVE PHASES ACROSS DIFFERENT DIMENSIONALITIES: AN EQUILIBRIUM AND TIME-RESOLVED ARPES STUDY

Niccolò Mignani - Supervisor: Ettore Carpene

A Charge Density Wave (CDW) is a broken-symmetry phase characterized by the low temperature stabilization of a periodic lattice distortion (PLD) through the opening of energy gaps at the Fermi level, and by a periodic spatial modulation of the electronic density. It was theoretically predicted long before any experimental observation by R. E. Peierls. The Peierls model describes the CDW phase transition for a one-dimensional metallic chain of atoms but fails whenever systems with higher dimensionality are considered.
However, CDWs are experimentally observed in many materials: in quasi-one-dimensional systems (q1D) such as Transition Metal Trichalcogenides (TMT), blue bronzes and Krogmann salts; but also in bi-dimensional materials (2D) such as Transition Metal Dichalcogenides (TMD), high temperature superconductors (cuprates) and Kagome metals. Many of the q1D systems can be understood within the one-dimensional Peierls model, while 2D CDWs challenge this simple picture and require different theoretical explanations. In general, there is agreement in saying that a strong momentum dependent electron-phonon coupling is needed to stabilize CDW phases, but their origin is still largely debated. This delicate relation between the electrons and the lattice is ultimately what has fascinated scientists for more than fifty years.
In this thesis, I present our investigation of the CDW phase of two materials with different dimensionality: $ZrTe_3$, a TMT with q1D properties, and 1T-$TaSe_2$, a TMD with 2D character; mainly employing photoemission spectroscopy.
Angular Resolved Photoemission Spectroscopy (ARPES) is a powerful technique: by shining ultraviolet light on the sample and measuring energy and emission angle of the photoemitted electrons, ARPES can detect the electronic structure of the material with energy and momentum resolutions, revealing its evolution across the CDW phase transition. Time-resolved-ARPES (trARPES) also allows to investigate the electronic dynamics and helps separating in the time domain the different degrees of freedom involved in the phase transition. Fig.1 schematically represents the trARPES technique, which exploits the so-called pump-probe scheme. Two ultrashort laser pulses are employed: the pump drives the investigated material out of equilibrium, while the probe photoemits electrons. By varying the delay between them it is possible to reconstruct the full excitation-relaxation dynamics of the system. We complemented photoemission measurements with broadband time-resolved optical reflectivity (trOR) measurements and Density Functional Theory (DFT) calculations.

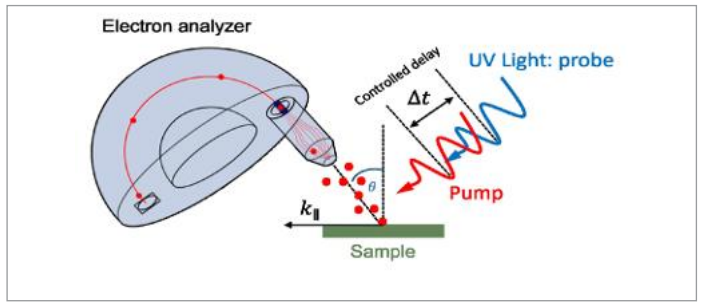

Fig.1 - Schematic representation of a trARPES experiment. The pump pulse excites the material, and the probe pulse induces photoemission at a controlled delay. The momentum and energy of the photoelectrons are measured by the analyzer.

The first material presented is $ZrTe_3$, which belongs to the family of transition metal trichalcogenides, a group of compounds that share a similar crystal structure and q1D properties. They have MX_3 formula units with M being a transition metal (Ti, Zr, Nb, Hf and Ta), and X a chalcogen atom (S, Se and Te). They are made of weakly bound one-dimensional prismatic chains along the b-axis direction. $ZrTe_3$ is a unique member because its Fermi surface comprises both a 3D hole-like pocket centered at Gamma and q1D bands at the Brillouin zone edges, placing this material at the crossroad of different dimensionalities. Extensive ARPES studies have shown that the CDW phase, setting in at 63 K, is compatible with the one-dimensional Peierls model. However, some of the observed changes in the band structure with temperature suggest the need for a larger view. We performed trARPES measurements, revealing interesting dynamical features: i) a transient photo-induced shift of the whole band structure, and (ii) the excitation of coherent oscillations compatible with two A_g phonon modes. Fig.2 shows a trARPES measurement performed with 6 eV probe photon energy that reveals the dynamics of the 3D state around the Gamma point. Our results suggest a strong electron-phonon coupling that plays a central role in CDW formation. Supported by theoretical calculations, we can disentangle the electronic and lattice contributions to the CDW transition.
The second material presented is 1T-$TaSe_2$, which belongs to transition metal dichalcogenides, a wide family of 2D layered materials with formula unit MX_2, where M is a transition metal and X is a chalcogen. The commensurate charge density wave (CCDW) phase of 1T-$TaSe_2$ is predicted to host several quantum states ranging from ID metal to 3D insulator depending on the lateral stacking of the layers. By means of ARPES with micrometer spatial resolution, we studied the charge-ordered 1T-$TaSe_2$, revealing the co-existence of metallic and insulating domains, as shown in Fig.3. Our investigation clarifies that metallicity is due to a specific lateral sliding of the CCDW layers, while insulating behaviour is driven by surface interlayer dimerization.

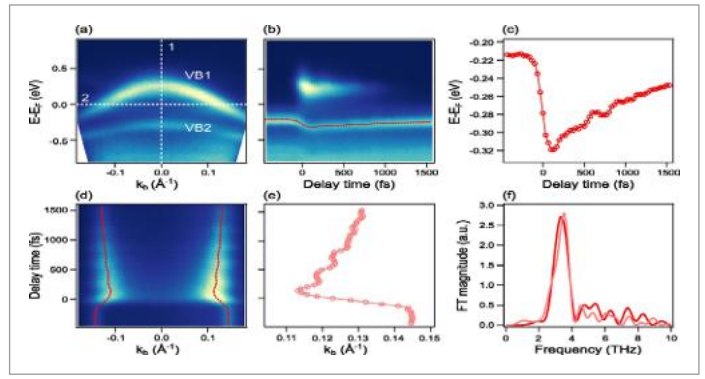

Fig.2 - TrARPES measurement on $ZrTe_3$ with probe photon energy 6 eV around the Gamma point. (a) Out of equilibrium band dispersion at Gamma, measured at a temporal delay of 150 fs. (b) Temporal evolution of photoemission along a vertical cut extracted at Gamma (cut 1 in (a)). The red dots are the peak positions of VB2 at each time delay obtained from Gaussian fits; shown in more detail in (c). (d) Temporal evolution of photoemission along a horizontal cut extracted at EF (cut 2, in (a)). The red dots are the peak positions of VB1 at each time delay obtained from Lorentzian fits; shown in more detail in (e). (f) Fourier Transform (FT) analysis of the oscillations observed in the bands positions dynamics, both in energy (red) and momentum (pink)

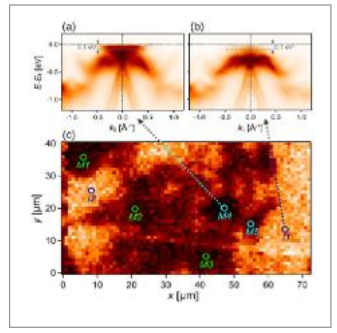

Fig.3 - NanoARPES measurements taken with 90 eV probe photon energy in two different domains on the same sample: (a) on a metallic region, (b) on an insulating one. (c) ARPES spatial map (lateral steps of 1 µm): the color contrast is obtained by integrating the photoemission intensity between 0 and 100 meV binding energy. Dark (metallic) domains are labeled M1-M5 and bright (insulating) domains are labeled I1-I2.

DIFFUSE OPTICS FOR THE CLINIC: TECHNIQUES, ANALYSIS AND DEVICE ENGINEERING IN MUSCLE AGING

Marco Nabacino - Supervisor: Caterina Amendola

Biomedical optics uses light to investigate the structure and function of biological tissues in a non-invasive and safe manner. By delivering near-infrared light into tissue and analyzing the returning photons, it is possible to extract quantitative information about blood oxygenation, microvascular perfusion, and cellular metabolism. Thanks to its portability, relatively low cost, and use of non-ionizing radiation, optical technology is particularly attractive for bedside monitoring and longitudinal studies in both clinical and physiological research.

The thesis work focuses on two complementary diffuse optical techniques: time-domain near-infrared spectroscopy (TD NIRS), which quantifies hemoglobin concentration and tissue oxygenation, and diffuse correlation spectroscopy (DCS), which measures microvascular blood flow by analyzing temporal fluctuations of scattered light. When combined, these methods provide a more complete description of tissue hemodynamics and oxidative metabolism than either technique alone.

A central application explored in this work is skeletal muscle aging. With increasing age, muscle structure and function change, affecting mobility, metabolic health, and overall quality of life. Traditional approaches to studying muscle metabolism often rely on invasive biopsies and laboratory assays. In contrast, optical techniques enable repeated in-vivo measurements, opening the possibility of monitoring physiological processes over time without tissue removal.

Part of this research was conducted within the Trajector-Age study, a large interdisciplinary project investigating muscle health across the lifespan. Figure 1 shows an example of the experimental setup used during these measurements. Optical probes were placed on the lower limb to monitor muscle oxygenation and blood flow at rest and during controlled vascular occlusion tests. By temporarily interrupting blood supply with an inflatable cuff and then releasing it, it is possible to probe oxygen consumption and vascular reactivity in a dynamic and reproducible way.

An example of the hemodynamic signals recorded during such an arterial occlusion is shown in Figure 2. The characteristic decrease in oxygenation during ischemia, followed by a rapid hyperemic response upon cuff release, provides insight into muscle oxidative metabolism and microvascular function. However, the analysis also revealed important methodological challenges. In particular, the thickness of the superficial adipose tissue layer strongly influences optical measurements, potentially masking subtle physiological differences between individuals. These findings highlight both the potential and the limitations of current optical approaches in heterogeneous human tissues.

To address these challenges, the thesis combines translational research with technological and methodological innovation. A novel hybrid TD NIRS and DCS device was designed, assembled, and thoroughly characterized using calibrated optical phantoms and in-vivo measurements.

The system demonstrated high stability and reproducibility, supporting its suitability for long clinical studies. Particular attention was devoted to depth sensitivity and signal quality, two key aspects when probing layered tissues such as skeletal muscle.

Beyond hardware development, substantial effort was devoted to improving data analysis. For TD NIRS, advanced modeling strategies were developed to mitigate biases introduced by the common assumption of tissue homogeneity. Using Monte Carlo simulations and experimental validation, correction schemes were proposed to reduce the influence of superficial layers and extend the range of reliable measurements.

These methods enhance the physiological interpretability of optical biomarkers, especially in populations with variable adipose tissue thickness.

For DCS, one of the main limitations is intrinsically low signal-to-noise ratio, which can obscure subtle flow dynamics.

To overcome this constraint without modifying hardware, a deep-learning-based denoising framework was developed. Instead of directly predicting blood flow, the approach reconstructs the underlying autocorrelation function from noisy measurements, preserving compatibility with established analysis models. Figure 3 illustrates an example of ground truth, noisy, and probabilistically denoised autocorrelation curves, highlighting the substantial improvement in signal quality and the associated uncertainty estimates.

Together, the thesis's contributions advance diffuse optical techniques along three complementary dimensions: instrumentation, quantitative modeling, and data-driven signal enhancement. By confronting practical limitations such as tissue heterogeneity and measurement noise, this work strengthens the reliability and translational potential of TD NIRS and DCS for studying skeletal muscle aging.

More broadly, the results support the role of biomedical optics as a powerful, non-invasive window into human physiology. With continued methodological refinement and integration with complementary clinical data, optical technologies hold promise for improving our understanding of muscle health, aging, and adaptation across the lifespan.

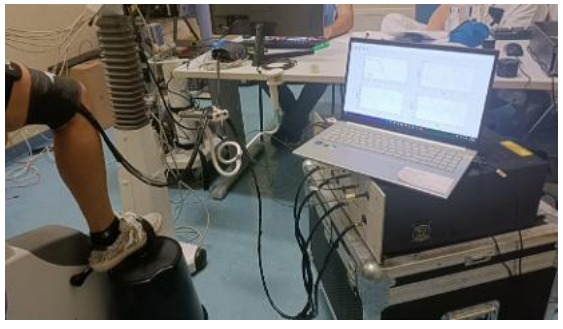

Fig.1 - Picture of the measurement setup. The participants sit on the cycle ergometer, with their right leg in a fixed, relaxed position. The optical probe is attached to the leg via black auto-adhesive bandage, allowing to measure oxygenation and blood flow. The pneumatic cuff placed on the proximal end of the thigh is used to induce arterial occlusions

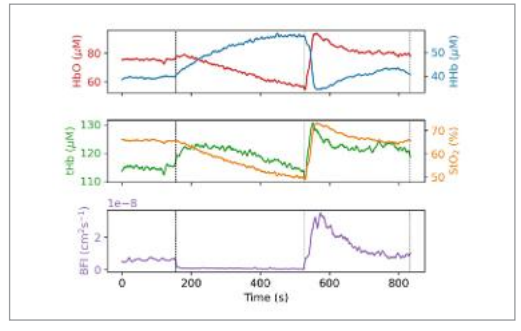

Fig.2 - Examples of time courses of the hemodynamic parameters measured during an arterial occlusion. HbO2: oxygenated hemoglobin concentration; HHb: deoxygenated hemoglobin concentration; tHb: total hemoglobin concentration; StO2: tissue oxygen saturation; BFI: blood flow index

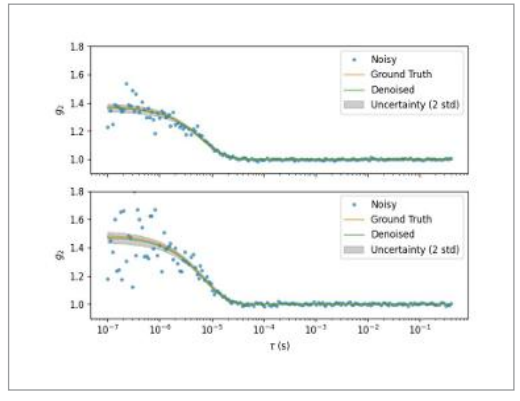

Fig.3 - Examples ground-truth, noisy, and denoised autocorrelation curves using the developed deep-learning model

ANISOTROPY, SURFACE PHOTOVOLTAGE EFFECT AND BAND GAP RENORMALIZATION IN II–V SEMICONDUCTOR, ZNAS2

Tarakameh Samani Narges - Supervisor: Alberto Crepaldi

This thesis investigates how crystallographic anisotropy controls equilibrium band dispersion and nonequilibrium photoinduced phenomena in the low-symmetry II–V semiconductor $ZnAs_2$. The experimental core combines equilibrium angle-resolved photoemission spectroscopy (ARPES), time-resolved ARPES (tr-ARPES), and pump–probe reflectivity. A central objective is to separate intrinsic, interaction-driven modifications of quasiparticle energies from extrinsic shifts of the measured binding energy scale that arise from near-surface electrostatics, including band bending and its photoinduced modification.
Equilibrium ARPES maps the occupied valence band manifold of $ZnAs_2$ and demonstrates that its pronounced macroscopic anisotropy originates from intrinsically anisotropic in-plane dispersion. Cleaved single crystals are oriented by Laue diffraction and measured along inequivalent crystallographic directions. A photon-energy scan between 18 and 200 eV reveals a reproducible periodicity of spectral features with photon energy, enabling repeated high-symmetry points to be identified and providing a controlled sampling of the three-dimensional Brillouin zone and clarifying which spectral variations reflect k-perpendicular dispersion and which reflect photoemission matrix elements. Within the surface plane, ARPES directly resolves markedly different dispersions along Γ–B and Γ–Z. The two directions exhibit distinct band curvatures, bandwidths, and velocities, implying strongly direction-dependent effective masses near the band edge. The anisotropy is therefore not merely a difference in spectral weight but a difference in the underlying energy–momentum relation. Polarization-dependent measurements show pronounced matrix-element selectivity: by switching between s and p polarization and by changing the measurement geometry, entire dispersions can be enhanced or suppressed in a symmetry-selective manner. The results are shown in Fig.1.
Time-resolved ARPES resolves the nonequilibrium carrier distribution and transient energy landscape after ultrafast optical excitation. Using a 6 eV probe and, independently, a high-harmonic-generation probe, the measurements access transient populations in previously unoccupied states together with hole depletion near the valence-band maximum. The pump produces a rapid redistribution of carriers in energy and momentum, followed by slower relaxation toward the band extrema. A key result is the identification and characterization of a surface photovoltage (SPV) response in $ZnAs_2$ that dominates the apparent energy motion of spectra if not corrected.
Under excitation, the near-surface electrostatic potential is modified by photoinduced charge separation in the space-charge region, producing an approximately rigid shift of spectral features in binding energy. In tr-ARPES this electrostatic shift appears as a concerted motion of valence and conduction features and can persist beyond the timescale of electronic thermalization. A characteristic negative-delay contribution further indicates that the pump-induced field can act on photoelectrons during propagation, reinforcing that the observed shift is electrostatic rather than a true pre-pump band-structure change.
After isolating the rigid SPV contribution, tr-ARPES reveals an additional, non-rigid modification of the near-gap electronic structure at higher excitation densities. In this regime, the relative separation between near-edge valence and conduction states changes transiently, providing direct evidence for carrier-induced many-body band-gap renormalization (BGR). The observed gap reduction is consistent with a dense photoexcited electron–hole plasma that enhances screening and modifies exchange-correlation contributions to the electronic self-energy.
Polarization-resolved pump–probe reflectivity provides an independent view of the same nonequilibrium physics through the transient dielectric response and confirms strong direction dependence of the photoinduced dynamics. Reflectivity transients recorded for inequivalent in-plane polarizations show distinct amplitudes and spectral fingerprints, mirroring the anisotropy observed in momentum-resolved photoemission. The transient optical conductivity is extracted using a Kramers–Kronig-consistent Drude–Lorentz parameterization, which captures intraband contributions from mobile photocarriers and interband resonance shifts near the absorption edge.
The reflectivity analysis further resolves how spectral weight is redistributed in time and with pump fluence. Photoexcitation introduces an intraband contribution consistent with a transient population of mobile carriers, while interband structures shift and broaden, indicating that both transition energies and effective damping evolve during relaxation. Tracking these parameters versus fluence shows that the response strengthens with excitation density and that recovery becomes slower, consistent with carrier-density-controlled screening and with space-charge dynamics that also drive SPV.
Across the datasets, phase-space effects are separated from genuine band-edge motion: Burstein–Moss filling reshapes near-edge optical response through Pauli blocking, while BGR shifts the quasiparticle edges themselves. This prevents misreading intensity changes as gap shifts now. Finally, measurements and analysis on the related semiconductor $CdGeAs_2$ provide a comparative reference for how composition and crystal symmetry alter near-gap optical and electronic response. This comparison highlights which ultrafast signatures are generic to polar semiconductors and which are amplified by the exceptionally strong in-plane anisotropy of $ZnAs_2$.
Overall, this work establishes $ZnAs_2$ as a benchmark bulk anisotropic semiconductor where intrinsic crystal symmetry, rather than reduced dimensionality or substrate coupling, sets both equilibrium dispersion and ultrafast response. The main outcomes are: (i) direct experimental confirmation of strong in-plane anisotropy of the band dispersion together with polarization-selective orbital visibility; (ii) identification of a sizable SPV response that rigidly shifts tr-ARPES spectra and produces negative-delay signatures; and (iii) observation of a carrier-density-dependent renormalization of the near-gap electronic structure consistent with many-body BGR.

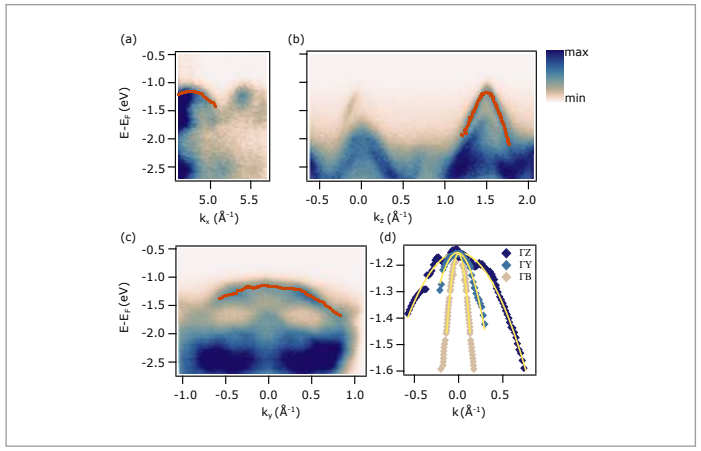

Fig.1 - (a-c) ARPES dispersions along kx, kz, and ky, respectively, with peak positions overlaid in red. (d) Compilation of the extracted points from all three directions with quadratic fits (yellow) used to determine the directional effective masses. The markedly different curvatures, steep along kz and flat along ky, yield a very large in-plane anisotropy

METHODOLOGICAL AND INSTRUMENTAL DEVELOPMENTS TOWARD RELIABLE AND UNBIASED HYBRID DIFFUSE OPTICS MONITORING OF NEONATAL BRAIN METABOLISM

Fabio Negretti - Supervisor: Davide Contini

During my PhD, I worked at the intersection of theoretical modeling, experimental validation and instrument engineering in the field of Diffuse Optics (DO), with the goal of enabling reliable and clinically meaningful monitoring of cerebral metabolism in preterm neonates. My research focused on Time Domain Near Infrared Spectroscopy (TD-NIRS) and Speckle Contrast Optical Spectroscopy (SCOS), within the European Horizon project PROMETEUS (Preterm Brain-Oxygenation and Metabolic EUSensing).

Diffuse Optics and multimodal monitoring

DO aims at non-invasively retrieving physiological information from biological tissues by exploiting photon migration driven by light absorption and scattering. In most practical configurations, light is injected and collected on the same side of the sample, as multiple scattering events allow photons to diffuse back toward the surface. Absorption encodes chromophore concentrations and enables quantitative spectroscopy through multi-wavelength measurements. In TD-NIRS, short picosecond pulses are injected and the broadened, attenuated and temporally shifted temporal signal is analyzed to recover both absorption and reduced scattering coefficients from a single measurement, with depth sensitivity encoded in photon arrival times. In this work, TD-NIRS at 685 and 830 nm was used to retrieve tissue oxygenation in terms of absolute concentrations of oxygenated and deoxygenated hemoglobin and tissue oxygen saturation, starting from the recovered absorption coefficients. SCOS is a relatively recent DO technique that measures deep tissue blood flow dynamics by exploiting intensity fluctuations of coherent light caused by microscopic motion of red blood cells. In its continuous-wave implementation, coherent laser light is injected and the resulting speckle pattern is imaged on a pixelated camera. Statistical analysis of the speckle frames, in space and/or time, provides a surrogate measure of blood flow. Since no single technique provides a complete physiological picture, this work promotes multimodality: combining TD-NIRS and SCOS enables simultaneous access to oxygenation and perfusion, thus to the full metabolic picture.

Efficient Monte Carlo–based modeling for two-layer media

The first research line addressed accurate modeling of photon migration in layered, heterogeneous media, a key requirement for quantitative TD-NIRS. The head is intrinsically stratified, with superficial layers and deeper brain regions exhibiting different optical properties. Although Monte Carlo (MC) simulations are the gold standard for modeling light transport in complex domains, their computational and storage demands are typically incompatible with real-time fitting of optical parameters.

To overcome this limitation, I validated a heuristic forward model for two-layer geometries based on scaling time-resolved white MC simulations. Instead of storing all simulated photon pathlengths in both layers, only average partial pathlengths within each temporal bin of the temporal point spread function are retained. This significantly reduces memory usage and computational time, making the approach suitable for inversion frameworks.

Extensive benchmarking against ground-truth MC simulations was performed over wide ranges of absorption, scattering, and layer thicknesses. The method shows near-perfect agreement at early photon arrival times and controlled deviations at late times, becoming relevant only under extreme differences in optical properties between layers. The model supports look-up-table-based inversion and enables more realistic multilayer fitting in controlled in-vivo scenarios while preserving computational feasibility.

Experimental validation of TD-NIRS robustness to skin pigmentation

The second branch of my work focused on the robustness and equity of TD-NIRS with respect to skin pigmentation. Recent evidence of systematic errors in pulse oximetry for individuals with darker skin tones highlighted the need to verify that optical technologies do not introduce unintended bias, especially in neonatal care.

Within a multidisciplinary consortium, I designed a reproducible methodology for fabricating thin skin-mimicking phantoms with controlled melanin-like absorption, based on silicone matrices doped with nigrosin. I defined standardized fabrication protocols and implemented their practical realization.

These phantoms were used in a structured validation campaign including static measurements on calibrated bulk phantoms, in-vivo measurements on volunteers at rest and dynamic arterial occlusion protocols.

The combined evidence demonstrated that strong absorption changes confined to a thin superficial layer have negligible impact on retrieved hemoglobin concentrations and tissue oxygen saturation. This confirms that TD-NIRS, thanks to its time-resolved nature and reduced sensitivity to superficial layers, is intrinsically robust against pigmentation-related bias, reinforcing its suitability as an equitable monitoring technology for clinical use.

PROMETEUS and development of the Neo-opticap hybrid instrument

The most applied component of my PhD was the realization of Neo-opticap, a six-channel hybrid TD-NIRS + SCOS instrument developed within PROMETEUS for continuous, non-invasive monitoring of preterm brain metabolism in the neonatal intensive care unit. The system retrieves cerebral oxygenation and blood flow, enabling estimation of an index of the cerebral metabolic rate of oxygen to support personalized nutritional strategies. My role covered the full development pipeline. I conceived the system architecture, balancing clinical requirements, performance targets and cost constraints. To limit detection-chain complexity and cost, a sequential architecture based on optical switching for both injection and detection was adopted, enabling spatial and temporal multiplexing with a reduced number of sources and detectors. I characterized commercial modules and developed custom solutions when necessary, including an in-house 8×1 optical detection switch. I designed and manufactured hybrid optodes optimized for neonatal application, integrating lightweight mechanics, appropriate source–detector separation and safety features. In parallel, I developed the low-level control software for synchronization, measurement execution, real-time preprocessing and bidirectional communication with a medical graphical user interface via structured WebSocket protocols.

A comprehensive characterization followed established community standards. For TD-NIRS, BIP and MEDPHOT protocols assessed responsivity, instrument response function stability, linearity, accuracy, noise behavior, reproducibility and long-term stability across all six channels. For SCOS, dedicated assays evaluated linearity of flow-related parameters, long-term stability and signal-to-noise thresholds for reliable estimation of blood flow. All results were in line with the state of the art. Multi-channel in-vivo functional tests during arterial occlusion demonstrated the capability of the hybrid system to track known oxygenation and perfusion dynamics.

The device can capture metabolic trends evolving on clinically relevant time scales. Its flexible software and modular hardware design allow adaptation to practical constraints of neonatal care, where probe number and positioning may vary.

Conclusions

Overall, my PhD integrates theoretical innovation, rigorous validation and translational instrumentation. By improving multilayer modeling efficiency, demonstrating robustness against pigmentation-related bias and delivering a clinically oriented hybrid device, this work advances reliable, unbiased and quantitative diffuse optical monitoring of neonatal brain metabolism.

PHOTOCEUTIC DEVICES FOR GENE-LESS, SPATIALLY AND TEMPORALLY SELECTIVE EXCITATION OF CELL

Herman Novik - Supervisor: Maria Rosa Antognazza

The possibility to control cellular activity with light is an important goal in bioelectronics, neurotechnology, and biomedical physics. Electrical stimulation has provided effective tools to interact with living tissues, but it often requires electrodes, wiring, or direct physical contact with the biological target. Light offers a different strategy. It can be delivered with high spatial and temporal precision, shaped across selected regions, and applied without direct electrical connection to the cells. Since most mammalian cells do not naturally respond to visible light, a material interface is needed to convert optical excitation into a signal that biological systems can process.

My PhD contribution addressed this challenge through the development and validation of photoceutic devices based on conjugated polymers and hybrid optoelectronic interfaces. The work focused on gene-less optical modulation, meaning that cellular excitation was pursued through engineered materials rather than genetic modification. The main objective was to study how the architecture of photoactive materials influences their interaction with aqueous media, cells, and neural tissue.

The research was centred on organic semiconducting polymers, mainly poly(3-hexylthiophene), known as P3HT, and PCPDTBT. These materials absorb light and can generate local interfacial effects when placed in contact with an electrolyte or a biological environment. Their properties make them attractive for biointerfaces: they are processable as thin films or nanoparticles, compatible with aqueous media, and mechanically softer than many inorganic materials traditionally used in bioelectronics. During the thesis, these polymers were studied in different geometries, including flat thin films, hybrid nanostructured substrates, and polymer nanoparticles.

A first part of the work investigated P3HT thin films deposited on glass or conductive substrates. These samples provided a reproducible platform to study the interface between light, organic semiconductors, electrolytes, and living systems. The films were fabricated and characterized in terms of optical response, thickness, surface properties, and stability in aqueous conditions. This stage established the material basis for later biological experiments, where optical access, tissue compatibility, and stable experimental conditions were essential.

The research was then extended to hybrid nanostructured interfaces developed in collaboration with CNR-IMM. Zinc oxide nanorods and silicon nanowires grown on conductive substrates were coated with P3HT and compared with flat P3HT reference samples. The goal was to evaluate whether the addition of inorganic nanostructures could modify the photoresponse of the polymer interface. Photocurrent measurements, local temperature recordings, and surface-potential experiments showed that the architecture of the substrate influences the intensity and dynamics of the light-induced response. This part of the thesis clarified how material geometry can affect the conversion of light into electrical and thermal signals at the polymer/electrolyte boundary.

A central outcome of the thesis was the biological validation of P3HT-coated substrates in mouse hippocampal slices. This ex vivo model allowed the material to be tested in a more complex neural environment than isolated cell cultures. The experiments focused on neuron-glia communication, with particular attention to astrocyte-mediated signalling. When P3HT-coated glass was illuminated, electrophysiological recordings revealed an increase in the frequency of slow inward currents, which are signals associated with communication between astrocytes and neighbouring neurons. The strength of individual events was not significantly altered, indicating that the material mainly affected how often these signalling events occurred. Control experiments showed that the effect was linked to the P3HT interface and to astrocyte-related signalling pathways, rather than to light exposure alone. This result is important because it demonstrates that a conjugated polymer substrate can translate optical stimulation into a measurable modulation of neuron-glia communication in intact neural tissue. In other words, the work moved beyond material characterization and showed that photoactive organic interfaces can influence a biologically relevant process in the brain.

A complementary part of the thesis explored photoactive polymer nanoparticles, with particular focus on PCPDTBT. Nanoparticles offer a different strategy compared with planar substrates because the active material can be dispersed in water-based media rather than fixed on a surface. PCPDTBT was selected because its absorption extends into the red and near-infrared spectral region, which is relevant for biological applications where deeper light penetration and compatibility with optical imaging are desirable. The nanoparticles were fabricated through a sterile miniemulsion process and characterized as aqueous dispersions suitable for biological use.

Overall, my PhD work contributed to the development of light-addressable biointerfaces for selective cell excitation without genetic modification. The thesis combined material fabrication, optoelectronic characterization, photothermal and surface-potential measurements, biocompatibility assessment, and ex vivo validation. Across these levels, the work showed that conjugated polymer interfaces can convert light into biologically relevant signals and that this effect can be observed in neural tissue through changes in astrocyte-mediated communication.

From a broader perspective, the thesis contributes to organic bioelectronics by extending the use of conjugated polymers from neuronal stimulation to glial modulation and neuron-glia signalling. It also provides a comparative view of how device geometry, from flat films to nanostructured substrates and nanoparticles, affects the interaction between light, material, electrolyte, and cells. These results support future studies on photoceutic platforms for controlled optical modulation of cellular function, with possible applications in neuroscience, biohybrid devices, and experimental tools for studying brain physiology.

A COMBINED *AB INITIO* AND HIGH-THROUGHPUT APPROACH TO FERROIC MATERIALS EXPLORATION

Federico Orlando - Supervisor: Silvia Picozzi

Density Functional Theory (DFT) has been, for over three decades, the standard computational method for predicting materials properties from first principles. Traditionally, DFT has flourished within a "calculation-first", system-by-system framework. Over time, however, this perspective has been complemented by data-oriented, high-throughput strategies, enabling systematic exploration. This paradigm shift has led to the development of extended, standardised materials databases and, more recently, has fostered the integration into computational materials science of Artificial Intelligence techniques, that allow the identification of patterns and trends hardly detectable on a case-by-case basis.

The present research advances materials characterisation by combining the power and accuracy of DFT simulations – embedded where appropriate into automated workflows – with the scalability of high-throughput frameworks. Two families of ferroic systems (displaying at least one emergent property related to magnetic, electric, or mechanical order) are selected as areas of interest, reflecting the intertwining of the theoretical and experimental research lines that shape the intellectual environment behind this project.

The first part of the work addresses the rapidly developing field of two-dimensional (2D) magnetism. For decades, the existence of long-range magnetic order in strictly 2D systems was considered unlikely on fundamental thermodynamic grounds. This view changed in the late 2010s, when experiments reported stable magnetism in monolayers of CrI_3 and $CrGeTe_3$. Since then, many additional compounds have been identified, exhibiting a rich variety of magnetic textures, with potential relevance for spintronic technologies. A central task in understanding these materials is the evaluation of exchange parameters, which collectively determine the nature of the magnetic ordering. These parameters are commonly extracted from DFT using approaches such as the "four-state method", which maps total energies of selected spin configurations onto a Heisenberg-like model Hamiltonian. This technique, however, is typically laborious and multi-step, since each parameter in the model requires four separate DFT calculations, performed in as many independent simulation cells, that also vary depending on the parameter.

To overcome this limitation, we designed AMaRaNTA (Automating Magnetic paRAmeters iN a Tensorial Approach), a Python-based computational workflow that automates the four-state method for 2D magnets. Starting solely from a crystal structure file, AMaRaNTA automatically generates the required simulation cells, submits and monitors calculations on high-performance computing facilities, retrieves total energies, and ultimately extracts exchange parameters.

In its current implementation, the code returns the nearest-neighbour exchange tensor, along with scalar parameters for second- and third-nearest-neighbour interactions and single-ion anisotropy. These form a minimal yet comprehensive set to capture the mechanisms stabilising diverse magnetic textures in 2D materials.

The functionality of AMaRaNTA was validated on a compact dataset of around 30 compounds. The workflow successfully reproduces expected features of well-established 2D magnets, including chromium trihalides (CrX_3, X = Cl, Br, I) and transition-metal dihalides (NiX_2, VX_2, MnX_2). It also captures the unusually strong antiferromagnetic interactions reported for VPS_3 (at the nearest-neighbour level), as well as for $NiPS_3$ and $NiPSe_3$ (at the third-nearest-neighbour level). Beyond this, our screening also predicts previously unreported features in selected systems, including antiferromagnetism in NiF_4Tl_2, sizeable Kitaev-like magnetism in $MnBi_2Te_4$, and antisymmetric Dzyaloshinskii–Moriya interactions in VF_4 and $VAgP_2Se_6$. Altogether, AMaRaNTA provides a robust, systematic and reproducible strategy for extracting exchange parameters in 2D magnets, with clear potential for a large-scale, high-throughput exploration.

The second part of the work is devoted to piezoelectric materials. These systems, in which electric and mechanical degrees of freedom are strongly coupled, have a long history of industrial and technological applications. Today, most such devices rely on lead-based compounds, whose toxicity, however, raises significant human health concerns; research is therefore increasingly directed towards the development of lead-free alternative materials.

A prominent example is the sodium–potassium niobate solid solution $K_xNa_{1-x}NbO_3$ (KNN), a random alloy with the perovskite ABO_3 structure. KNN has attracted significant attention over the past two decades, during which a substantial body of experimental work has provided a general understanding of its composition–temperature phase diagram. By contrast, DFT studies of this system remain limited in number and scope, due to the presence of several competing phases and to the challenges of modelling chemical disorder in random alloys, which require large supercells to accurately capture the multifaceted local environment.

Our contributions originated as theoretical support to the ongoing activity of our in-house experimental collaborators. In this context, we first addressed the experimentally observed tendency of KNN to segregate into Na-rich and K-rich domains. We investigated this behaviour via DFT simulations of idealised, tetragonal KNN systems, thereby disentangling chemical substitution from lattice relaxation effects. Analysis of total energies revealed that the preference for regions of unbalanced composition already emerges at the first-principles level, albeit with a very small associated energy gain.

We then turned to a deeper exploration of how KNN properties evolve with composition. After preliminary validation on the sodium niobate end member, we focused on a specific KNN phase, of monoclinic symmetry and intermediate structural complexity, and examined its behaviour on the Na-rich side of the phase diagram. We unveiled how this phase tends to "breathe" with increasing Na content, undergoing alternating flattening and elongation distortions. Accordingly, the polarisation follows this structural evolution by progressively oscillating around its reference direction. Analysis of the piezoelectric tensors reveals an overall enhancement of the response at intermediate compositions, corresponding to maximal chemical disorder; the same regime also favours polarisation rotation towards the non-polar y axis. These results are in reasonable agreement with the limited DFT literature available; the calculated d_{33} piezoelectric coefficient also shows moderate resemblance to our in-house experimental data, within a specific compositional window. Finally, repeating the energetic stability analysis within the more realistic monoclinic framework, we found that the energy gain associated with decomposition towards the end members increases by an order of magnitude with respect to the idealised tetragonal case; this strengthens our earlier conclusion regarding the intrinsic preference of KNN for non-equimolar compositions. Beyond complementing experimental observations, our investigation contributes to the more ambitious goal of establishing a foundation for a systematic, large-scale DFT survey of KNN across phases and compositions.

TAILORING MAGNETIC ENERGY LANDSCAPES FOR RECONFIGURABLE CHIRAL TEXTURES AND MOIRÉ SUPERSTRUCTURES VIA DIRECT LASER WRITING

Matteo Panzeri - Supervisor: Edoardo Albisetti

The development of energy-efficient, beyond-CMOS computing architectures has identified non-collinear spin textures, such as magnetic skyrmions and domain walls, as promising carriers for next-generation logic-in-memory and neuromorphic technologies. However, the technological implementation of these textures is currently limited by the lack of flexible, non-destructive methods to control their nucleation, stability, and spatial arrangement at the nanoscale. Conventional nanopatterning techniques, such as electron-beam lithography or ion irradiation, typically rely on permanent structural modifications. These irreversible approaches preclude reconfigurability and often degrade the intrinsic material properties required for high-performance spintronic applications.

This thesis introduces a versatile, non-contact platform for the deterministic engineering of magnetic energy landscapes via laser-assisted local field cooling. By utilizing a focused 405 nm continuous-wave laser, we locally heat a magnetic heterostructure near the blocking temperature of its antiferromagnetic layer while applying an external magnetic field. This technique allows for the spatial tailoring of the local exchange bias anisotropy with quantitative precision. To probe the ultimate resolution limits of this methodology, we explored thermally assisted magnetic Scanning Probe Lithography (tam-SPL). While the thermal gradient generated by the scanning probe tip is highly localized, our investigation into low-DMI (Dzyaloshinskii-Moriya interaction) systems revealed that the minimum stable magnetic feature size is intrinsically limited to approximately 300 nm by the width of the magnetic domain walls, rather than the technique itself.

The experimental framework first establishes quantitative control over the exchange anisotropy in a low-DMI stack, specifically Ta/IrMn/Ru/Ta/CoFeB/MgO/Ta. By mapping the spatial switching fields, we demonstrated that the local magnetic energy density can be continuously tuned, allowing for grayscale magnetic patterning. This capability was utilized to create complex remanent states, illustrated by a "Gradient Tree" structure (Figure 1). These programmed gradients generate continuous variations in the local switching fields, dictating the nucleation and propagation of domain walls without physical boundaries. We further exploited this control to demonstrate functional static encoding, creating multi-level magnetic QR codes with field-gated readability, where information becomes accessible only within specific external magnetic field windows.

This methodology was also extended to a high-DMI Ta/Pt/Co/NiFe/IrMn/Pt heterostructure engineered to host chiral spin textures at room temperature. By locally tuning the exchange bias, we achieved the on-demand generation of reconfigurable spin-texture lattices with square, hexagonal, and Kagome symmetries. The most advanced realization of this platform is the creation of artificial magnetic Moiré superlattices (Figure 2). Unlike conventional Moiré materials, which arise from the physical stacking of twisted atomic lattices, the superstructures presented here are the result of an interference pattern between two independently written potential landscapes. We realized these superstructures through two distinct approaches: by overlapping identical periodic lattices with a controlled rotational misalignment (twisted Moiré patterns), and by superimposing lattices with identical symmetry but mismatched periodicities.

The structural and dynamic properties of these complex magnetic textures were validated through advanced nanoscale characterization. Nitrogen-Vacancy (NV) center magnetometry revealed that the internal morphology of the Moiré lattice sites evolves from clusters of small skyrmions to extended single-domain chiral features as the laser writing power increases. Furthermore, Brillouin Light Scattering (BLS) spectroscopy and micromagnetic simulations demonstrated that these programmed lattices exhibit dynamic responses that are distinctly different from those of the unpatterned film. Specifically, we identified localized breathing eigenmodes in the GHz frequency range, characterized by the coherent expansion and contraction of the domain cores.

In conclusion, this research bridges fundamental chiral magnetism with the engineering of functional magnetic metamaterials. By demonstrating that complex symmetries and Moiré superlattices can be encoded through the interference of programmable magnetic potentials, this thesis provides a robust framework for deterministic, reprogrammable design of energy landscapes and spin textures. The ability to tailor magnetic energy landscapes with nanoscale precision offers a powerful tool for the realization of adaptive information technologies, paving the way for reprogrammable magnonics and unconventional computing architectures without the need for permanent structural alterations.

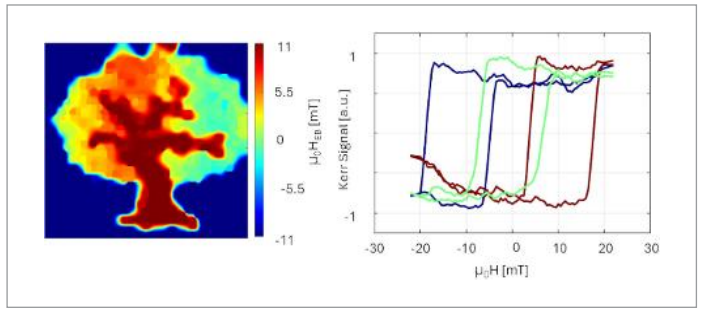

Fig.1 - Grayscale magnetic patterning. The spatial map of the exchange bias for a "Gradient Tree" structure (left) and the corresponding hysteresis loops extracted from the map (right) demonstrate the smooth, continuous modulation of the local magnetic energy landscape

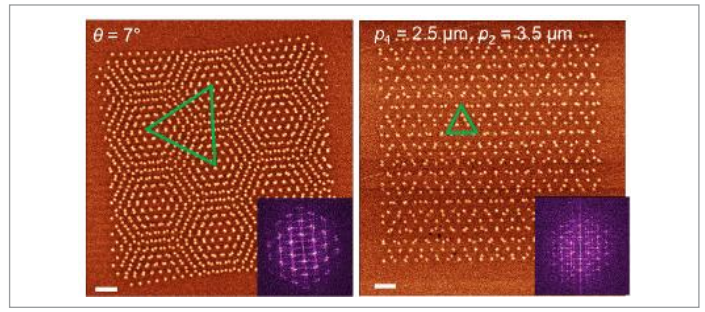

Fig.2 - Magnetic Force Microscopy (MFM) of artificial Moiré superlattices. A twisted Moiré lattice with a 7° misalignment (left) and a periodicity-mismatched lattice superimposing 2.5 µm and 3.5 µm periods (right). Insets show the corresponding Fast Fourier Transforms (FFT). Scale bars: 10 µm

WAFER-SCALE INTEGRATION OF $K_xNa_{1-x}NbO_3$ FILMS FOR MEMS

Giulia Pavese - Supervisor: Miguel Angel Badillo Avila

PZT is a widely used and industrially relevant material that has been integrated into micro-electromechanical systems (MEMS) and is essential for the realization of actuators, sensors, and energy harvesters. However, driven by the European Directive on the Restriction of Hazardous Substances (RoHS), which aims to reduce the use of lead in electronic equipment, the pursuit of alternatives to lead zirconate titanate (PZT) has become a primary objective for the field of piezoelectric materials. Due to its excellent piezoelectric properties in bulk form, potassium sodium niobate ($K_xNa_{1-x}NbO_3$, KNN) has emerged as one of the most promising substitutes. Nevertheless, KNN thin films have not yet achieved widespread industrial adoption and remain largely confined to research environments. This is related to high leakage currents and formation of secondary phases commonly reported for KNN, that are detrimental for devices performance. Therefore, overcoming such challenges and understanding their underlying mechanisms is essential for the reliable integration of KNN thin films into functional devices.

My research thesis addresses the growth and characterization of composition-tailored $K_xN_{1-x}NbO_3$ thin films on 8" wafers using industrial magnetron sputtering techniques. Optimized stoichiometries were used for the integration of KNN into microfabrication processes to produce Piezoelectric Micromachined Ultrasonic Transducers (PMUTS).

In the first stage of research, $K_{0.5}Na_{0.5}NbO_3$ films were deposited at 500 °C under different Ar flow conditions and annealed at different temperatures. Depending on growth and processing, the films exhibited mixed (100)/(001) out-of-plane orientations and, despite a ferroelectric response with P_r around 10 μC/cm², the films exhibited high leakage currents ranging from 10^{-5} up to 1×10^2 A/cm² at 100 kV/cm. Detailed micro-scale analysis revealed phase segregation of K and Na. Such phase separation leads to the formation of a stable ferroelectric Na-rich perovskite phase, accompanied by a K-rich, yet alkali-deficient, pyrochlore phase in the surrounding areas. The sodium enriched areas attain compositions near the second and third morphotropic phase boundaries of KNN (at Na ~70 and 80 at.%). The findings suggested the hypothesis that films enriched in Na might display improved chemical stability of KNN and thus reduce phase segregation.

In the second stage of research, deposition temperature was increased to 600 °C, and other processing conditions were adjusted. Such multidimensional parameter optimization resulted in columnar KNN films with a preferential (001) orientation out of plane. We then aimed to reduce leakage currents in KNN films through doping with multivalent ions, such as Mn, an aspect that is critical to achieve functioning and reliable piezoelectric devices. The introduction of buffer interlayers between Pt and KNN further reduced leakage and stabilized the ferroelectric response after high-temperature annealing, achieving values as low as 3.46 × 10^{-7} A /cm², on par with device integration requirements.

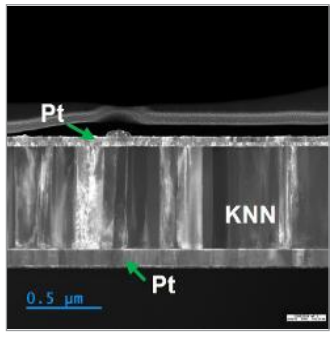

Fig.1 - TEM cross section of a KNN film.

In the final stage, a detailed compositional study was performed on $K_xNa_{1-x}NbO_3$ films. The phase diagram for KNN ceramics exhibits morphotropic phase boundaries (MPB) at x ≈ 0.55, 0.35, and 0.17. While the first MPB has been widely studied, the other two remain largely unexplored. These boundaries correspond to regions of phase coexistence that promote lattice softening and polarization rotation, enhancing piezoelectric response. All three boundaries, and intermediate compositions ($0.17 < x < 0.6$), were investigated to determine the optimal stoichiometry for high piezoelectric performance of KNN films.

Structural and functional properties were analyzed using Transmission Electron Microscopy (TEM), Energy Dispersive X-ray Spectroscopy (EDX), X-ray diffraction (XRD), and ferroelectric and piezoelectric measurements. By increasing Na content above ~70 at.%, spurious pyrochlore formation was suppressed, phase segregation reduced, and a compact and dense columnar structure produced, as shown in Figure 1. The piezoelectric response also improved with increasing Na content, as evidenced by the enhanced strain shown in Figure 2 a, reaching maximum values of $d_{33,f}$ ~79 pm/V and $e_{31,f}$ ~10 C/m² at 78 at.% Na. Interestingly, P_r peaked, instead, at ~68 at.% Na (~14 μC/cm²) (see Figure 2 b). XRD confirmed preferential {001} orientation for all KNN films. Also, the progressive lattice contraction with increasing Na content, together with the inversion of lattice parameters above ~73 at.% Na, indicated strain-driven structural reorientation. The persistence of out-of-plane remanent polarization despite such reconfiguration suggested a transition toward a monoclinic phase, facilitating polarization rotation and thus higher piezoelectric coefficients.

Optimized KNN films were employed for the microfabrication and experimental characterization of PMUT devices based on Na-rich KNN compositions. Circular PMUT membranes with a diameter of approximately 600 μm each, yielded a displacement of about 2 μm at resonance and low driving voltage, surpassing the performance of other lead-free alternatives, such as AlScN- and AlN-based devices. Moreover, towards the end of this thesis, effective passivation and wet-etching protocols for KNN films were also established, enabling the prospective of patterning continuous KNN films and fabricating suspended MEM structures such as cantilevers in the immediate term.

The achievement of lead-free PMUTS represents the first proof of concept of a MEMS device fully planned, grown, and fabricated at Polifab, the micro and nanofabrication facility of Politecnico di Milano. Our results demonstrate the feasibility of integrating lead-free KNN films into MEMS architecture and highlight the robustness and scalability of the developed technological processes with industrial equipment in collaboration with STMicroelectronics.

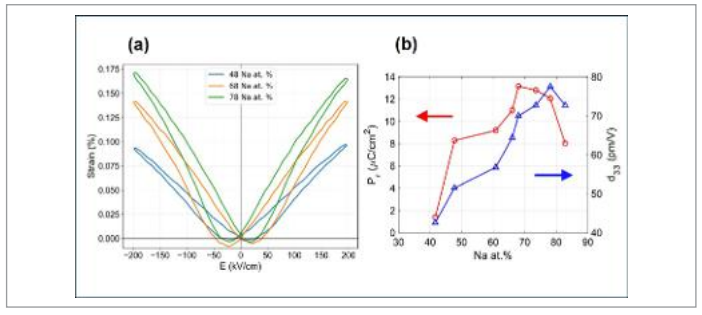

Fig.2 - (a) Strain vs electric fields loops for films with 48, 68 and 78 Na at.%, (b) Pr and d_{33} trends versus Na at. %.

SYNCHRONIZED ULTRAFAST NEAR-INFRARED FIBER LASERS FOR HYPERSPECTRAL VIBRATIONAL MICROSCOPY APPLIED TO HISTOPATHOLOGY

Fedele Pisani - Supervisor: Gianluca Galzerano

Histopathology, the microscopic examination of tissue to study disease manifestation, serves as a cornerstone of diagnostic medicine, particularly in oncology. Conventional evaluation relies on visual inspection of stained tissue sections. While established, this method remains inherently subjective, dependent on variable staining protocols, and prone to inconsistent diagnostic outcomes. Consequently, there is a critical clinical demand for standardized, quantitative imaging approaches that do not require labelling. Vibrational spectroscopy, specifically Stimulated Raman Scattering (SRS) microscopy, has emerged as a powerful candidate. By probing the intrinsic molecular vibrations of biochemical constituents, SRS provides chemically specific, label-free imaging with high spatial resolution and speed. However, the clinical translation of SRS has been impeded by the technical complexity of the required laser sources. To achieve high chemical specificity, SRS microscopy requires access to both the high-frequency C-H stretching region and the diagnostically rich fingerprint region. Accessing these regions simultaneously requires a complex optical setup involving three distinct synchronized pulse trains: two narrowband pump beams and one broadband Stokes beam. Historically, achieving the necessary temporal overlap and stability required bulky, maintenance-heavy solid-state lasers or optical parametric oscillators, rendering them impractical for clinical environments.

This doctoral work addresses these limitations by developing a compact, robust, and fiber-integrated laser platform designed specifically for simultaneous, multiplexed SRS microscopy. The core innovation is the realization of a passively synchronized, three-color mode-locked fiber laser system. This system eliminates the need for active electronic feedback by exploiting Cross-Phase Modulation (XPM) within shared passive fiber segments to lock the repetition frequencies of independent oscillators. The research begins with the design and characterization of a novel Neodymium-doped (Nd) fiber oscillator operating at 920 nm. Developing a fiber laser at this wavelength is challenging due to the strong competition from the dominant four-level transition of Neodymium at 1064 nm. The presented design utilizes a polarization-maintaining (PM) linear cavity with a custom fiber Bragg grating (FBG) to suppress the 1064 nm emission and enforce oscillation on the quasi-three-level transition at 920 nm. Mode-locking is achieved via a Semiconductor Saturable Absorber Mirror (SESAM). The resulting oscillator delivers stable 3 ps pulses at a repetition rate of 18.5 MHz. A comprehensive noise analysis reveals outstanding performance, with an integrated Relative Intensity Noise (RIN) of just 0.04% and a pulse timing jitter below 2 ps, making it an ideal low-noise pump source for probing the fingerprint region. Building on this foundational source, the dissertation details the implementation of the three-color synchronized system.

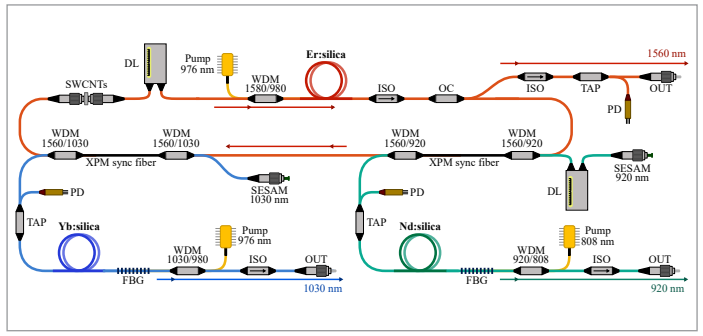

Fig.1 - Experimental layout of the three synchronized passively mode-locked lasers. SWCNTs: HiPCO SWCNTs saturable absorber; DL: tunable optical delay line; WDM: wavelength division multiplexer; ISO: optical isolator; OC: output coupler; TAP: 99/1% polarizing beam splitter; PD: photodetector; OUT: FC/APC fiber connector at the output; SESAM: semiconductor saturable absorber mirror; FBG: chirped fiber Bragg grating

The setup comprises three independent fiber oscillators: an Erbium (Er) ring oscillator at 1560 nm, an Ytterbium (Yb) linear oscillator at 1030 nm, and the aforementioned Nd linear oscillator at 920 nm. Synchronization is achieved through a coupling-only configuration where the oscillators share segments of passive polarization-maintaining fiber. The theory of XPM-based synchronization is elaborated, describing how the interaction between overlapping pulses induces spectral shifts that, via cavity dispersion, translate into temporal corrections, effectively locking the repetition rates. Experimental results demonstrate robust, simultaneous locking of all three lasers for extended periods without active stabilization. The system achieves sub-picosecond timing jitter between the synchronized pulse trains, with Allan deviation measurements confirming the stability of the phase difference. This represents the first realization of a passively synchronized three-color fiber system based exclusively on a coupling configuration, significantly reducing complexity compared to master-slave injection schemes. To translate these synchronized oscillators into a functional microscopy source, a complex amplification and modulation architecture is developed. The requirements for multiplexed SRS are stringent: pump pulses must be narrowband to obtain high spectral resolution, while Stokes pulses must be broadband to cover the vibrational spectrum. To translate the synchronized oscillators into a functional microscopy source, the system employs tailored amplification and conversion schemes. The Erbium line is frequency-doubled to 792 nm to serve as the pump for the high-frequency C-H stretching region, incorporating high-frequency amplitude modulation to enable sensitive lock-in detection. The Neodymium line at 920 nm is amplified to probe the molecular fingerprint region, utilizing spectral compression to maintain the narrow bandwidth necessary for high chemical specificity. Finally, the Ytterbium line generates the broadband Stokes beam; by employing a specialized photonic crystal fiber, it achieves the wide spectral coverage required to span both vibrational regions without compromising pulse quality. In conclusion, this work presents a significant advancement in fiber laser technology for biomedical imaging. By solving the challenge of multi-color synchronization through passive nonlinear optical effects and engineering tailored amplification schemes, the dissertation provides a blueprint for a fully integrated, compact SRS microscope. This technology paves the way for rapid, quantitative, and automated histopathological analysis, potentially transforming diagnostic workflows in clinical settings. The successful demonstration of the Nd-doped 920 nm oscillator, the three-color XPM synchronization, and the broadened Stokes source constitutes a significant step toward alignment-free, turnkey vibrational imaging platforms.

LARGE AREA PULSED LASER DEPOSITION OF FUNCTIONAL OXIDES

Lorenzo Quaresmini - Supervisor: Andrea Cattoni

This Ph.D activity is carried out within the framework of the NFFA-DI (Nano Foundries and Fine Analysis – Digital Infrastructure) project which aims to establish an infrastructure that allows users, that have previously submitted proposals, to have access to a vast catalogue of instruments. Thanks to this project, our group had the opportunity to purchase a new large area PLD (Pulsed Laser Deposition) system that is able to deposit thin films up to 4" wafers with thickness uniformity of ±5%.

Pulsed laser deposition is a physical vapor deposition technique (PVD) in which highly energetic laser pulses are focused on a ceramic target leading to the so called laser ablation process. In this process a small fraction of target material is vaporized and interacts with the background gas inserted into the chamber generating a plasma plume that expands toward a heated substrate where atoms eventually deposit. The process can be tuned by controlling different parameters such as laser fluence, i.e. energy density of a single laser pulse per unit area, repetition frequency, pressure of the background gas (usually oxygen) inside the chamber, target-to-substrate distance and substrate temperature to achieve the desired quality of the film in terms of thickness, crystallinity, morphology and stoichiometry. The most important advantages of this technique are its reliability to precisely transfer the correct stoichiometry from the target to the film making it especially suitable for the growth of complex oxides (e.g. high temperature superconductors, multiferroics, wide bandgap semiconductors, etc...) and its versatility that gives the possibility of depositing virtually any material ranging from metals to nitrides or oxides.

The two major drawbacks of this deposition technique are the interplay of different deposition parameters that hinder an easy tuning of a growth recipe and the strong directionality of the deposition process itself. Focusing on the latter mentioned disadvantage, it is widely known that the angular deposition profile of this process prevents the possibility of achieving uniform deposition over large areas (more than 1 cm^2). In the case of the system used during this work, large area deposition is obtained thanks to an external optical system that is able to move linearly changing the reciprocal position between the centre of the plasma plume and the substrate without modifying the dimensions and the shape of the laser pulse. In addition, it is possible to variate the velocity of the optical system stage during the raster to improve the uniformity of the deposited film. Thin films grown by PLD are then characterized to assess their crystalline, morphological quality. Techniques used for characterization are X-ray diffraction (XRD) to evaluate the crystal orientation in both out-of-plane and in-plane directions and scanning electron microscopy (SEM) used to evaluate surface morphology and have a semi-quantitative estimate of the chemical composition using EDX (Energy Dispersive X-ray Spectroscopy).

In the initial stages of my research I was actively involved in the acceptance and commissioning of the PLD system. My activity then divided into two different paths: on one side I am involved in the deposition and characterization of films that are requested by proposals submitted inside the NFFA-DI project while on the other hand I have my personal research activity that is mainly dedicated to the integration of films of complex oxides on 4" Si wafers for different applications that range from superconducting materials such as YBCO on Si using buffer layers to lead-free piezoelectric materials such as KNN on Pt(111) template grown on Si.

Within the NFFA-DI framework, to date, I was involved mainly in two different activities namely the growth and characterisation of thin films of yttrium barium cuprate (YBCO) on strontium titanate (STO) single crystals to pave the way to the possibility of depositing high quality infinite layer nickelates and the growth of high entropy oxide $Co_{0.2}Ni_{0.2}Cu_{0.2}Mg_{0.2}Zn_{0.2}O$ (5HEO) on MgO substrates to extend the work on characterisation already present in literature. It is worth mentioning that these efforts represent only the preliminary stages of substantially larger projects involving several research groups.

In parallel with the activities mentioned above, my research effort is also focused on the deposition of complex oxides and their integration on Si on a large area scale (i.e. 4 inches diameter wafers).

Integration of complex oxides on Si is currently one of the most significant challenges in extending the performance and functionality of microelectronic devices by overcoming the intrinsic limitations typically imposed by silicon.

The first step toward this goal is to create a template that allows the deposition of oxide films with high crystalline and morphological quality. The most suitable candidate to fulfill these requirements is strontium titanate (STO) that is already used in its bulk form as a substrate for the growth of many different perovskite oxides. The easiest route to integrate high-quality films of strontium titanate on Si substrate is by using intermediate buffer layers. In our work, buffer layers are yttria-stabilized zirconia (YSZ) and yttrium barium cuprate (YBCO). YSZ is fundamental mainly for two reasons: on one side it prevents interfacial problems related to the oxidation of Si and the presence of native oxide layer while on the other hand it is used as chemical barrier to avoid interdiffusion between Si and YBCO. Moreover, YSZ acts as a structural bridge between Si and YBCO, reducing the lattice mismatch between them and thereby promoting high-quality growth of the subsequent layers. YBCO serves instead as an additional structural buffer layer promoting epitaxial growth of strontium titanate.

To obtain PLD-grown strontium titanate films that have good crystalline and morphological quality, optimization of the deposition conditions for single buffer layers is fundamental and scaling this optimization to 4-inch diameter wafers poses an even more demanding challenge due to the increased requirements for thickness uniformity and temperature homogeneity.

It is worth mentioning that, starting from this activity, there was the opportunity to investigate the effectiveness of the adopted approach by depositing YBCO on Si with YSZ as a buffer layer to later test its superconductive properties and first resistivity measurements showed promising results.

Another activity that is intended to prove the quality of the work done during this research is the epitaxial growth of potassium-sodium niobate (KNN) thin films on STO/YBCO/YSZ/Si platform. KNN is a perovskite-structured ferroelectric and piezoelectric material that has recently gained interest as a candidate to substitute PZT in sensor, actuators and microelectromechanical systems (MEMS). This increasing interest is mainly driven by the need to replace lead-based piezoelectric materials due to environmental and health concerns as well as increasingly strict regulations such as European RoHS directive.

The early stages of my research work dedicated to this topic focused on the PLD growth of KNN films using an alternative template for the integration on Si, namely a $Pt/Ti/SiO_2/Si$ stack that can ensure film adhesion, electrical conductivity (that is crucial for ferroelectric and piezoelectric measurements) and good chemical stability during deposition. Through a systematic optimization of the deposition parameters, growth conditions of KNN were refined in terms of crystallinity, morphology and ferroelectric/piezoelectric performances. Optimized parameters will be then transferred to the deposition of KNN films on the STO on Si template mentioned before, allowing a comparative assessment of structural and functional properties.

LARGE AREA TOPOLOGICAL INSULATORS FOR NOVEL SPIN CHARGE INTERCONVERSION APPLICATIONS

Mahmoud Galal Ahmed Rehab

Supervisors: Carlo Zucchetti, Roberto Mantovan, Claudia Wiemer

Three-dimensional topological insulators (3D-TIs) have generated intense research interest in condensed matter physics due to their strong spin-orbit coupling (SOC) and spin-momentum locking, which dictate the spin orientations of their topologically-protected surface states (TSS). These properties make TIs ideal for emerging applications such as Spin-Orbit Torque MRAM and MESO devices. In particular, since spin-charge conversion (SCC) phenomena are often at the core of devices' functionalities, increasing SCC efficiency in TI-containing spintronic devices is demanding. This work presents a comprehensive investigation of the TI Sb_2Te_3 integrated with silicon, progressing from fundamental material synthesis to its functional integration into spintronic devices.

This work begins with the wafer-scale growth via metal organic chemical vapor deposition (MOCVD) of Sb_2Te_3 thin films with controlled thicknesses in the range from 20 to 40 nm on a full 4-inch wafer Si(111) substrate. A systematic study was conducted to evaluate the influence of key growth parameters and sample characteristics, namely, film thickness, wafer position (affecting precursor flux and temperature uniformity), and crystalline quality, on the topological insulating properties of the material. High-quality thin films were obtained across the full 4-inch substrate. Scanning electron microscopy (SEM) images revealed a smooth, homogeneous surface morphology free of voids or granular features. X-ray diffraction (XRD) analysis confirmed a highly-crystalline structure for both film thicknesses, with the 40 nm films exhibiting enhanced crystallinity and a stronger preferential orientation along the (00l) direction, as shown in Fig. 1. Building directly on these foundational growth studies, a functional investigation of room-temperature SCC was carried out on MOCVD-grown Sb_2Te_3 (40 nm) films across the full 4-inch area. In particular, SCC is probed by conducting broadband ferromagnetic resonance (FMR) and spin-pumping FMR on Sb_2Te_3/Au/Co/Au heterostructures. A significant and spatially uniform SCC over the full wafer scale was observed, and the signal was predominantly attributed to the presence of topological surface states in Sb_2Te_3, as shown in Fig. 2. The SCC is interpreted within the Edelstein effect framework, which allows for the quantification of the SCC efficiency through the inverse Edelstein effect length λ_{IEE}, lying in the 0.14 ÷ 0.30 nm range along the diameter of the 4-inch substrate. The observed SCC variability is connected to variations in the chemistry, structure, and morphology of Sb_2Te_3 across the probed wafer area and provides a technologically relevant background for the future use of TIs in spintronic devices.

A comprehensive understanding of native oxidation was required, in order to understand its role in stabilizing (or not), the TIs' TSS. Despite promising SCC in as-grown films, rapid surface oxidation of Sb_2Te_3 upon ambient exposure was encountered, which occurs within days to months following storage. X-ray photoemission spectroscopy (XPS) was conducted before and after a developed chemical etching process, optimizing a recipe to remove OH-group contamination using dilute HCl. It is demonstrated that this treatment effectively removes native oxides, producing a clean, stoichiometric, and oxide-free surface while preserving the underlying crystalline quality. The recovery of the pristine surface is confirmed by magnetoconductance measurements, which reveal the restoration of the weak anti-localization (WAL) effect and topological surface transport channels.

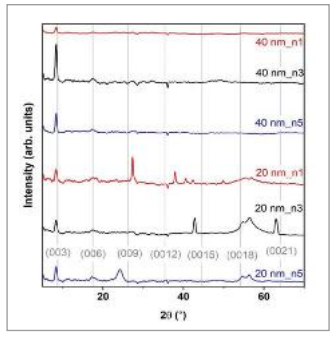

Fig.1

Based on this reliable surface-recovery step, interface engineering in Sb_2Te_3/Au/Co/Au heterostructures was systematically undertaken to assess its impact on SCC efficacy and spin transport. Three interfacial conditions were compared: (i) pristine Sb_2Te_3 with native oxide, (ii) chemically etched Sb_2Te_3 free of oxide layers, and (iii) Sb_2Te_3 with intentionally O_2 plasma-oxidized surfaces. XPS verification of interfacial chemistry in all cases was obtained, including the formation of a stable, complex plasma-induced oxide. While the spin transparency and spin-mixing conductance were improved by chemical etching, this is not directly reflected in the electrically-probed SCC where, quite counterintuitively, the plasma-oxidized interface yielded the highest SCC efficiency, with $\lambda_{IEE} \approx 0.36$ nm, being higher than both oxide-free and native-oxide cases. These original findings opens prospectives towards engineering TSS protection through appropriate oxidations, going beyond the typically accepted scenario, perceiving it as an obstacle to achieve optimal interfacial spin transport and SCC.

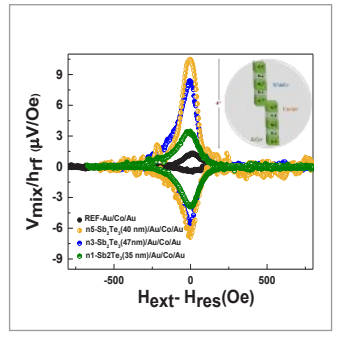

Fig.2

During a short-term visit to the Institut de Ciència de Materials de Barcelona (ICMAB-CSIC), spin-orbit torque (SOT) efficiency was evaluated in the same heterostructures using second-harmonic measurements. The pristine Sb_2Te_3 sample with native oxide exhibited the highest damping-like torque efficiency, while the chemically etched, oxide-free sample showed the lowest. This trend mirrors the spin-charge conversion (SCC) results from spin-pumping measurements, where oxide-containing interfaces consistently outperformed the oxide-free case, demonstrating that a controlled oxide layer enhances both SCC and SOT.

Finally, the focus is placed on device fabrication and demonstration. Photolithography-defined Hall bars and stripe structures were fabricated on Sb_2Te_3/Si (111) to study spin transport from silicon into the TSS. Optical spin injection experiments, combined with intensity and polarization modulation techniques, revealed a spin-dependent electrical signal attributed to SCC at the TSS surface. These results demonstrate efficient interfacial spin detection and provide a pathway toward scalable, silicon-compatible (and eventually optically-driven) spin-logic architectures.

SPIN AND ORBITAL PROPERTIES OF INFINITE-LAYER NICKELATES AND CUPRATES

Francesco Rosa - Supervisor: Giacomo Ghiringhelli

My PhD experimental activity has been devoted to the investigation, by resonant soft x-ray spectroscopies, of the magnetic and orbital properties of infinite-layer nickelates and cuprates, gathering the majority of the work I carried out during the last three years in collaboration with the PolimiX group led by Prof. Giacomo Ghiringhelli at the Physics Department of Politecnico di Milano, Italy. The group has a worldwide reputation for having obtained many impactful results concerning the physics of strongly-correlated materials, particularly cuprates, and gave fundamental contributions to the development of the Resonant Inelastic X-ray Scattering (RIXS) as an experimental technique for such systems. After forty years from the discovery of cuprate superconductors, the origin of unconventional high-temperature superconductivity in these compounds remains one of the most fascinating and puzzling mysteries of modern physics, still lacking a universal theoretical explanation. The presence of strong electron-electron correlations, nowadays recognized as a key ingredient of unconventional superconductors, causes a strict entanglement between different excitations and interactions, preventing the formulation of simple, NFE-like models. Despite being the first discovered unconventional superconductors, copper oxides are still the leading materials as it concerns critical temperature at atmospheric pressure. Justifying their anomalously large T_c values has therefore been the object of innumerable theoretical and experimental efforts. In this context, a promising strategy consists in looking for other materials which are able to reproduce the key features of copper oxides and showcase high-T_c superconductivity. Among these features: a layered crystal structure with tetragonal in-plane Cu-O coordination, strongly enhancing electronic interactions; a $3d^9$ configuration of the transition metal atoms, with only one hole per site; the presence of cation layers interleaved to CuO_2 planes, acting as a charge reservoir. Several attempts have been made on *3d* transition metal oxides different from copper, with little results. Nickel looks like a significant exception, after the report of superconductivity in infinite-layer (IL) nickelate thin films in 2019. The study of analogies and differences between copper and nickel oxides is therefore expected to be very valuable in order to discriminate the essential physical mechanisms leading to the appearance of a zero-resistance state in these materials. During my PhD, I investigated IL nickelate and cuprate thin films by means of x-ray spectroscopies. Given the wide variety of different phenomena characterizing our systems, we focus our attention on magnetism, which is known to have a strong and often competing relationship with superconductivity. After the introductory chapters, the first part of my work consists in an extensive RIXS analysis on several IL nickelate thin films: we analyze the dispersion of dynamic spin excitations, comparing results for different rare-earth species, doping level and substrate material. The effectiveness and the advantages of the RIXS techniques for this purpose have already been widely demonstrated for cuprates, and comparison with copper oxides indeed constitutes an important part of our work.

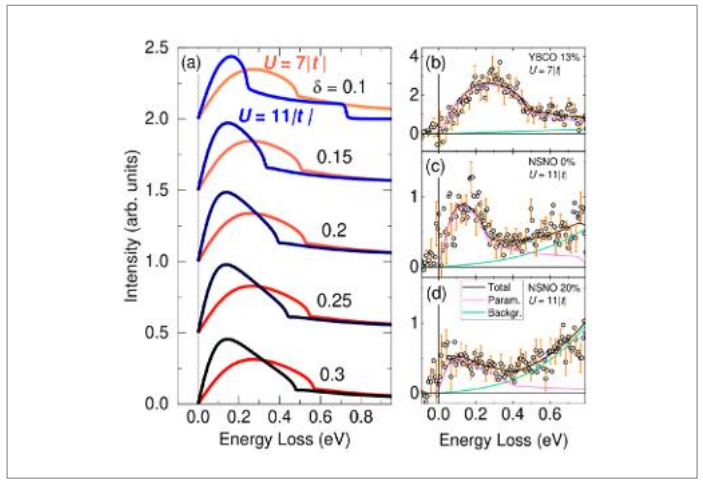

Fig.1 - (a) Hubbard-based theoretical susceptibilities and (b-d) fittings of cross-polarized RIXS data.

We first focus on the Sr-doped class $Nd_{1-x}Sr_xNiO_2$ (NSNO), where superconductivity was originally reported. A dispersive magnetic excitation is reported at about half the energy of cuprates, consistently with previous observations. Polarization-resolved RIXS measurements allow us to precisely extract the shape of the magnetic peak, which we then fit with a magnetic susceptibility calculated from an original Hubbard-based model, formulated by Fidrysiak et al. (see figure 1). Besides giving a direct view on the microscopic mechanisms, such model provides us with a unifying framework for the two classes of compounds: in particular, from comparative fittings of RIXS data from cuprates and nickelates we estimate a similar value of the hopping parameter *t*, while the Mott energy *U* is about double in IL nickelates than in cuprates. Our NSNO study finds a natural continuation in the following chapter, where superconducting $PrNiO_2$ thin films are investigated with the same technique. Besides the better quality of the samples, the key factor in this case is that superconductivity in these samples is not achieved through chemical doping, but is believed to occur due to a self-doping from the rare-earth, a phenomenon which has no counterpart in cuprates. We report a relatively sharp magnon dispersion even close to the superconducting T_c, suggesting that self-doping does not have such a disruptive effect on magnetism as chemical doping. The extracted magnetic exchange couplings are a factor 2 lower than in the isostructural cuprate $CaCuO_2$, as expected. We then performed a polarization-resolved study of orbital transitions, finding good agreement with single-ion predictions. We notice a dispersion of the lowest-energy *dd* peak opposite to cuprates, which we interpret as a next-neighbor based orbiton propagation mechanism, which is no longer hindered by the long-range antiferromagnetic order present in cuprates. In the second part of the thesis, we adopt a different perspective: the static magnetic order in the NSNO films is investigated with X-ray Magnetic Circular Dichroism (XMCD), reporting the occurrence of a strong out-of-plane magnetic moment. After ruling out possible paramagnetic contributions, we attribute the phenomenon to the canting of antiferromagnetically in-plane correlated spins, proposing as its possible origin a symmetry lowering of the NiO_2 planes. In the final chapter, we deal with the effect of possible magnetic confinement from non *c*-axis YBCO cuprate thin films, which we found to have a sizable impact on the magnetic dispersion. Overall, our result contribute to shed new light on the peculiar magnetic and electronic properties of IL nickelates, although it is still a long way to get a complete picture of their physics. Encouraging signals coming from the report of phenomena which have no counterpart in cuprates: the case of self-doping is emblematic, endowing IL nickelates with a way to achieve superconductivity that avoids the increase of structural disorder associated to chemical doping. Moreover, the highlighted analogies and differences with cuprates will be hopefully useful to clarify relevant elements at the root of unconventional superconductivity in these materials.

SPIN MANIPULATION AND DETECTION IN SEMICONDUCTOR PLATFORMS

Francesco Scali - Supervisor: Federico Bottegoni

The scaling trend associated with Moore's law, first articulated in 1965, is increasingly difficult to sustain as electronic devices approach nanometer dimensions. Today, further miniaturization is limited not only by fabrication complexity, but also by power density and interconnect bottlenecks, making it harder to keep improving performance while reducing energy consumption. This situation has intensified the search for alternative ways to efficiently manipulate information that remain compatible with the established semiconductor supply chain. One promising direction is spintronics, which aims to exploit and control the spin of particles, enabling device concepts based on new operating principles. Spintronics has already successfully advanced information storage technology exploiting metals with MRAM, STT-MRAM, and SOT-MRAM, but it still lacks widely adopted applications for logic operations. In this framework, my PhD thesis investigates how spin information can be converted into an electrical signal and dynamically controlled in semiconductors. Semiconductors are attractive because they naturally connect to scalable electronics. However, they also pose a clear challenge: spin signals are typically weak, and their characteristic lengths and times depend sensitively on band structure, scattering, and spin relaxation. In this thesis, I address these aspects by combining theoretical analysis of the electronic structure and spin depolarization with opto-spintronic measurements and drift-diffusion modelling.

The work follows two complementary lines. First, it demonstrates spin-to-charge conversion in the chalcopyrite cadmium germanium arsenide ($CdGeAs_2$) through a photoinduced inverse spin Hall effect (ISHE) experiment. Second, it studies how fast a spin signal can be electrically modulated in the drift-diffusion regime by solving time-dependent spin transport equations under oscillating electric fields. Taken together, these results clarify an important trade-off in semiconductor spintronics: short spin diffusion lengths are challenging for signal amplitude, yet they can enable very fast electrical control.

$CdGeAs_2$ is a non-centrosymmetric semiconductor with strong spin-orbit coupling and bulk inversion asymmetry. These ingredients shape the band structure and, in turn, the electronic and spin-transport properties of the material. In particular, they allow efficient conversion of spin currents into detectable charge currents, which is essential for electrical readout of spin information. Moreover, they influence the spin diffusion length, i.e., the characteristic distance over which a spin-polarized carrier population preserves its polarization. While a long spin diffusion length is desirable for transporting spin over large distances (e.g., in spin interconnects), a shorter spin diffusion length can also be advantageous because it allows faster electrical control of spin currents, which is the focus of the second part of the thesis.

Using angle-resolved photoemission spectroscopy (ARPES), we resolved the valence-band manifold near the top of the valence band in $CdGeAs_2$. Building on this band-structure knowledge, the ISHE response of optically injected spin-polarized electrons is interpreted. Spin injection is achieved through optical orientation based on interband transitions allowed by dipole selection rules and driven by circularly polarized light. Optical orientation is a well-established technique, widely used in the literature since the early 1970s. It was first demonstrated in silicon (Si) in 1968 and later investigated extensively in gallium arsenide (GaAs) and germanium (Ge) to generate spin-polarized carriers and diffusive spin currents in semiconductors. By tuning the photon energy across the near-infrared region above the band gap, I measure the spectral dependence of the ISHE signal. To interpret the spectrum, I employ a spin diffusion model that relates the measured voltage to (i) the optically injected spin polarization, (ii) the absorption coefficient of the semiconductor, and (iii) the spin diffusion length. The first two quantities are directly evaluated from band structure calculations performed using an 8-band k·p model, whose parameters are constrained by essential information extracted from the ARPES measurements. The model predicts a high injected electron spin polarization (about 40-70%) for photon energies only ~200 meV above the direct band gap of the semiconductor, showing that optical orientation is a valuable route to generate spin currents in $CdGeAs_2$ as well. A key outcome from the comparison between the experiment and theory is that the observed spectral behaviour is consistent with a short spin diffusion length in $CdGeAs_2$ ($L_s \lesssim$ 100 nm). This value is comparable to that in GaAs and much smaller than the micrometer-scale values often found in Si and Ge. This short spin diffusion length suppresses the overall ISHE amplitude, but the measured signal remains sizable. Moreover, when compared with a similar experiment on Ge where the spin-to-charge conversion efficiency is on the order of 10^{-4}, the ISHE voltage measured in $CdGeAs_2$ is about one order of magnitude larger under comparable conditions. These results suggest a large spin-to-charge conversion response in $CdGeAs_2$, making it a potential semiconductor platform for spin current detection.

The second part of the work turns this "short-length" picture into an opportunity: a reduced spin diffusion length can enable faster electrical modulation of spin-dependent signals. I analyse the frequency response of spin drift-diffusion by solving the time-dependent drift-diffusion and continuity equations under a sinusoidal electric field, using finite-element simulations. The spin density response contains harmonics at f and 2f, whose amplitudes define cut-off frequencies that quantify the maximum usable modulation bandwidth. By inserting material parameters for n-doped Ge, Si, and GaAs at room temperature and scanning doping density and injector-detector distance, the simulations provide practical bandwidth estimates. In the three semiconductors, I evaluate the Elliott-Yafet and Dyakonov-Perel spin depolarization mechanisms describing effective magnetic fields during collisions and transport. The analysis indicates that the spin relaxation rate scales proportionally with the momentum scattering rate in Ge and Si, whereas it shows an inverse dependence in GaAs. The strong difference in scattering and depolarization processes yields large variations in the spin diffusion length of these semiconductors. The simulations highlight two regimes, linked to field amplitude, and show that the characteristic cut-off frequency increases as the spin diffusion length decreases. In the strong-field regime, the results reflect the doping dependence of the spin diffusion length and lead to modulation frequencies that can reach values as high as ~35 GHz in heavily doped Ge, ~480 MHz in heavily doped Si, and ~15 THz in lightly doped GaAs. These values represent transport-limited speeds and neglect additional device constraints (for instance, detection-junction capacitances), yet they show that drift-diffusion itself does not prevent operation in the multi-GHz range with bias voltages commonly used in electronics. The similar spin diffusion length in $CdGeAs_2$ and GaAs, in addition to the very fast frequency response of the latter, points to high-speed manipulation of spin currents in $CdGeAs_2$ as well.

Overall, the thesis develops a coherent path from band structure and optical orientation to ISHE detection and time-dependent spin transport, showing how microscopic properties set the scale of measurable spin signals and how, in turn, these scales can be leveraged for high-speed spin manipulation in semiconductor platforms.

ORGANIC NANOFIBERS FOR MUSCLE CELL DIFFERENTIATION AND OPTOSTIMULATION

Giulia Simoncini - Supervisor: Guglielmo Lanzani

The development of functional engineered tissues requires the integration of biomimetic structural materials with precise and minimally invasive actuation strategies. In excitable cells such as skeletal, functionality emerges from the interplay between a structured architecture, coordinated electrophysiology, and synchronized contraction. Reproducing a biohybrid actuator able to combine tissue-like cell organization with the possibility of external control of cell activity remains a central challenge in tissue engineering. In the first part of this work we addresses this problem by combining nanostructured electrospun scaffolds with a rationally-designed membrane-targeting azobenzene molecule (Ziapin2), establishing a materials-driven substrate for the growth and the optical control of engineered skeletal muscle tissues.
Electrospinning was employed to fabricate 2D aligned nanofibrous substrates made of poly(vinyl alcohol) (PVA) and poly(caprolactone) (PCL), selected for their biocompatibility, biodegradability, and established use in muscle cell culture. A comparison between the two materials was conducted to evaluate which of them were more suitable to promote skeletal muscle cell differentiation and to support the photo-induced contraction. The resulting fiber networks structurally resemble the native extracellular matrix and provide morphological and mechanical characteristics that guide differentiated skeletal muscle cell (myoblast) adhesion, fusion, and maturation. In particular, highly aligned PVA fibers show the highest number and performance of contractile myotubes able to contract following perfectly the frequency of the light stimulation. Indeed, the PVA aligned fibers were selected for several reasons: First, the self-standing electrospun membrane allows us to induce a quasi-3D cell differentiation and a tissue-like cell organization. Second, the functionalization to create an "all-in-one device" able to promote cell differentiation and contemporaneous cell contraction. The anisotropic scaffold architecture is essential for promoting cellular alignment and enabling synergistic contractile behavior. Upon stimulation, engineered constructs generated stresses up to 3.3 kPa, strains on the order of 4×10^{-4}, linear displacements of approximately 4 μm, and forces of 460 μN: values that fit the range reported for three-dimensional C2C12 systems. These results highlight the importance of structural guidance and mechanical properties to achieve tissue-level actuation.
As reported at the beginning, to control remote and non-genetic cell excitability, this work shows a photostimulation strategy based on amphiphilic azobenzene derivatives that localize non-covalently into the plasma membrane. Upon reversible trans–cis photoisomerization, these molecules convert light stimulus into the modulation of membrane properties, like membrane potential, capacitance or membrane surface charge. In the second part of this work, we focused on the design, photophysical and electrophysiological characterization of a new azobenzene compound combining the main effects of the two previous generations of phototransducers already characterized in our group, and with a molecular structure suitable for the PVA fibers functionalization. These azobenzenes demonstrated two principal mechanisms: an opto-mechanical pathway (Ziapin2), in which isomerization alters membrane thickness and capacitance through dimer formation, and an electro-optical pathway (MTP2), in which dipole reorientation modifies membrane surface charge. Ziapin2 (Z2), used previously for the stimulation of muscle cell biohybrid actuator, shows opto-mechanical actuation inducing variation in membrane capacitance and consequently a hyperpolarization of the membrane potential. The push-pull molecule MTP2, thanks to its strong dipole moment, upon isomerization induced a redistribution of surface membrane charges.

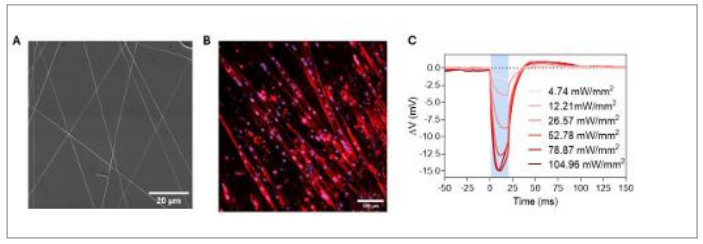

Fig.1 - A) SEM image of PVA aligned fibers,B)Confocal image of differentiated myotubes on nanofibrous structure, C) Patch-clamp traces of membrane potential variation induced by SZ upon illumination with a LED at 470 nm..

Building on this mechanistic framework, a next-generation dual-action phototransducer, called SZ, was rationally engineered to integrate opto-mechanical and electro-optical contributions within a single molecular architecture. Before testing this molecule with cells, photophysical characterization was carried out to understand the behaviour and the isomerization kinetics of SZ in different solvents. Molecular dynamics simulations and electrophysiological recordings demonstrated that SZ induces robust and reversible hyperpolarization at significantly reduced molecular concentration than Ziapin2. Electrophysiology was tested first on HEK-293T cells to understand the SZ effects on simpler model cells and then we selected a more complex system like hiPSC-derived cardiomyocytes: muscle cells that do not require alignment and differentiation. Also, in these cells SZ induced a strong hyperpolarization followed by rebound depolarization capable of eliciting deterministic action potentials.
The cooperative interplay between capacitance modulation and dipole reorientation expands the operational window of non-genetic optical control and strengthens the causal link between molecular-level events and cellular electrophysiological responses.
The convergence of anisotropic biofabrication and dual-mechanism molecular phototransduction provides a versatile platform for regenerative medicine, in vitro disease modeling, high-throughput drug screening, and soft biohybrid robotics, advancing the design of optically actuated, tissue-like constructs with controllable function.

FEMTOSECOND LASER-FABRICATED POROUS GLASS MEMBRANES FOR TUNABLE TRANSPORT IN LAB-ON-CHIP SYSTEMS

Federica Torre - Supervisors: Roberto Osellame, Anna Valente

Biological barriers regulate transport in living systems through a delicate interplay of selectivity, permeability, and stability. From epithelial layers to highly specialized interfaces, their function relies not only on biological activity but also on the physical structure of the barrier itself. Reproducing these properties in artificial systems remains a major challenge, particularly in microfluidic and lab-on-chip platforms, where membranes are often treated as passive elements rather than as engineered components.
In most existing devices, porous membranes are introduced to separate compartments while enabling molecular exchange. However, widely used polymeric membranes were not originally designed for microfluidic applications and exhibit intrinsic limitations, including uncontrolled adsorption, autofluorescence, limited chemical stability, and poor tunability of pore geometry.
The core idea driving my research is that membranes should instead be regarded as tunable physical interfaces, whose geometry and transport properties can be designed and controlled. By focusing on the physical structure of the barrier, it becomes possible to decouple geometry-driven transport phenomena from biological effects, enabling more reproducible and quantitative experimental platforms.
In this context, glass represents an appealing alternative to polymers, offering optical transparency, chemical inertness, and long-term stability. However, fabricating porous structures with sub-micrometric features in glass is technically challenging and lies beyond the reach of most conventional microfabrication approaches. During my PhD, I explored the use of femtosecond laser micromachining combined with selective chemical etching to overcome these limitations. This fabrication approach relies on the localized modification of the glass bulk using ultrashort laser pulses, followed by chemical etching of the modified regions to generate through-holes with diameters in the nanometer range. A systematic study of the laser focal spot and writing strategy was carried out to ensure uniform and reproducible modification. This investigation enabled the identification of stable fabrication windows for producing reproducible nanopores.
The resulting membranes were characterized from a transport perspective through permeability measurements performed on glass substrates with controlled pore size and density. These experiments allowed direct correlations between geometry and transport behavior, highlighting the role of membrane thickness, porosity, and pore size in regulating molecular flux independently of biological components.
A key element of this work is the development of a glass-based microfluidic architecture in which the membrane is directly defined within the substrate itself. The system consists of two laser-fabricated channels: one positioned very close to the glass surface to form a thin membrane region, and a second open channel fabricated on the opposite side of the substrate. When the two parts are aligned and sealed, the channels form a closed microfluidic system separated by a glass membrane with a thickness on the order of a few tens of micrometers. Nanopores are selectively introduced within this membrane, enabling controlled transport across a physically well-defined interface that bridges micrometer and nanometer length scales.

Overall, the membranes developed in this work are conceived as tunable physical interfaces rather than application-specific components. By independently controlling membrane thickness at the micrometer scale and pore size down to the nanometer regime, the same platform can be adapted to different transport scenarios and experimental needs. This flexibility enables systematic studies of nanoscale transport phenomena and supports a broad range of applications where size-selective filtration, optical accessibility, and material stability are essential.
Looking ahead, this work naturally opens toward the development of more integrated and versatile glass-based microfluidic systems. Future directions include exploring advanced assembly strategies for combining multiple glass components, as well as the integration of additional functionalities such as on-chip sensing and controlled interfaces with biological systems. These perspectives aim at extending the platform beyond its current configuration, toward experimental setups that enable more comprehensive studies of transport phenomena across engineered physical barriers.

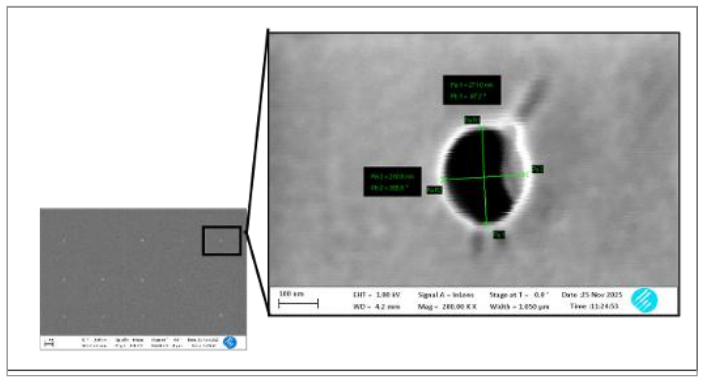

Fig.1 - SEM images showing nanometer-scale pores fabricated in glass by femtosecond laser micromachining and selective chemical etching.

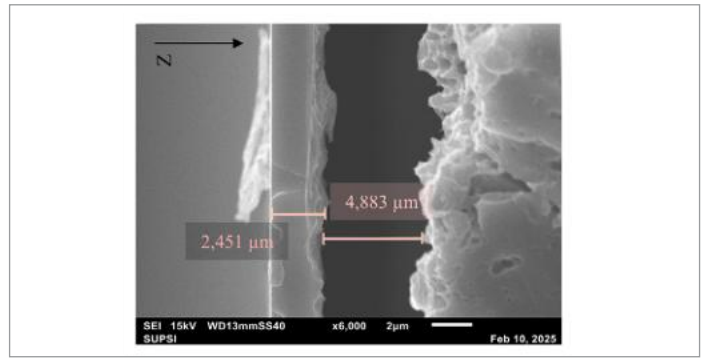

Fig.2 - SEM cross-section of a laser-fabricated glass membrane showing the membrane region defined by a single etched cavity. The image is used to investigate the minimum achievable membrane thickness.

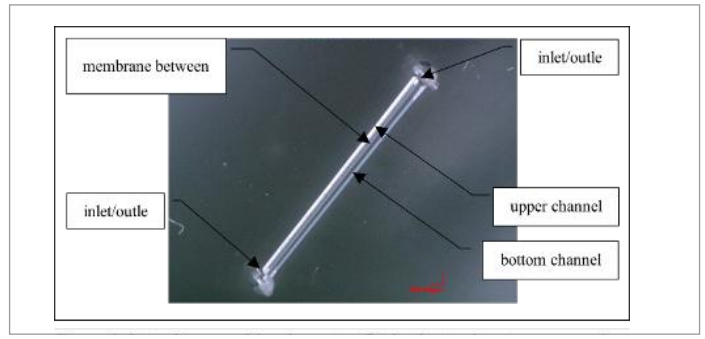

Fig.3 - Optical image of the glass microfluidic device showing upper and lower channels separated by a thin membrane region, together with inlet and outlet ports.

HYPERSPECTRAL IMAGING FOR BIOPHYSICAL APPLICATIONS IN MICROSCOPY AND REMOTE SENSING

Lorenzo Vinco - Supervisor: Dario Polli

In my research I used a common-path interferometer based on birefringent crystals to work in the field of time-resolved spectroscopy. This device measures the interferogram of the incoming electro-magnetic signal and the corresponding power spectrum is retrieved upon a Fourier transformation. When a camera is placed in front of the device, a stack of images at a single wavelength is obtained and the spectral response of each pixel can be used to infer the local composition of the specimen.
In my research, I used the interferometer in imaging mode in several configurations, ranging from microscopy to diffuse reflectance.
A commercial version of this device (GEMINI-X, NIREOS S.r.l.) was used to measure the fluorescence of multi-stained tissue on a Nikon microscope (Nikon Eclipse Ti2). Different regions exhibited characteristic emissions associated with three of the four fluorophores present in the specimen. A clear representation of the fluorophore distribution (Fig. 1) is obtained by unmixing the hyperspectral data using non-negative matrix factorization. This algorithm estimates the spectral shape of the fluorophores under the assumption that each pixel can be described as the linear superposition of spectra, called endmembers, and that the abundance of each endmember is non-negative. In figure 1, the stack of the abundance distribution of the endmember detected by the algorithm is shown. This image reveals the estimated abundance fraction of each fluorophore. Bright, saturated pixels are mapped by the algorithm at the corners of a simplex and are associated with the presence of a pure component.
Another important application of hyperspectral imaging is diffuse reflectance from unstained bulk tissues. When light impinges on the surface of a tissue, the transmitted fraction undergoes multiple scattering events which depend on the scattering coefficient of the specimen. Furthermore, specific wavelengths are absorbed by different chromophores depending on the absorption spectra. A small fraction of the light which travelled into the tissue and was re-emitted back from the surface is collected by the camera and carries useful information on the chemical components present in the tissue. Tumoral tissue and healthy tissue are characterized by different concentrations of hemoglobin, lipids, water and collagen. Thus, diffusively reflected light has absorption features that can be used to distinguish between these two tissue types. Figure 2 shows a false-color reconstruction of a datacube obtained from a breast cancerous biopsy. Absolute spectra were normalized over a white reference target and preprocessed using a standard normal variate procedure, which subtracts the mean spectrum and normalizes over the standard deviation. Fat tissue shows a remarkable absorption at 1210 nm and reduced absorption at 970 nm, which stems from a reduced water content. On the contrary, diseased tissue and fibrotic tissue exhibit a large absorption band above 1400 nm and the absorption of hemoglobin below 600 nm. These results are framed in the context of a project funded by the EU called SpectraBreast. In the first 18 months of the project, the main task I worked on was the design and characterization of the hyperspectral system, which is made of a VIS-SWIR hyperspectral camera ranging from 400 nm to 1700 nm, a light system and a mechanical structure to enclose the specimen. Compared to the previous measurements, which were taken placing a macro lens in front of the camera and placing the sample at a distance of about 20 cm, in the new configuration the camera was moved farther away with no additional lenses. This ensures a larger field-of-view which can contain the whole sample and allows operators and surgeons to easily place and remove the specimen from the system without any issues. The chosen distance ensures a pixel size of 50 microns per pixel. In terms of spatial resolution, the modulation transfer function of the camera was calculated upon measuring a lithographic USAF pattern tilted at a small angle and differentiating the edge spread function. By taking a Fourier transform of the result, a contrast transfer of 50% was estimated for patterns modulated with a period of 370 micrometers.
Several illumination configurations were also tested. The simplest illumination system consists of fourteen white LEDs and two halogen lamps split between the left and right side of the sample. When these lamps are oriented towards the white-painted ceiling of the enclosure, the sample is illuminated with diffused light. Compared to direct illumination, this configuration reduces glares and shadowing effects at the cost of reduced throughput. However, with this illumination source, little light is present between 700 nm and 1000 nm, as well as below 435 nm. Thus, a multi-LED illumination source was tested and selected as the source that will be used for the remaining of the project.
SpectraBreast aims at developing a prototype for a device that integrates hyperspectral technology with Raman spectroscopy for the intraoperative assessment of margins during breast conserving surgery. It is a project which involves multiple partners from all Europe, including Politecnico di Milano and NIREOS S.r.l.
In conclusion, during my research I employed hyperspectral imaging technology for measuring biological specimens in a wide variety of configurations, including microscopy, macro imaging and remote imaging.

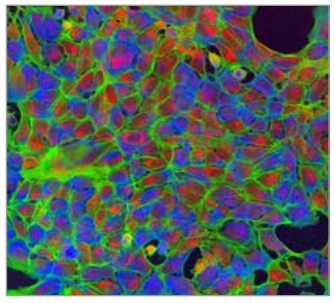

Fig.1 - Stack of three abundance maps obtained through unmixing of hyperspectral fluorescence data on U-2OS cells stained with multiple dyes

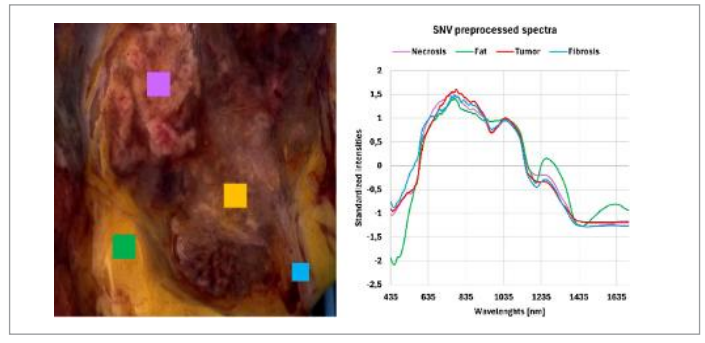

Fig.2 - False-color reconstruction of a breast cancerous specimen reconstructed from hyperspectral data and average SNV preprocessed spectra of selected regions of interest

PHASE NANOENGINEERING OF CRYSTALLINE YTTRIUM IRON GARNET FILMS VIA DIRECT LASER WRITING FOR MAGNONIC APPLICATIONS

Matteo Vitali - Supervisor: Daniela Petti

Co-Supervisor: Edoardo Albisetti

Magnonics is a rapidly expanding field focused on the excitation, propagation and control of spin waves (SWs), which are collective magnetic excitations in the ordered spin lattices of magnetic materials. Unlike traditional currents, SWs (whose quanta are called magnons) propagate through collective oscillations of magnetic moments without moving charges. The resulting lack of Joule heating and their intrinsic GHz frequencies at nanoscale wavelengths make SWs candidates for next-generation, low-power information processing devices.

Yttrium Iron Garnet (YIG) stands out as one of the most promising materials in this field due to its exceptionally low magnetic damping, allowing SWs to propagate for hundreds of micrometres. To harness these phenomena, precise nanoscale control over magnetic thin films is essential.

My PhD work focused on tuning the magnetic properties of YIG films through Phase Nanoengineering, a method that modifies thin films without material disruption using a highly localized energy source. Specifically, I employed a technique called Direct Laser Writing (DLW) powered by a continuous-wave UV laser. This allowed for precise, point-by-point raster scanning to irradiate custom shapes, successfully modifying the magnetic structure of single-crystal YIG films, starting with a 1 µm-thick sample. Once a laser power threshold is exceeded in irradiated areas, the original magnetic stripe domains of the film are permanently affected; their size is reduced by more than a factor of two, as measured by Magnetic Force Microscopy (MFM) as shown in Fig 1c. The size of these new domains can be tuned with the laser power, which directly correlates with an increase in the saturation field, as observed in the hysteresis loops measured via the Magneto-Optical Kerr Effect (MOKE). Scanning Electron Microscopy (SEM) cross-sectional images of irradiated YIG areas show that the modification is confined to a top layer, whose thickness can be tuned by the irradiation power (Fig. 1a).

Through micromagnetic simulations of the domain structure (Fig. 1b), I was able to link the magnetic properties in this modified volume to an increase in perpendicular magnetic anisotropy (PMA). This mechanism is driven by the high optical absorption of YIG at the laser wavelength. Due to the limited penetration depth of the laser, the absorbed optical power heats a vertically confined volume above its melting temperature, followed by recrystallization after irradiation. To confirm this mechanism, I performed simulations of the heat profile generated by the gaussian laser beam propagating through the YIG, linking the depth of the PMA-enhanced layer to the laser power.

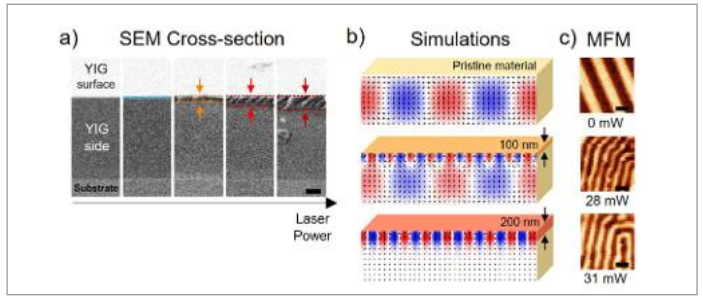

Fig.1 - a) SEM cross section images showing the increasing depth of the modified volume with the laser power. Scale bar 200 nm. b), c) Micromagnetic simulations (b) reproducing the magnetic domain structure of the corresponding MFM measurements (c), considering increasing thicknesses of the top layer with increased PMA. Scale bars 1 mm

Raman spectroscopy revealed that this PMA increase results from the strained state of the YIG post-irradiation, which is also associated with the creation of oxygen vacancies. Furthermore, by employing single-shot irradiation, a minimum feature size of 100 nm was achieved for individual irradiated dots.

The resulting PMA profiles have a substantial impact on the SW band structure of the YIG and were exploited to fabricate one- and two-dimensional magnonic crystals (MCs), which are structures with periodic magnetic properties. Measured spin-wave transmission through the 1D-MC exhibits frequency gaps introduced by the patterned crystal. Meanwhile, micro-focused Brillouin Light Scattering (µ-BLS) experiments on the 2D-MC demonstrated control over SW localization, which I further confirmed via micromagnetic simulations.

I also investigated the effects of this DLW technique on a thinner, 100 nm thick single-crystal YIG film. The laser patterning on this sample produced effects similar to those previously described for the thicker sample. Once again, above an optical power threshold, the material undergoes significant changes. The irradiated patterns acquire a distinctive blue colour, and MFM measurements reveal the emergence of magnetic stripe domains (Fig. 2a). This indicates an increase in PMA compared to the pristine material, which exhibits a uniform magnetization parallel to the film surface. By further increasing the irradiation power, the domain structure transitions from stripe domains to a fully out-of-plane (OOP) state, where the magnetization lies entirely perpendicular to the film plane. This is reflected in local square hysteresis loops whose coercivity increases with the laser power, as measured by micro-MOKE (Fig. 2b).

Eventually, the film loses its magnetic properties if the laser power is increased even further. In this high-power regime, I used the DLW technique to pattern waveguides that successfully confine SW propagation. Through micromagnetic simulations, I analysed the localization of the SW modes propagating within these patterned waveguides.

Ultimately, this work validates Phase Nanoengineering via Direct Laser Writing as a highly effective method for tuning the magnetic properties of YIG down to the nanoscale. The technique paves the way for the fast and reliable fabrication of SW-based proof-of-concept devices.

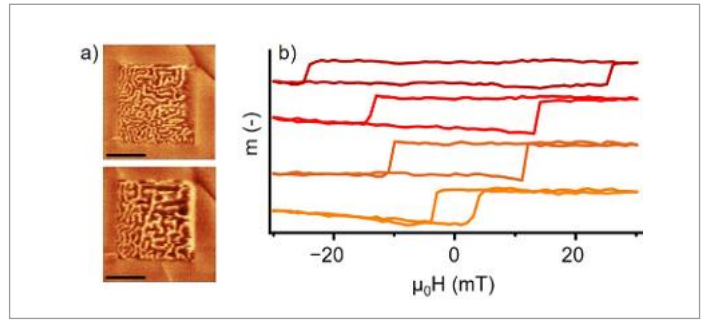

Fig.2 - a) MFM measurements of irradiated square areas near the power threshold, showing magnetic stripe domains. Scale bars 5 mm. b) OOP hysteresis loops measured on uniformly irradiated areas at higher powers with respect to the ones in a).

PHOTOPHYSICAL PROPERTIES AND MECHANISMS OF AMPLIFIED SPONTANEOUS EMISSION IN 2D LAYERED PEROVSKITES

He Yarong - Supervisor: Annamaria Petrozza

Metal halide perovskites are promising semiconductors for photonic applications due to their tunable emission, high efficiency, and solution processability, making them attractive for silicon photonics and for addressing challenges such as the "green gap" in lasers. While three-dimensional perovskites have achieved continuous-wave lasing, two-dimensional (2D) systems offer improved stability and strong excitonic effects, but achieving optical gain in n = 1 layered structures remains challenging due to high thresholds and nonradiative losses.

Lead-based 2D perovskites show limited and poorly reproducible amplified spontaneous emission (ASE), whereas tin-based counterparts exhibit more promising optical gain, including low-temperature lasing and emerging room-temperature operation. However, the fundamental origin of their distinct behavior remains unclear. Recent studies highlight the importance of structural rigidity: aromatic π-conjugated spacers enhance lattice cohesion and radiative recombination, while flexible alkyl spacers introduce disorder and defect-related losses. In parallel, quasi-2D (n > 1) Ruddlesden–Popper perovskites provide improved optical gain properties through reduced exciton binding energy and longer carrier lifetimes, though tin-based systems remain less explored.

In this study, comprehensive optical and structural characterization, which includes temperature-dependent PL, power-dependent ASE measurements, and ssNMR spectroscopy, was employed to elucidate the interplay between lattice dynamics, exciton-phonon coupling, and ASE thresholds.

We first investigate the role of metal cation composition by comparing PEA_2PbI_4, PEA_2SnI_4, and their mixed systems. Structural and optical analyses reveal that Sn-to-Pb substitution strongly affects crystallinity, bandgap tuning, and defect formation. Defect-related states are identified as a major factor limiting ASE, while temperature-dependent and time-resolved studies elucidate the role of exciton–phonon coupling, exciton binding energy, and Auger recombination in governing optical gain.

$Fth = F0 * \exp(TT0)$, where Fth is the threshold fluence, $F0$ is the threshold fluence at 0 K, and T0 is the characteristic temperature, which results to be 42±2 K for PEA2SnI4 and 38±5 K for PEA2PbI4.

To further understand ASE in tin-based systems, we explore the effects of structural rigidity and dimensionality. By comparing Ruddlesden–Popper (BA_2SnI_4) and Dion–Jacobson ($DABSnI_4$) phases, we show that stronger interlayer coupling and reduced spacer flexibility enhance lattice rigidity, suppress nonradiative recombination, and significantly lower the ASE threshold. In contrast, the more flexible RP structure exhibits pronounced defect-related emission and limited ASE performance.

Additionally, dimensionality engineering from n = 1 to quasi-2D systems further improves optical gain by optimizing structural balance and carrier dynamics. Overall, this work establishes a clear framework linking metal cation composition, lattice rigidity, and dimensionality to ASE behavior in 2D perovskites. By suppressing defect-related losses and enhancing structural stability, efficient optical gain can be achieved. These insights provide practical design guidelines for developing stable, high-gain, lead-free perovskite materials for photonic and optoelectronic applications

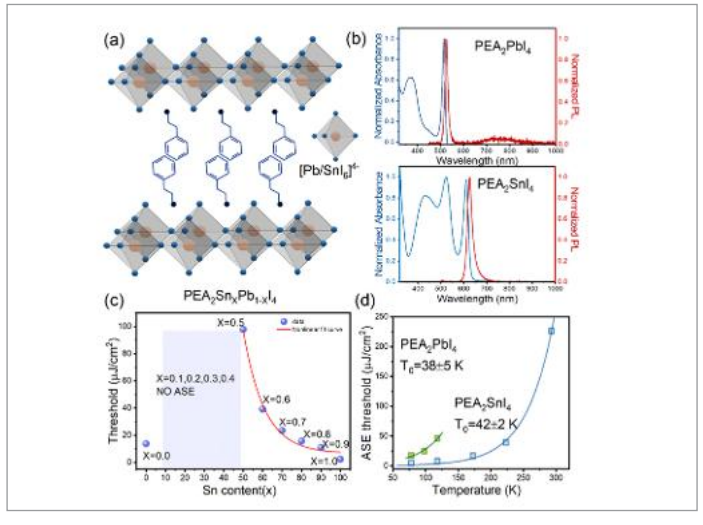

Fig.1 - Influence of metal cation composition on ASE properties in two-dimensional perovskites. (a) Schematic illustration of the 2D layered perovskite structure, consisting of alternating organic (PEA) and inorganic ($[Pb/SnI_6]^{4-}$) layers. (b) The UV-vis absorption and photoluminescence spectra of PEA2PbI4 and PEA2SnI4 thin films at room temperature. (c) ASE threshold as a function of the Sn content (x) (78 K). No ASE is observed in the range of Sn content (x=0.1- 0.4). (d)ASE threshold evolution versus temperature; the experimental data were fitted using the exponential function

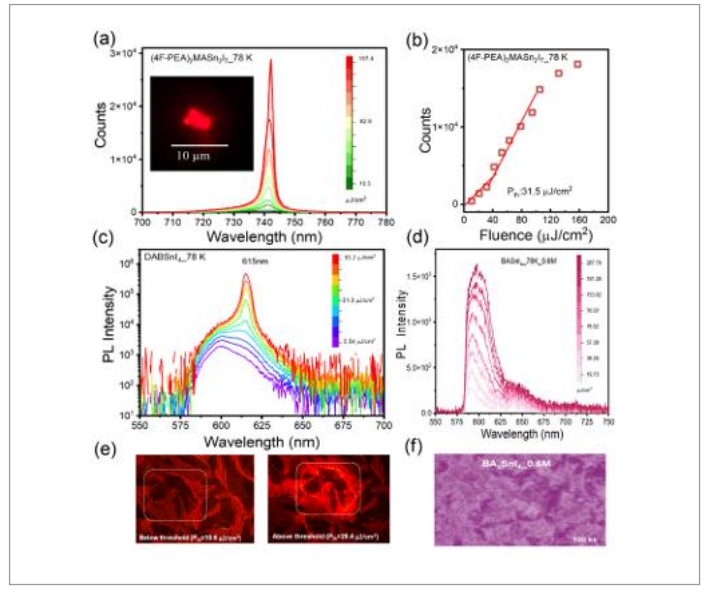

Fig.2 - Phase rigidity and dimensionality effects on ASE in 2D layered perovskites. (a) Fluence-dependent PL spectra in the two microflakes of (4F-PEA)2MASn2I7, fluence increasing from 10.5 to 157.4 μJ/cm2 and from 10.5 to 236 μJ/cm2.Insets show optical images of the microflakes above the threshold. (b) Integrated emission intensity as a function of excitation fluence, revealing a clear ASE threshold. (c) Fluence-dependent photoluminescence of Dion-Jacobson DABSnI4 at 78 K, exhibiting sharp spectral narrowing and efficient ASE. (d) Corresponding emission behavior of BA2SnI4 thin films, showing broader emission and no ASE appears as the fluence increases. (e), Optical images of DABSnI4 thin films when the excitation is below and above the threshold. (f) Optical images of BA2SnI4 thin films under the white light.

ENHANCED NONLINEAR FREQUENCY CONVERSION AND POLARIZATION CONTROL AT THE NANOSCALE

Luan Yigong - Supervisor: Michele Celebrano

Light-matter interactions at the nanoscale are crucial for modern photonic technologies, such as optical communication, biosensing, and advanced imaging. Nonlinear light-matter interactions at the nanoscale are particularly relevant, underpinning frequency conversion and enabling a range of processes such as chiral-dependent polarization control. However, these effects are intrinsically weak and scaling with power laws of the field amplitude. Therefore, to attain efficient frequency conversion they require high field intensities and long interaction lengths only achievable in bulk materials. As a result, in nanoscale volumes, this results in small nonlinear chiroptical responses and limits miniaturization and on-chip integration. Nanophotonics overcomes these challenges by structuring materials at subwavelength scales, concentrating and shaping electromagnetic fields to enhance weak nonlinear effects and control polarization. This enables nanoscale devices to replicate or exceed the functionality of bulk optical components.

Optical metasurfaces are two-dimensional ensembles of nanoantennas (commonly termed meta-atoms), which allow to broaden the spectra of optical functionalities by collective effects, especially in periodic arrangements. Coupling between resonators gives rise to lattice resonances and symmetry-protected modes with high quality factors, enabling stronger and more spectrally selective light-matter interaction. Metasurfaces therefore offer versatile control over light's intensity, phase, spectrum, and polarization within an ultrathin footprint, making them ideal for compact laser sources, metalenses, smart cameras, and enantiomer sensing. While many metasurface functionalities are defined at the design stage, an important frontier is reconfigurable metasurfaces whose optical response can be actively tuned. Electrical or optical control allows dynamic modulation of resonances, enabling real-time adjustment of light intensity and polarization.

My PhD research follows this progression, from engineering resonant nanoantennas to exploiting collective metasurface resonances to enhance weak nonlinear and chiroptical responses, ultimately achieving dynamic polarization control in reconfigurable nonlinear metasurfaces.

The first challenge I addressed during my PhD thesis was achieving efficient, spectrally narrow second-harmonic generation (SHG) in lithium niobate (LN) at the nanoscale, where fabrication constraints typically limit resonant structures. This was solved using an etchless thin-film lithium niobate (TFLN) platform, realized by nanoimprinting a slanted titanium dioxide (TiO2) nanograting onto the LN film. The resulting hybrid structure supports high-Q quasi-bound states in the continuum (q-BICs), strongly confining the optical field within the nonlinear material and enhancing SHG. A key feature is a simple spectral-tuning mechanism: small mechanical rotation of the sample (< 1°) continuously shifts the q-BIC resonance relative to the pump wavelength, allowing precise optimization of the nonlinear interaction without active tuning elements. This approach achieves a maximum normalized SHG efficiency of $\eta\eta II,\mathrm{norm}=0.15\%\ \mathrm{cm}^2/\mathrm{GW}$, comparable to state-of-the-art LN devices with a relatively low pump intensity (3.6×10^{-6} GW/cm^2). Additionally, larger rotation angles (> 1°) enable wavelength-tunable SHG with nearly constant efficiency, alongside rotation-controlled modulation of the emitted polarization from linear to circular. Building on the understanding of q-BIC resonances, the second part investigates chiral q-BIC metasurfaces that combine structural chirality with symmetry-protected resonances to achieve strong polarization-selective light-matter interactions. Both planar (2D) Si and three-dimensional (3D) WS_2 chiral geometries were designed, enabling direct comparison of dimensionality effects on the chiroptical response. The 2D Si structures, easy to fabricate, support q-BIC resonances with strong circular-polarization selectivity in THG through polarization conversion, exhibiting near-unity nonlinear circular dichroism and THG conversion efficiencies on the order of 10^{-2} W^{-2}. In contrast, the 3D WS_2 metasurface design exhibits intrinsic chirality by breaking symmetry both in-plane and out-of-plane, generating strong longitudinal fields. This design maintains maximum chirality in TH signals for oblique incidences up to 20°, offering a new degree of freedom for sub nanometer control of resonance wavelengths.

Finally, a dynamic polarization-control scheme was demonstrated in symmetric AlGaAs metasurfaces. By coherently combining sum-frequency (SFG) and third-harmonic generation (THG) driven by dual femtosecond pumps ($\omega\omega$+$2\omega\omega$), the opposite parity of these nonlinear contributions enables continuous tuning of the emitted polarization from linear to circular, reaching a circular polarization degree of 83%. The circularly polarized light of opposite handedness is symmetrically distributed along the first diffraction orders and introducing a $\pi\pi$ phase shift reverses the handedness within the same diffraction order.

This approach establishes polarization as an independent degree of freedom for all-optical beam control, offering new opportunities for chiral-sensitive detection and advanced imaging applications.

Overall, this thesis demonstrates the design, fabrication, and dynamic control of nonlinear dielectric metasurfaces for efficient, tunable, and polarization-sensitive nonlinear light conversion at the nanoscale. By combining high-Q resonant photonic platforms, engineered structural chirality, and coherent nonlinear processes, multiple routes for reconfigurable nonlinear nanophotonic functionality are established, laying the groundwork for future developments in actively controllable metasurfaces and advanced optical manipulation at the nanoscale.

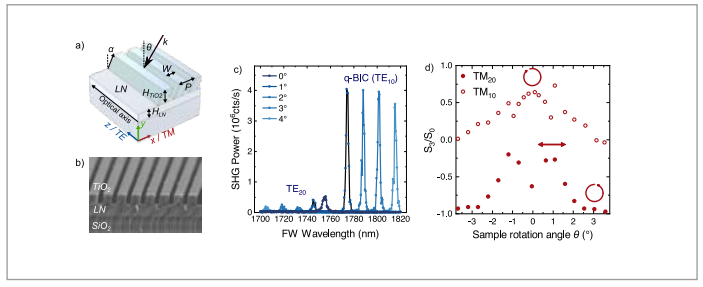

Fig.1 - a) Schematic of the TiO2 nanograting on a $LiNbO_3$ film, with the LiNbO3 optical axis along the z-axis. b) Cross-sectional scanning electron micrograph of the fabricated structure. c) Experimental SHG spectra under TE-polarized excitation for tilt angles from 0° to 4°, demonstrating wavelength-tunable SHG with nearly constant efficiency. d) Rotation-angle ($\theta\theta$) dependence of the normalized Stokes parameter $SS3/SS0$ for modes under TM-polarized excitation

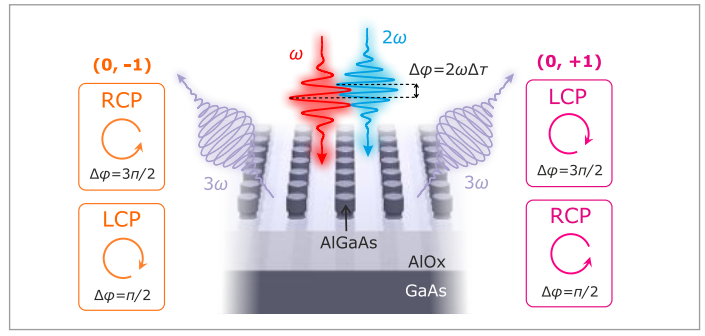

Fig.2 -Schematic of all-optical polarization control via nonlinear interferometry in a fully symmetric AlGaAs metasurface. SFG and THG from dual pump beams ($\omega\omega$+$2\omega\omega$) produces upconverted light at $3\omega\omega$. Circularly polarized light with opposite handedness appears in the specular diffraction orders due to broken mirror symmetry in detection and introducing a $\pi\pi$ phase shift reverses the handedness